

Toxic si/shRNAs that kill cancer cells by targeting survival genes

William Putzbach^{1,6}, Quan Q. Gao^{1,6}, Monal Patel^{1,6}, Stijn van Dongen⁴, Ashley Haluck-Kangas¹, Aishe A. Sarshad⁵, Elizabeth Bartom², Kwang-Youn A. Kim³, Denise M. Scholtens³, Markus Hafner⁵, Jonathan C. Zhao¹, Andrea E. Murmann¹
and Marcus E. Peter^{1,2,*}

¹ Department of Medicine/Division Hematology/Oncology and ² Department of Biochemistry and Molecular Genetics, ³ Department of Preventive Medicine, Feinberg School of Medicine, Northwestern University, Chicago, IL 60611, USA; ⁴ European Bioinformatics Institute (EMBL-EBI), Hinxton, Cambridge CB10 1SD, UK; ⁵ Laboratory of Muscle Stem Cells and Gene Regulation, NIAMS, NIH, Bethesda, MD 20892, USA.

Corresponding author: Marcus Peter, E-mail: m-peter@northwestern.edu, phone: 312-503-1291; FAX: 312-503-0189.

⁶ Shared first authorship

Keywords:
RNAi, Fas, cancer, CRISPR, cell death, DISE, OTE

Abstract

Over 80% of multiple tested siRNAs and shRNAs targeting CD95 or CD95 ligand (CD95L) induce a form of cell death characterized by simultaneous activation of multiple cell death pathways preferentially killing transformed and cancer stem cells. We now show these si/shRNAs kill cancer cells through canonical RNAi by targeting the 3'UTR of critical survival genes in a unique form of off-target effect we call DISE (death induced by survival gene elimination). Drosha and Dicer deficient cells, devoid of most miRNAs, are hypersensitive to DISE, suggesting cellular miRNAs protect cells from this form of cell death. By testing 4666 shRNAs derived from the CD95 and CD95L mRNA sequences and an unrelated control gene, Venus, we have identified many toxic sequences - most of them located in the open reading frame of CD95L. We propose that using specific toxic RNAi-active sequences present in the genome can kill cancer cells.

Introduction

One of the most popular methods utilized to reduce gene expression in cells is RNA interference (RNAi). RNAi has been used in several studies to identify genes critical for the survival of human cancer cell lines (Cowley et al., 2014; Hadji et al., 2014; Hart, Brown, Sircoulomb, Rottapel, & Moffat, 2014; Morgens, Deans, Li, & Bassik, 2016; Wang et al., 2015). During RNAi, gene expression is inhibited by small interfering (si)RNAs, small hairpin (sh)RNAs or micro (mi)RNAs. miRNAs are generated as primary transcripts in the nucleus where they undergo processing to pre-miRNAs by the Drosha-DGCR8 complex before being exported to the cytosol by exportin 5 (Ha & Kim, 2014; Krol, Loedige, & Filipowicz, 2010). Once in the cytosol, pre-miRNAs and shRNAs are cleaved by Dicer, a type III RNase that functions in complex with TRBP, generating 21-23 nucleotide long fragments of double-stranded RNA (dsRNA) that have two nucleotide 3' overhangs (Zamore, Tuschl, Sharp, & Bartel, 2000). DsRNA fragments or chemically synthesized double stranded siRNAs are loaded into the RNA-induced silencing complex (RISC) as single stranded RNAs (the guide RNA) (Siomi & Siomi, 2009). A near-perfect complementarity between the guide strand of the si/miRNA and the target mRNA sequence results in cleavage of the mRNA (Pratt & MacRae, 2009). Incomplete complementarity results in inhibition of protein translation and contributes to mRNA degradation (Guo, Ingolia, Weissman, & Bartel, 2010). mRNA targeting is mostly determined by the seed sequence, positions 2-7/8 of the guide strand, which is fully complementary to the seed match in the 3'UTR of targeted mRNAs. Similar to miRNAs, although not fully explored, siRNAs and shRNAs also target multiple mRNAs besides the mRNAs they were designed to silence—a phenomenon commonly referred to as off-target effect (OTE)—that is generally sought to be avoided (Birmingham et al., 2006; Jackson et al., 2006; Lin et al., 2005).

The death receptor CD95 (Fas/APO-1) mediates induction of apoptosis when bound by its cognate CD95L, most prominently in the context of the immune system (Krammer, 2000). However, more recently, it has become apparent that the CD95/CD95L system has multiple tumor-promoting activities (Peter et al., 2007). CD95 signaling promotes cell growth (Chen et al., 2010), increases motility and invasiveness of cancer cells (Barnhart et al., 2004; Kleber et al., 2008), and promotes cancer stemness (Ceppi et al., 2014; Drachsler et al., 2016; Qadir et al., 2017). In fact, we reported tumors barely grew *in vivo* when the CD95 gene was deleted (Chen et al., 2010; Hadji et al., 2014). Therefore, it appeared consistent that multiple shRNAs and siRNAs targeting either CD95 or CD95L slowed down cancer cell growth (Chen et al., 2010) and

engaged a distinct form of cell death characterized by the activation of multiple cell death pathways (Hadji et al., 2014). This unique form of cell death cannot be inhibited by conventional cell death or signaling pathway inhibitors or by knockdown of any single gene in the human genome (Hadji et al., 2014); it preferentially affects transformed cells (Hadji et al., 2014) including cancer stem cells (Ceppi et al., 2014). Here we report that loading of CD95 and CD95L derived sequences (si/shRNAs targeting CD95 or CD95L) into the RISC elicits a distinct form of cell death that results from the targeting of multiple survival genes in a unique form of OTE.

Results

si/shRNAs kill cells in the absence of the targeted site

More than 80% of multiple tested shRNAs or siRNAs designed to target either CD95 or CD95L were toxic to multiple cancer cells (Hadji et al., 2014). We have now extended this analysis to Dicer substrate 27mer DsiRNAs designed to target CD95L (*Figure 1 - figure supplement 1A*, (D. H. Kim et al., 2005)). All five DsiRNAs displayed toxicity when introduced into HeyA8 cells at 5 nM (*Figure 1 - figure supplement 1B*) reinforcing our previous observation that the majority of CD95 and CD95L targeting si/shRNAs are toxic to cancer cells. We also analyzed a data set of a genome-wide analysis of 216 cells infected with a pooled library of the TRC shRNAs (Cowley et al., 2014). Most of the shRNAs we have tested were found to be depleted in the infected cell lines included, in this study. The following shRNAs were found to be depleted in the listed percentage of the 216 cell lines tested: shL4 (99.5%), shL1 (96.8%), shR6 (88.9%), shR7 (75%), shL2 (67.1%), shR5 (38.4%), shL5 (26.4%), and shR8 (21.3%) (*Figure 1 - figure supplement 1C*). Consistent with our data, shL1 and shR6 were found to be two of the most toxic shRNAs. Again in this independent analysis, the majority of tested shRNAs (67%) targeting either CD95 or CD95L killed more than half of all tested cancer cell lines.

Interestingly, a more recent RNAi screen did not report toxicity after expressing shRNAs against CD95 or CD95L (Morgens et al., 2016). The authors of this study used a second-generation shRNA platform based on a miR-30 backbone. To determine the source of the discrepancy in the data, we generated miR-30 based Tet-inducible versions of some of our most toxic shRNAs (shL1, shL3, shL4, shR5, shR6, and shR7, *Figure 1- figure supplement 2A*) and found none of them to be highly toxic to HeyA8 cells (*Figure 1- figure supplement 2B*). To determine their knockdown efficiency, we induced their expression in cells carrying sensor

plasmids in which the fluorophore Venus was linked to either the CD95L or CD95 open reading frame (ORF). Expression of most of these miR-30-based shRNAs also did not efficiently silence Venus expression (**Figure 1- figure supplement 2C**). In contrast, two of our most toxic shRNAs shL3 and shR6 when expressed in the Tet inducible pTIP vector not only killed HeyA8 cells, but also very efficiently suppressed Venus fluorescence in cells expressing the targeted Venus sensor (**Figure 1- figure supplement 2D**). These data suggest that the levels of shRNAs produced from the miR-30 based vector may not be sufficient to be toxic to the cancer cells. Because expression levels of shRNAs are difficult to titer, we used siRNAs to determine the concentration of the toxic CD95L-derived siL3 required to kill HeyA8 cells (**Figure 1- figure supplement 2E**). Growth was effectively blocked (and cells died, data not shown) when siL3 was transfected at 1 nM—a concentration well below the commonly used and recommended siRNA concentration of 5-50 nM—but not at 0.1 nM. These data suggest this form of toxicity does not require high amounts of si- or shRNAs; however, that the low expression we achieved from the miR-30 based shRNA vectors was not enough to effectively induce the toxicity. Because these miR-30 based shRNA vectors were developed to reduce off-target effects, the toxicity of CD95 and CD95L targeting si/shRNAs described by us and others could be due to an OTE. While this was a plausible explanation, the high percentage of toxic si/shRNAs derived from CD95 and CD95L seemed to exclude a standard OTE and pointed at a survival activity of CD95 and CD95L.

We therefore tested whether exogenously added recombinant CD95L protein could protect cells from the toxicity of CD95L-derived shRNAs. When NB7 cells were incubated with different concentrations of a soluble form of CD95L (S2), toxicity exerted by shL1 was not affected (**Figure 1A, left panel**). NB7 neuroblastoma cells were chosen for these experiments because they lack expression of caspase-8 (Teitz et al., 2000) and hence are completely resistant to the apoptosis inducing effects of CD95L. An ostensible moderate and dose-dependent protection was detected when cells were treated with a highly active leucine-zipper tagged CD95L (LzCD95L) (**Figure 1A, center panel**). However, this effect is likely due to the growth-promoting activities of soluble CD95L, which also significantly affected the growth of the cells expressing a scrambled control shRNA (seen for both S2 and LzCD95L). The recombinant LzCD95L protein was active, as demonstrated by its apoptosis-inducing capacity in CD95 apoptosis sensitive MCF-7 cells (**Figure 1A, right panel**).

To test whether CD95L or CD95 proteins could protect cancer cells from death, we introduced silent mutations into the targeted sites of three very toxic shRNAs: shL1 and shL3 (both targeting CD95L) and shR6 (targeting CD95). We first introduced eight silent mutations into the sites targeted by either shL1 or shL3 (**Figure 1B**) and expressed these proteins in NB7 cells (**Figure 1C**). Both mutant constructs were highly resistant to knockdown by their cognate shRNA but still sensitive to knockdown by the other targeting shRNA (**Figure 1C**). Overexpression of these shRNA-resistant versions of the CD95L ORF did not protect the cells from shL1 or shL3, respectively (**Figure 1D**). Interestingly, expression of full length CD95L slowed down the growth of the NB7 cells right after infection with the lentivirus despite the absence of caspase-8 (data not shown). Infection with shRNAs was therefore performed 9 days after introducing CD95L when the cells had recovered and expressed significant CD95L protein levels (**Figure 1C**). We then mutated the CD95 mRNA in the targeted site of shR6 (**Figure 1E**). Neither expression of wild-type (wt) nor mutated (MUT) CD95 in MCF-7 cells (**Figure 1F**) reduced the toxicity when cells were infected with the pLKO-shR6 or another toxic lentiviral shRNA, pLKO-shR7 (**Figure 1G**). These data suggested that neither exogenously added recombinant CD95L or exogenously expressed CD95L or CD95 protein can protect cells from toxic shRNAs derived from these genes.

To determine whether we could prevent cancer cells from dying by this form of cell death by deleting the endogenous targeted sites, we used CRISPR/Cas9 gene-editing to excise sites targeted by different shRNAs and siRNAs in both alleles of the CD95 and CD95L genes. We first deleted a 41 nt piece of the CD95L gene in 293T cells, that contained the target site for shL3 (**Figure 2A, 2C**). While internal primers could not detect CD95L mRNA in three tested clones, primers outside of the deleted area did detect CD95L mRNA (**Figure 2D**, and data not shown). Three clones with this shL3 Δ 41 deletion were pooled and tested for toxicity by shL3 expressed from a Tet-inducible plasmid (pTIP-shL3). Compared to a pool of control cells transfected only with the Cas9 plasmid, the 293T shL3 Δ 41 cells were equally sensitive to the toxic shRNA (**Figure 2G**). This was also observed when the clones were tested individually (data not shown).

To exclude the possibility that shL3 was inducing cell death due to a unique activity of shL3 and/or 293T cells, we deleted the same 41 nt in CD95L in the ovarian cancer cell line HeyA8; We also generated HeyA8 clones in which we either removed a 64 nt region containing the target site for the siRNA siL3 in the CD95L coding sequence or a 227 nt region containing the target site for shR6 in CD95 (**Figure 2A, 2B** and **Figure 2 - figure supplement 1**). In all cases,

homozygous deletions were generated (**Figure 2E**). To confirm the deletion of the shR6 target site, we infected HeyA8 cells treated with the Cas9 plasmid only and HeyA8 with a homozygous deletion of the shR6 site with shR6 and, as positive controls, with shR2 (targeting the CD95 ORF) and shR6' (targeting the CD95 3'UTR). Five days after infection, CD95 mRNA was quantified by real time PCR using a primer located outside the 227bp deletion (**Figure 2F**). The mutated CD95 mRNA was still detectable in the shR6 Δ 227 cells. While shR2 and shR6' (both targeting outside the deleted region) caused knockdown of CD95 mRNA in both the Cas9 expressing control and the shR6 Δ 227 cells, shR6 could only reduce mRNA expression in the Cas9 control cells. These data document that HeyA8 CD95 shR6 Δ 227 cells no longer harbor the sequence targeted by shR6.

Now having HeyA8 cells lacking one of three RNAi-targeted sites in either CD95 or CD95L, we could test the role of the CD95 and CD95L gene products in protecting HeyA8 cells from the death induced by either shRNA (shL3 and shR6, two different vectors: pLKO or the Tet inducible pTIP) or the siRNA siL3. In all cases, the shRNA or siRNA that targeted the deleted region was still fully toxic to the target-site deleted cells (**Figure 2H** and **2I**). We saw efficient growth reduction and cell death in siL3 site deleted cells transfected with as little as 1 nM siL3 (**Figure 2I**, and data not shown). These data firmly establish that cells were not dying due to the knockdown of either CD95 or CD95L.

Involvement of canonical RNAi

shRNAs and early generation naked siRNAs showed general toxicity when introduced in large amounts, presumably by eliciting an interferon (IFN) response (Marques & Williams, 2005) or by saturating the RISC (Grimm et al., 2006). However, both chemically modified siRNAs at very low concentrations and lentiviral shRNAs at an MOI<1 were still toxic (data not shown). We therefore decided to test whether the observed toxicity involved canonical RNAi and activity of the RISC. To test shRNAs or siRNAs targeting CD95L, we introduced the Venus-CD95L sensor (inset in **Figure 3A**, right panel) into HeyA8 CD95 protein k.o. cells we had generated in the process of deleting the shR6 site (**Figure 2 - figure supplement 1**, clone # 2 was used for the following studies; see figure legend for strategy and characterization of the clones). While double-stranded (ds)-siL3 effectively silenced Venus expression and induced toxicity, neither the sense nor the antisense single-stranded (ss)RNAs significantly decreased Venus expression or induced toxicity (**Figure 3A**). In addition, no activity was found when ds-siL3, synthesized as

deoxyribo-oligonucleotides, was transfected into the cells (**Figure 3B**). Using this type of analysis, we tested a number of modified siRNAs for RNAi activity and toxicity. For siRNAs to be fully active they require 3' overhangs on both strands (Bernstein, Caudy, Hammond, & Hannon, 2001). Converting siL3 to a blunt-ended duplex resulted in substantial loss of RNAi activity and toxicity (**Figure 3C**). Due to the topology of the RISC, siRNA activity is decreased by modification of the 5' end of the antisense/guide strand (Chiu & Rana, 2003). To test whether cell death induced by siL3 would be affected by a bulky modification, we placed a Cy5 moiety at any of the four possible ends of the siL3 duplex. Only when the siL3 duplex carried a 5' modification in the guide strand did it prevent RNAi activity and toxicity; modifications in the three other positions had no effect (**Figure 3C**). This was confirmed for another siRNA, siL2. To test whether the toxicity of siL3 required association with a macromolecular complex, which would be consistent with RISC involvement, we performed a competition experiment. HeyA8 cells were transfected with 10 nM of siL3, and a mutated nontoxic oligonucleotide, siL3MUT, was titrated in (**Figure 3D**). siL3MUT reduced the growth inhibitory activity of siL3 in a dose-dependent fashion suggesting that siL3 and siL3MUT compete for the same binding site in the cells, pointing at involvement of the RISC.

To determine involvement of RNAi pathway components in the toxicity of CD95 and CD95L-derived sequences, we tested HCT116 cells deficient for either Drosha or Dicer (Y. K. Kim, Kim, & Kim, 2016). Growth of parental HCT116 cells was impaired after infection with shL3 or shR6 viruses (**Figure 3E**, left panel). Consistent with the requirement of Dicer to process shRNAs, Dicer^{-/-} cells were completely resistant to the toxic shRNAs (**Figure 3E**, center panel). This was also supported by the inability of shR6 to silence CD95 protein expression in these cells (**Figure 3F**). Dicer^{-/-} cells were not resistant to toxic siRNAs as these cells died when transfected with siL3, which is consistent with mature siRNAs not needing further processing by Dicer (**Figure 3G**, center panel). Interestingly, Drosha^{-/-} cells were hypersensitive to the two toxic shRNAs (**Figure 3E**, right panel, $p < 0.0001$, according to a polynomial fitting model), and shR6 efficiently knocked down CD95 expression in Drosha^{-/-} cells (**Figure 3F**). Both Drosha^{-/-} and Dicer^{-/-} cells were much more susceptible to the toxicity induced by siL3 than parental cells (**Figure 3G**, center and right panel, $p < 0.0001$, according to a polynomial fitting model). The hypersensitivity of the Drosha^{-/-} cells to toxic si/shRNAs and of Dicer^{-/-} cells to toxic siRNAs can be explained by Drosha^{-/-} and Dicer^{-/-} cells allowing much more efficient uptake of mature toxic

RNAi-active species into the RISC because they are almost completely devoid of competing endogenous miRNAs (Y. K. Kim et al., 2016).

To determine the contribution of the siRNA seed sequence to their toxicity, we generated a set of chimeric siRNAs in which we systematically replaced nucleotides of the toxic siL3 siRNA with nucleotides of a nontoxic scrambled siRNA. We did this starting either from the seed end or from the opposite end (**Figure 3H**). HeyA8 cells expressing both the Venus-CD95L sensor (to monitor level of knockdown) and a Nuc-Red plasmid to fluorescently label nuclei (to monitor the effects on cell growth) were transfected with 5 nM of the chimeric siRNAs; total green fluorescence and the number of red fluorescent nuclei were quantified over time. The siL3 control transfected cells showed an almost complete suppression of the green fluorescence and high toxicity. In the top panel of **Figure 3H**, the data are summarized in which siL3 nucleotides were stepwise replaced with siScr nucleotides from the seed sequence end. Both RNAi and toxicity were profoundly reduced when three of the terminal siL3 nucleotides were replaced with the siScr nucleotides in those positions, suggesting the seed region (6mer highlighted in blue) is critical for both activities. Consistently, as shown in the bottom panel of **Figure 3H**, when siL3 nucleotides were replaced with siScr nucleotides from the non-seed end, neither RNAi nor the toxicity was diminished until replacements affected residues in the seed region. These data suggest the 6mer seed sequence of siL3 was critical for both RNAi activity and its toxicity.

Toxic si/shRNAs cause downregulation of survival genes

A general OTE by RNAi has been reported (Birmingham et al., 2006; Jackson et al., 2006; Lin et al., 2005). However, this was been found to cause toxicity in most cases, and the targeted mRNAs were difficult to predict (Birmingham et al., 2006). The fact that 22 of the tested CD95 and CD95L-targeting sh- and si/DsiRNAs were toxic to many cancer cells evoking similar morphological and biological responses (Hadjil et al., 2014) generated a conundrum: Could an OTE trigger a specific biology? To test this, we expressed two toxic shRNAs - one targeting CD95L (shL3) and one targeting CD95 (shR6) - in cells lacking their respective target sequences and subjected the RNA isolated from these cells to an RNA-Seq analysis. In order to detect effects that were independent of cell type, delivery method of the shRNA, or targeted gene, we expressed shL3 in 293T (Δ shL3) cells using the Tet-inducible vector pTIP and shR6 in HeyA8 (Δ shR6) cells using the pLKO vector. In each case, changes in RNA abundance were compared to cells in which expressing a non-targeting shRNA in matching vectors. Total RNA was

harvested in all cases at either the 50-hour time point (before the onset of cell death) or at the 100-hour time point (during cell death) (**Figure 4A**). To achieve high stringency, the data were then analyzed in two ways: first, using a conventional alignment-based analysis to identify genes for which the mRNA changed more than 1.5-fold (and an adjusted p-value of less than 0.05) and second, by a read-based method, in which we first identified all reads that changed >1.5-fold and then subjected each read to a BLAST search to identify the gene it was derived from. Only RNAs that were detected by both methods were considered (**Table S1**). The combination of the analyses resulted in one mRNA that was upregulated and 11 mRNAs that were downregulated (**Figure 4B**). Using an arrayed qPCR approach, most of these detected mRNA changes were validated for both cell lines (**Figure 4 - figure supplement 1A**). Interestingly, for nine of the eleven genes, published data suggest they are either highly upregulated in cancer and/or critical for the survival of cancer cells, as their inhibition or knockdown resulted in either growth reduction or induction of various forms of cell death (see legend of **Figure 4 - figure supplement 1** for details). Significantly, six of these eleven downregulated genes were recently identified in two independent genome-wide RNAi lethality screens to be critical for cancer cell survival (Blomen et al., 2015; Wang et al., 2015) (**Figure 4B** and **Figure 4 - figure supplement 1B**) (**Table S2**). Considering these two screens only identified 6.6% of human genes to be critical for cell survival, we found a significant enrichment (54.5%, p-value = 3×10^{-6} according to binomial distribution) of these survival genes among the genes downregulated during the cell death induced by either shL3 or shR6. All six survival genes are either highly amplified or mutated in human cancers (**Figure 4 - figure supplement 2A**). In addition to these six genes, GNB1 and HIST1H1C were reported to be required fitness genes in a recent high-resolution CRISPR-based screen (Hart et al., 2015). A kinetic analysis showed most of the deregulated mRNAs were downregulated early with a significant effect already at 14 hours, more than two days before the onset of cell death (**Figure 4 - figure supplement 1C** and data not shown). This suggested the cells were dying because of the silencing of multiple critical survival genes, providing an explanation for why multiple cell death pathways were activated. We therefore call this type of cell death DISE (for Death Induced by Survival gene Elimination).

To confirm some of the downregulated genes were also critical survival genes for HeyA8 cells, we transfected HeyA8 cells with siRNA SmartPools targeting each of the eleven genes. Individual knockdown of seven of the targeted genes resulted in reduced cell growth when compared to cells transfected with a pool of scrambled siRNAs (**Figure 4C**). To mimic the effect

of the CD95 and CD95L-derived shRNAs, we treated HeyA8 cells with a combination of siRNA pools targeting these seven genes. Remarkably, 1 nM of this siRNA mixture (35.7 pM of each individual siRNA) was sufficient to effectively reduce growth of the cells (**Figure 4 - figure supplement 2B**) and also cause substantial cell death (**Figure 4 - figure supplement 2C**), suggesting it is possible to kill cancer cells with very small amounts of siRNAs targeting a network of these survival genes.

To test the generality of this phenomenon, we inducibly expressed another CD95L derived shRNA, shL1, in 293T cells using the pTIP vector, and transfected HeyA8 cells with 25 nM siL3. We subjected the cells to RNA-Seq analysis 100 hours and 48 hours after addition of Dox or after transfection, respectively. To determine whether survival genes were downregulated in all cases of sh/siRNA induced cell death, we used a list of 1883 survival genes and 423 genes not required for survival (nonsurvival genes) recently identified in a CRISPR lethality screen (**Table S2**). We subjected the four ranked RNA-Seq data sets to a gene set enrichment analysis using the two gene sets (**Figure 4D**). In all cases, survival genes were significantly enriched towards the top of the ranked lists (most downregulated). In contrast, nonsurvival genes were not enriched. One interesting feature of DISE that emerged was the substantial loss of histones. Of the 16 genes that were significantly downregulated in cells treated with any of the four sh/siRNAs, 12 were histones (**Figure 4E**). While it might be expected that dying cells would downregulate highly expressed genes such as histones, we believe that losing histones is a specific aspect of DISE because a detailed analysis revealed the downregulated histones were not the most highly expressed genes in these cells (**Figure 4 - figure supplement 3**). In addition, almost as many genes with similarly high expression were found to be upregulated in cells after DISE induction.

A Metascape analysis revealed genes involved in mitotic cell cycle, DNA conformation change, and macromolecular complex assembly were among the most significantly downregulated across all cells in which DISE was induced by any of the four sh/siRNAs (**Figure 4F**). These GO clusters are consistent with DISE being a form of mitotic catastrophe with cells unable to survive cell division (Hadjji et al., 2014) and suggest a general degradation of macromolecular complexes.

Toxic si/shRNAs target survival genes in their 3'UTR

To test whether the toxic shRNAs directly targeted genes through canonical RNAi, we subjected the two gene lists obtained from the RNA-Seq analysis (the cell lines treated with either shL3 or

shR6 at the 50 hour time point) to a Sylamer analysis (van Dongen, Abreu-Goodger, & Enright, 2008) designed to find an enrichment of miRNA/siRNA targeted sites in the 3'UTR of a list of genes ranked according to fold downregulation (**Figure 5A**). This analysis identified a strong enrichment of the cognate seed match for shL3 and shR6 in cells treated with either of these two shRNAs. The analyses with cells treated with shRNAs for 100 hours looked similar but less significant, suggesting early targeting by the shRNAs followed by secondary events (data not shown). Enrichment in 6mers and 8mers were both detected (only 8mers shown) in the 3'UTRs but not the ORF of the ranked genes (data not shown).

Interestingly, the seed matches detected by the Sylamer analysis were shifted by one nucleotide from the expected seed match based on the 21mer coded by the lentivirus. RNA-Seq analysis performed for the small RNA fraction confirmed in all cases (shScr and shL3 in pTIP, and shScr and shR6 in pLKO), the shRNAs in the cells were cleaved in a way resulting in the predominant formation of an siRNA shifted one nucleotide away from the shRNA loop region (black arrow heads in **Figure 5 - figure supplement 1A**). This allowed us to design toxic mature siRNAs based on the sequences of shL3 and shR6. These shRNA-to-siRNA converts were toxic to HeyA8 cells (**Figure 5 - figure supplement 1B**) confirming that the observed toxicity was not limited to the TRC shRNA platform, but based on a sequence-specific activity of the si/shRNAs.

The generalizability of the Sylamer results for shL3 and shR6 was tested with cells treated with either shL1 or siL3. In both cases, when the ranked RNA Seq data were subjected to a Sylamer analysis, the seed matches of the si/shRNA introduced were again significantly enriched in the 3'UTR of downregulated RNAs (**Figure 5 - figure supplement 2**). In none of the Sylamer analyses of the four data sets, did we see enrichment of seed matches in the 3'UTRs of downregulated RNAs that matched the passenger strand. In all cases, the only significantly enriched sequences matched the seed sequences in the guide strand of the si/shRNAs we introduced.

Our data suggested that DISE inducing si/shRNAs caused an early loss of survival genes, and at the same time downregulated RNAs through canonical RNAi targeting their 3'UTR. However, it was not clear whether the most highly downregulated survival genes were targeted in their 3'UTR by RNAi-active sequences. We determined as little as 6 nucleotides dictated whether an siRNA killed cancer cells (see **Figure 3H**). 10 of the 11 targeted genes identified in the RNA-Seq analysis described in **Figure 4A and 4B** contained multiple 6mer seed matches for either shL3 and/or shR6 (**Figure 5B**). It is therefore likely the two shRNAs, shL3 and shR6, killed cells

by targeting a network of genes enriched in critical survival genes through RNAi. The only gene without an shL3 or shR6 seed match was HIST1H1C. Interestingly, only four of the histones downregulated in cells after treatment with any of the four tested sh/siRNAs had a 3'UTR (underlined in **Figure 4E**) suggesting that most histones were not directly targeted by the sh/siRNAs.

Using multiplex qPCR, we tested whether other toxic shRNAs targeting either CD95 or CD95L also caused downregulation of some of the 11 genes silenced by shL3 and shR6. HeyA8 cells were transfected with the toxic siRNA siL3 (RNA harvested at 80 hours) or the toxic shRNAs shL1, shL3 or shR7 (RNA harvested at 100 hrs.). While shL1 did not have much of an effect on the expression of these genes, shR7 caused downregulation of 7 of 11 of the same genes targeted by shL3 even though the 6mer seed matches of the two shRNAs are very different (CTTTGT for shL3 and GGAGGA for shR7) (**Figure 4 - figure supplement 1D**).

To determine whether preferential targeting of survival genes was responsible for the death of the cells, we tested whether there was an association between the presence or absence of a predicted seed match in the 3'UTR for the si/shRNA introduced and whether a gene would be downregulated (>1.5 fold downregulated, $p < 0.05$) among survival genes using the Fisher's Exact test (**Figure 5C**). In almost all cases, this analysis revealed that survival genes containing a predicted seed match in their 3'UTR were statistically more likely to be downregulated than survival genes without such a motif. The analysis with shL1 treated cells did not reach statistical significance, likely due to the fact that this shRNA was found to be very toxic and the 100 hour time point may have been too late to observe evidence of significant targeting. This interpretation is supported by the observation that the significance for both shL3 and shR6 to target survival genes was higher at 50 hours when compared to the 100 hour time points (**Figure 5C**) and that the Sylamer analysis of the shL1 treated cells was less significant after 100 hours of treatment than any of the other Sylamer analyses (**Figure 5 - figure supplement 2**).

Now that we had established that the toxicity of the studied shRNAs involved targeting of survival genes rather than CD95 or CD95L we had to assume that when studying a larger set of shRNAs that the level of knockdown of the targeted genes and the toxicity were not strictly correlated. This was confirmed for the TRC shRNAs targeting the ORF or 3'UTR of CD95 in CD95 high expressing HeyA8 cells (**Figure 5 - figure supplement 3**). While some of the toxic shRNAs efficiently silenced CD95 (i.e. shR6 and shR2) others did not (i.e. shR5). In summary,

our analyses suggest that cells die by DISE due to an early and selective silencing of survival genes through targeting seed matches in their 3'UTR followed by the downregulation of histones.

Identification of toxic shRNAs in the CD95L and CD95 mRNAs

The majority of commercially available si- Dsi-, and shRNAs targeting either CD95 or CD95L were highly toxic to cancer cells. We therefore asked whether these two genes contained additional sequences with similar activity. To test all shRNAs derived from either CD95L or CD95, we synthesized all possible shRNAs, 21 nucleotides long, present in the ORF or the 3'UTR of either CD95L or CD95 starting with the first 21 nucleotides after the start codon, and then shifting the sequence by one nucleotide along the entire ORF and 3'UTR (**Figure 6A**). We also included shRNAs from a gene not expressed in mammalian cells and not expected to contain toxic sequences, Venus. All 4666 oligonucleotides (700 Venus, 825 CD95L ORF, 837 CD95L 3'UTR, 987 CD95 ORF, and 1317 CD95 3'UTR shRNAs) were cloned into the Tet-inducible pTIP vector (**Figure 6B**) as five individual pools. We first tested the activity of each individual pool to be toxic and to target the Venus sensor protein (fused to either the ORF of CD95 or CD95L). NB7 cells were again used because of their resistance to the Venus-CD95L sensor which was found to be slightly toxic to CD95 apoptosis competent cells. NB7-Venus-CD95L cells infected with the Venus-targeting shRNA pool showed some reduction in fluorescence when Dox was added, however, the shRNA pool derived from the CD95L ORF was much more active in knocking down Venus (**Figure 6 - figure supplement 1A**). No significant green fluorescence reduction was detected in cells after infection with the shRNA pool derived from the CD95L 3'UTR since the targeted sequences were not part of the sensor. Similar results were obtained when NB7-Venus-CD95 cells were infected with the Venus, CD95 ORF, and CD95 3'UTR targeting shRNA pools. To determine their ability to reduce cell growth (as a surrogate marker for toxicity), we infected NB7 parental cells with each of the five pools (parental cells were used for this experiment to avoid a possible sponge effect by expressing either CD95L or CD95 sequences that were part of the Venus sensors). Interestingly, the pool of 700 shRNAs derived from Venus did not cause any toxicity (**Figure 6 - figure supplement 1B**). In contrast, the pool of the shRNAs derived from CD95L significantly slowed down growth, while no toxicity was observed when cells were infected with the pool of shRNAs derived from the CD95L 3'UTR. In the case of CD95, both the shRNAs derived from the ORF and the 3'UTR showed some toxicity. However, the shRNAs derived from the 3'UTR caused greater toxicity

compared to those derived from the ORF. The data suggests that overall the shRNAs derived from the CD95L ORF and the CD95 3'UTR contain the most toxic sequences.

To determine the toxicity of each of the shRNAs in the pools, NB7 cells were infected with the libraries of shRNA viruses (MOI<1), and after puromycin selection cells were pooled 1:1:1 (Venus ORF/CD95L ORF/CD95L 3'UTR pools or Venus ORF/CD95 ORF/CD95 3'UTR pools) to allow for competition between shRNAs when Dox was added (**Figure 6B**). Cells were cultured for 9 days with and without Dox to allow for cell death to occur. To identify depleted shRNAs, shRNA barcodes were detected through next generation sequencing of PCR products to determine the relative abundance of each shRNA in three pools: 1) the cloned plasmid libraries, 2) cells after infection and culture for 9 days without Dox, and 3) cells infected and cultured with Dox for 9 days. A total of 71,168,032 reads were detected containing a complete sequence of one of the cloned shRNAs. Virtually all shRNAs were substantially represented in the cloned plasmids (**Table S3**). The shRNAs in the CD95L pool (comprised of the Venus, CD95L ORF, and CD95L 3'UTR subpools) and the CD95 pool (comprised of the Venus, CD95 ORF, and CD95 3'UTR subpools) were ranked from highest (most toxic) to lowest underrepresentation. During this and subsequent analyses, we noticed in many cases, Dox addition did cause a reduction of shRNAs, indicating an increase in toxicity; however, in other instances, infection alone and without the addition of Dox was toxic. This effect was likely due to the well-described leakiness of the Tet-on system (Pham, Moretti, Goodall, & Pitson, 2008), which we confirmed for shR6 in NB7 cells (**Figure 6 - figure supplement 2A**). To capture all toxic shRNAs, we therefore decided to split the analysis into two halves: 1) the changes in abundance after infection compared to the composition in the plasmid pool (infection -Dox) and 2) the changes in abundance after Dox addition compared to the infected -Dox cells (infection +Dox). In subsequent analyses shRNAs underrepresented after infection are either boxed (**Figure 6C**) or shown (**Figure 6D, 7B and Figure 7 - figure supplement 1B**) in blue and the ones underrepresented after Dox addition are either boxed or shown in orange. The results for all shRNAs are shown in **Figure 6 - figure supplement 2B**. Grey dots represent all shRNAs and red dots represent only the ones that were significantly underrepresented at least 5-fold. Interestingly, the highest abundance of downregulated shRNAs was found in the CD95L ORF and the CD95 3'UTR pools of shRNAs, which is consistent with the increased toxicity observed when NB7 cells were infected with either of these two pools individually (see **Figure 6 - figure supplement 1B**). The shRNAs of these two toxic pools were highly enriched in the

underrepresented shRNAs in the two pooled experiments (CD95L and CD95). Their toxicity was also evident when all shRNAs in each pool (2362 shRNAs in the CD95L and 3004 shRNAs in the CD95 pool) were ranked according to the highest fold downregulation (**Figure 6C**). The three subpools in each experiment are shown separately. Thus, again this analysis identified the ORF of CD95L and the 3'UTR of CD95 as the subpool in each analysis with the highest enrichment of underrepresented shRNAs (**Figure 6C**).

This analysis allowed us to describe the toxicity landscape of CD95L and CD95 ORFs and their 3'UTRs (**Figure 6D**). All shRNAs significantly underrepresented at least five-fold (red dots in **Figure 6 - figure supplement 2B**) are shown along the CD95L pool (**Figure 6D**, left) and the CD95 pool (**Figure 6D**, right) sequences. For both CD95L and CD95, toxic shRNAs localized into distinct clusters. The highest density of toxic sequences was found in the stretch of RNA that codes for the intracellular domain of CD95L (underlined in green in **Figure 6D**).

Predicting shRNA toxicity - the toxicity index (TI) and GC content

Our data suggest toxic shRNAs derived from either CD95L or CD95 kill cancer cells by targeting a network of genes critical for survival through canonical RNAi. Therefore, we wondered how many 8mer seed sequences derived from these toxic shRNAs would have corresponding seed matches in the 3'UTR of critical survival genes in the human genome. Would it be possible to predict with some certainty in an *in silico* analysis what shRNAs would be toxic to cells? To calculate such a hypothetical toxicity index, we used the ranked CRISPR data set (Wang et al., 2015) with 1883 survival genes (SGs) and 423 nonSGs. Based on our RNA-Seq analyses, we hypothesized the survival genes contained more putative seed matches for toxic shRNAs in their 3'UTRs than the nonsurvival genes (**Figure 7A**, left) and that the number of seed matches in the 3'UTRs of survival genes divided by the number of seed matches in the 3'UTR of nonsurvival genes would, to some extent, predict toxicity of an si/shRNA (**Figure 7A**, right).

To establish a Toxicity Index (TI) for each shRNA, we first gathered 3'UTR sequences for 1846 of the survival genes and 416 of the nonsurvival genes. We then generated a list containing a normalized ratio of occurrences of every possible 8mer seed match in the 3'UTRs of the survival and non-survival gene groups. This resulted in a ratio for each of the 65,536 possible 8mer combinations (**Table S4**), the TI. We then assigned to each of the 4666 shRNAs in our screen its TI, and ranked each pool within the two experiments of our screen according to the

highest TI (red stippled lines in **Figure 7B**). We then further separated the shRNAs into two groups: those that were toxic just after infection and those toxic after addition of Dox (**Figure 7B, Table S5**). In each ranked list, we could now assess whether the experimentally determined toxicity of shRNAs correlated with the *in silico* predicted TI. Remarkably, the highest enrichment of toxic shRNAs was found amongst those with higher TI for the subpool of shRNAs targeting the CD95L ORF followed by shRNAs in the subpool targeting the CD95 3'UTR. To confirm the significance of this finding, we repeated the analysis 10,000 times by randomly assigning 8mers and their associated TIs to the two shRNA pools and again sorted the data from highest to lowest TI. The reported p-values were calculated based on these permuted datasets using Mann-Whitney U tests.

We noticed that survival genes tend to be more highly expressed than nonsurvival genes (data not shown). To address the question whether toxic si/shRNAs only target survival genes or all genes that are highly expressed, we recalculated the TI based on a set of 850 highly expressed and expression matched survival and nonsurvival genes (**Figure 7 - figure supplement 1A**). This alternative TI tracked slightly less well with the toxic shRNAs we identified, but the enrichment of toxic shRNAs towards the top of the list ranked according to the new TI was still statistically significant (**Figure 7 - figure supplement 1B**). This analysis demonstrates survival genes contain more seed matches for toxic shRNAs in their 3'UTR than nonsurvival genes regardless of the expression level. This suggests, to a certain extent, it is possible to predict the experimental toxicity of shRNAs based on the *in silico* calculated TI.

Our data suggest DISE results from a sequence-specific off-target activity that depends on the presence of certain seed matches in the 3'UTR of survival genes. Thus, DISE inducing RISC associated small RNAs behave in manner similar to miRNAs. This raised the question whether these seed matches have special properties. While we did not find a sequence motif that was present in all toxic si/shRNAs, we did find that sequence composition, specifically GC content, which has been reported to affect the specificity of shRNAs (Gu et al., 2014; Ui-Tei et al., 2004), correlated with the toxicity of shRNAs. When the GC content of the 6mer seed sequences of all underrepresented shRNAs detected in the shRNA screen across the CD95L ORF was plotted we found a significant correlation between the GC content and higher toxicity (indicated by underrepresentation) (**Figure 7C and 7D**). This correlation was even more pronounced when plotting GC content versus the 6mer toxicity index (**Table S4**) (**Figure 7E**). While not an absolute requirement, higher GC content made shRNAs more toxic, consistent with reports

519 demonstrating that shRNAs with high GC content in the seed region showed decreased on-
 520 target and increased off-target activity (Gu et al., 2014; Ui-Tei et al., 2004). In summary, our
 521 data suggest that si- and/or shRNAs with certain seed sequences are toxic to cancer cells by
 522 targeting critical survival genes through an RNAi mechanism independent of both Drosha and
 523 Dicer. Furthermore, the data suggest high miRNA content, presumably through competing for
 524 occupancy in the RISC, might render cells less sensitive to DISE.
 525

Discussion

Most current uses of RNAi are aimed toward highly specific silencing with little OTE. In fact, OTEs represent one of the largest impediments to the use of RNAi in phenotypic screening applications. We now demonstrate DISE is a unique form of OTE that results in the simultaneous activation of multiple cell death pathways in cancer cells. The discovery that DISE involves loss of multiple survival genes now provides an explanation for the unique properties we described for this form of cell death, especially the observation that cancer cells have a hard time developing resistance to this cell death mechanism (Hadji et al., 2014; Murmann et al., 2017).

DISE represents a specific form of RNAi OTE

There are a number of rules that have been elucidated for designing si/shRNAs (Bramsen et al., 2009) to avoid undesired effects such as OTE (Petri & Meister, 2013), general toxicity due to the presence of toxic sequence motifs (Fedorov et al., 2006; Petri & Meister, 2013), poisoning/saturating of the RISC (Grimm et al., 2006), or evocation of an IFN response (Marques & Williams, 2005). The following arguments and evidence support our prediction that DISE is a manifestation of a novel, functionally important, conserved mechanism of genome regulation, and not the result of one of the above-mentioned effects:

- 1) The sheer number of toxic shRNAs embedded in CD95L or CD95. A number of genome-wide shRNA and siRNA lethality screens have revealed that 2-5% of shRNAs targeting human genes are toxic to cells. We recently reported in 12 independent arrayed shRNA lethality screens the identification of 651 genes out of about 18,000 targeted genes that are critical for the survival of 8 different cancer cell lines (Hadji et al., 2014). Many of the genes targeted by these shRNAs were actually established survival genes (as discussed in (Hadji et al., 2014)). That means that the number of shRNAs that are toxic due to a possible OTE or general toxicity would be expected to be very small. In contrast, we found that >80% of the shRNAs and siRNAs that were designed to target either CD95 or CD95L exhibited toxicity in multiple cell lines. Consistent with our data analysis a parallel genome-scale loss of function screen confirmed that the majority of the tested shRNAs derived from either CD95L and CD95 were toxic to a majority of the tested 216 cell lines when used as a pooled library (Cowley et al., 2014). These also included a number of hematopoietic cell lines suggesting that the DISE effect is not limited to solid cancers. Interestingly, in this study the authors did not consider the data on most of the CD95L and CD95 targeting shRNAs to be significant as they received

- a low consistency score. A high consistency score predicts the observed phenotype (cell death or growth reduction in this case) is caused by knocking down the targeted gene (Shao et al., 2013). However, we have demonstrated here that the toxicity of an shRNA is solely dependent on its seed and the transcriptome of the treated cells. Therefore, the results of every shRNA should be considered individually as far as the DISE inducing effect is concerned.
- 2) High concentrations of siRNAs can saturate the RISC, preventing the access of crucial endogenous miRNAs (Khan et al., 2009). We have demonstrated that, in general, 5 nM of CD95L-derived siRNAs are sufficient to kill cancer cells. We have even seen very efficient cell death with as little as 1 nM of siRNA (see **Figure 2I** and **Figure 1 - figure supplement 2E**). It is therefore unlikely we are poisoning the RISC. It has been reported that in siRNA overexpression experiments, changes in mRNA expression can be caused by blocked access of endogenous miRNAs to the RISC, such as the highly expressed miRNA family, let-7 (Khan et al., 2009). However, we can exclude such an effect in our analysis, as there was no significant enrichment (or depletion) of the let-7 seed match motif (or that of any other miRNA) in our analyses (black lines in **Figure 5A**).
 - 3) No IFN response was observed. We have performed multiple RNA-Seq and gene array analyses of cells in which DISE was induced by multiple si/shRNAs targeting CD95 or CD95L. In none of these analyses did we detect an increase in any of the known IFN response genes (Schoggins et al., 2011) (data not shown). In addition, we demonstrated the latest generation of Dicer optimized 27mer DsiRNAs that do not elicit an IFN response (D. H. Kim et al., 2005) and the shRNAs expressed from within the cells shown to have low IFN triggering activity (Robbins et al., 2006) have the same toxic activities as the standard 21mer siRNAs (see **Figure 1 - figure supplement 1A and 1B**).
 - 4) Mutation of just one position destroys activity. A major argument against DISE toxicity being caused by overloading the RISC, an IFN response or the presence of known toxic sequences, lies in the analysis of the chimeras we generated between siL3 and a non-toxic scrambled oligonucleotide (see **Figure 3H**). This analysis demonstrated that the seed match positions of siL3 are critical for its toxicity. In fact, just replacing one nucleotide in a critical position in the center of the seed match almost completely abolished toxicity of the siRNA.

What are the requirements for an si/shRNA to induce DISE?

Our data provide strong evidence that the toxicity observed is a sequence-specific event caused by seed matches present in the targets of the toxic si/shRNAs rather than by a toxic motif enriched in all toxic si/shRNAs (i.e. the UGGC motif described before (Fedorov et al., 2006)). We did find a correlation between the toxicity of shRNAs (both predicted by the TI and experimentally determined in the shRNA screen) and the GC content in their seed region. While this correlation was significant, it was not a requirement as some of the most toxic si- and shRNAs had a low 8mer seed GC content (shL3, 25%; shR6, 25%; siL3, 37.5%). Our data suggests that survival genes may contain different types of seed matches (based on base composition or sequence) when compared to nonsurvival genes. Such a distinction has indeed been described before (Stark, Brennecke, Bushati, Russell, & Cohen, 2005). In a study in *Drosophila*, it was determined that survival genes are depleted of seed matches targeted by highly expressed miRNAs. These authors concluded that evolution must have selected against the presence of seed matches for highly expressed miRNAs in the 3'UTR of survival genes. It is therefore not surprising that a gene ontology (GO) analysis of all miRNA targets (the "targets") in this study described these genes as being involved in development and differentiation (Stark et al., 2005). In contrast, genes not targeted by miRNAs (the "antitargets") grouped in GO clusters that were consistent with cell survival (Stark et al., 2005). A similar phenomenon was also shown in mammalian cells; genes with fewer miRNA target sites, as predicted by Targetscan, contained distinct enriched GO terms from those enriched in genes with many predicted target sites. The genes with fewer sites were enriched in GO terms like ribosomal subunits and respiratory chain, whereas target-heavy genes were more enriched in regulatory-related GO terms (Zare, Khodursky, & Sartorelli, 2014). It is possible the DISE inducing si/shRNAs carry seed sequences that preferentially target seed matches present in the 3'UTRs of the "anti-targets". However, as our data on the miR-30 based shRNAs suggest, DISE-inducing shRNAs must be expressed at a certain level to be toxic.

DISE is caused by loading of the guide strand of toxic si/shRNAs into the RISC

Part of our data was generated using a widely used first generation stem loop shRNA platform, the TRC library. The TRC shRNAs have recently been found to be prone to cause OTE. Gu *et al.* showed that the loop design of this system results in imprecise Dicer cleavage and, consequently, the production of different mature small-RNA species that increase passenger loading, one major source of OTE (Gu et al., 2012). More recently it was reported that most guide RNAs derived

from the TRC hairpin were shifted by 4 nt 3' of the expected 5' start site (Watanabe, Cuellar, & Haley, 2016). While we did see a shift in processing of these stem loop shRNAs, we did not see such a high level of imprecision in the cleavage of our toxic shRNAs. In fact, 99.4% of the shR6 guide RNAs started at the same nucleotide position (**Figure 5 - figure supplement 1A**). The majority of the processing of both our pTIP and pLKO-based shRNAs was shifted by one nucleotide (**Figure 5 - figure supplement 1A**). This shift was consistent with the defined seed matches that were detected in the Sylamer analyses. In general, one major seed match was detected with one other minor species (this was less obvious for shL1, **Figure 5 - figure supplement 2**). Furthermore, all four Sylamer analyses only detected enrichments in the 3'UTR of downregulated mRNAs that were consistent with only the guide strand targeting the mRNA and not the passenger strand. In all cases, including in cells transfected with the siRNA siL3, the primary enriched sequence motifs were either 7, or 8mers present in the 3'UTR of the targeted mRNAs.

DISE has features of the RNAi OTE previously reported

Our data on DISE are consistent with a number of properties of RNAi OTE that have previously been reported. Similar to DISE, OTE mediated silencing requires a 6/7nt seed sequence of complementarity (Birmingham et al., 2006; Jackson et al., 2006; Lin et al., 2005) and it targets mRNAs in the 3'UTR (Birmingham et al., 2006). Our data on shRNAs, siRNAs, and DsiRNAs suggest that DISE is not limited to one platform and requires sequence specific targeting. This conclusion is also consistent with a previous report that suggested that sequence-dependent off-target transcript regulation is independent of the delivery method (Jackson et al., 2006). The authors found the same enrichment of 6mers and 7mers in 3'UTRs of targeted mRNAs for siRNAs and shRNAs (Jackson et al., 2006).

The role of Dicer in DISE

We previously reported that Dicer^{Exo5^{-/-}} HCT116 cells (with deleted Exon 5) were at least as sensitive to induction of DISE (by either shL3 or shR6) than wt cells suggesting that Dicer deficient cells could be killed by DISE (Hadji et al., 2014). It has been reported that these Dicer deficient cells are hypomorphs (Ting et al., 2008) and indeed, we detected low residual Dicer expression by Western blotting (Hadji et al., 2014). We have now revisited this issue with HCT116 cells rendered completely deficient for Dicer using CRISPR/Cas9 gene editing (Y. K.

Kim et al., 2016). The fact that these Dicer^{-/-} cells were now completely resistant to the toxic effects of shL3 or shR6 demonstrates the complete absence of Dicer protein and activity. Similar to the Drosha^{-/-} cells, in the absence of mature miRNAs, which seem to attenuate DISE, Dicer^{-/-} cells are hypersensitive to DISE induced by siRNAs.

Open questions regarding the relevance of DISE

We are proposing an entirely new concept of killing cancer cells that is based on the toxicity of CD95 and CD95L derived small RNAs. Naturally, there are many open questions such as:

1) Is DISE part of an anti-cancer mechanism? We are proposing that DISE kills cancer cells in a way that they usually cannot escape from. We have not found a way to block cancer cells from dying by DISE. We provide strong evidence to suggest this is due to the simultaneous targeting of multiple survival genes that result in the activation of multiple cell death pathways. It will be difficult to prove cells are dying due to the preferential targeting of survival genes. It may never be possible to express multiple siRNA resistant survival genes at the same time at physiological levels to render cancer cells resistant to the action of countless small RNAs. This prediction alone makes DISE a promising new strategy to kill cancer cells.

2) Does CD95L induce DISE *in vivo*? We recently found that overexpression of the CD95L ORF is toxic to cancer cells and that this kills cancer cells in a manner very similar to DISE induction (unpublished data). We and others have noticed upregulation of CD95L in multiple stress related conditions such as treatment with chemotherapy ((Friesen, Fulda, & Debatin, 1999) and data not shown). While the amount of CD95L RNA and the level of upregulation alone may not be enough to induce DISE, it could result from the combined expression of multiple RNAs that when generated kill cells by DISE. We view CD95L as just one of many RNAs that have this activity.

3) Are there other genes in the human genome containing toxic seed sequences? We recently identified other genes in the genome that contain DISE inducing shRNAs (Patel & Peter, 2017). It is therefore possible that when cells are subjected to genotoxic or oncogenic stress that they generate numerous small RNAs that can be taken up by the RISC and in combination execute DISE. Hence, our analysis of CD95/CD95L will likely be applicable to other genes.

A model for why DISE preferentially kills cancer cells

We interpret the hypersensitivity of both Drosha^{-/-} and Dicer^{-/-} cells to DISE in the following

way: Most of the small RNAs in the cells that are loaded into the RISC are miRNAs. Using AGO pull-down experiments we determined 98.4% of AGO associated RNAs in HCT116 cells to be miRNAs (99.3% in HeyA8 cells, data not shown). It was recently reported that Drosha^{-/-} cells showed a reduction of miRNA content from roughly 70-80% to 5-6%, and Dicer^{-/-} cells showed a reduction down to 14-21% (Y. K. Kim et al., 2016). Since neither Drosha^{-/-} nor Dicer^{-/-} cells express reduced AGO2 protein levels (see subset **Figure 3E**), it is reasonable to assume that their RISC can take up many more of the toxic DISE inducing RNAs than the RISC in wt cells explaining the super toxicity of both DISE inducing si/shRNAs and CD95L mRNAs in these cells.

We previously showed expression of either shL3 and shR6 induced DISE in immortalized normal ovarian fibroblasts much more efficiently than in matching nonimmortalized cells (Hadji et al., 2014), suggesting that this form of cell death preferentially affects transformed cells. Our data now provide an interesting model to explain the higher sensitivity of cancer cells to DISE when compared to normal cells. It is well documented that cancer cells in general have global downregulation of miRNAs when compared to normal tissues (Lu et al., 2005). This might free up the RISC for DISE inducing RNAs and would imply that miRNAs may protect normal cells from DISE.

Overall our data allow us to predict that any small RNA with DISE inducing RNAi activity that does not require Dicer processing can kill cancer cells regardless of Dicer or Drosha status. In fact, in an accompanying manuscript we demonstrate that DISE can be triggered *in vivo* to treat ovarian cancer in mouse xenografts by delivering CD95L-derived siRNAs using nanoparticles (Murmann et al., 2017). No toxicity was observed in the treated mice. These data suggest that it might be possible to develop a novel form of cancer therapy based on the DISE OTE mechanism.

Materials and methods

Reagents and antibodies

Primary antibodies for Western blot: anti-β-actin antibody (Santa Cruz #sc-47778), anti-human CD95L (BD Biosciences #556387), and anti-human CD95 (Santa Cruz #sc-715), anti-human AGO2 (Abcam #AB186733), anti-human Drosha (Cell Signaling #3364), and anti-Dicer (Cell Signaling #3363). Secondary antibodies for Western blot: Goat anti-rabbit; IgG-HRP (Southern Biotech #SB-4030-05 and Cell Signaling #7074) and Goat anti-mouse; IgG1-HRP; (Southern

BioTech #1070-05). Conjugated antibody isotype control for CD95 surface staining were FITC-mouse anti-human CD95 (BD Biosciences #556640) and FITC-mouse IgG1, κ isotype control (BD Biosciences #551954). Recombinant soluble S2 CD95L and leucine-zipper tagged (Lz)CD95L were described before (Algeciras-Schimmich et al., 2003). Reagents used: propidium iodide (Sigma-Aldrich #P4864), puromycin (Sigma-Aldrich #P9620), G418 (Affymetrix #11379), zVAD-fmk (Sigma-Aldrich #V116, used at 20 μ M), doxycycline (Dox) (Sigma-Aldrich #9891), Lipofectamine 2000 (ThermoFisher Scientific #11668027), and Lipofectamine RNAiMAX (ThermoFisher Scientific #13778150).

Cell lines

The ovarian cancer cell line HeyA8, the neuroblastoma cell line NB7, and the breast cancer cell line MCF-7 were grown in RPMI 1640 medium (Cellgro #10-040-CM), 10% heat-inactivated FBS (Sigma-Aldrich), 1% L-glutamine (Mediatech Inc), and 1% penicillin/streptomycin (Mediatech Inc). The human embryonic kidney cell line 293T and Phoenix AMPHO cells were cultured in DMEM (Cellgro #10-013-CM), 10% heat-inactivated FBS, 1% L-Glutamine, and 1% penicillin/streptomycin.

HCT116 Drosha^{-/-} and Dicer^{-/-} cells were generated by Narry Kim (Y. K. Kim et al., 2016). HCT116 parental (cat#HC19023), a Drosha^{-/-} clone (clone #40, cat#HC19020) and two Dicer^{-/-} clones (clone #43, cat#HC19023 and clone #45, cat#HC19024) were purchased from Korean Collection for Type Cultures (KCTC). All HCT116 cells were cultured in McCoy's medium (ATCC, cat#30-2007), 10% heat-inactivated FBS, 1% L-Glutamine, and 1% penicillin/streptomycin. All cell lines were authenticated using STR profiling and tested monthly for mycoplasma using Plasmotest (Invitrogen).

All lentiviruses were generated in 293T cells using pCMV-dR8.9 and pMD.G packaging plasmids. Retroviruses were generated in Phoenix AMPHO cells using the VSVg packaging plasmid.

NB7 cells overexpressing wild type and mutant CD95L cDNAs used in **Figure 1C and D** were generated by infecting cells seeded at 50,000 to 100,000 cells per well on a 6-well plate with empty pLenti, pLenti-CD95L-WT, pLenti-CD95L-L1MUT, and pLenti-CD95L-L3MUT (described below) with 8 μ g/ml polybrene. Selection was done with 3 μ g/ml puromycin for at least 48 hours.

#R0537) and SphI-HF (NEB #R3182) were used to digest both the pTIP-shR6 vector (to excise the shR6 insert) and the double-stranded shRNA DNA cassette insert followed by ligation with T4 DNA ligase. The template oligos were purchased from IDT. The poly-N represents the two 21bp sequences that transcribe for the sense (*N*) and antisense (*n*) shRNA.

miR-30 based shRNAs were generated by The Gene Editing & Screening Core, at Memorial Sloan Kettering, NY, by converting the 21mers expressed in the pLKO and pTIP vectors into 22mers followed by cloning into the Dox-inducible LT3REPIR vector as described (Dow et al., 2012). A vector expressing an shRNA against Renilla luciferase was used as control (Dow et al., 2012).

CRISPR deletions

We identified two gRNAs that target upstream and downstream of the site to be deleted. These gRNAs were expected to result in the deletion of a DNA piece just large enough to remove the target site. The CRISPR gRNA scaffold gene blocks were from IDT and consisted of the DNA sequence 5'-*TGTACAAAAAGCAGGCTTTAAAGGAACCAATTCAGTCGACTGGATCCGGTACCAAGGTCGGGCAGGAAGAGGGCCTATTTCCCATGATTCCTTCATATTTGCATATACGATACAAGGCTGTTAGAGAGATAATTAGAATTAATTTGACTGTAAACACAAAGATATTAGTACA* AAATACGTGACGTAGAAAGTAATAATTTCTTGGGTAGTTTGCAGTTTTAAATTATGTTTTAA AATGGACTATCATATGCTTACCGTAACTTGAAAGTATTTGATTTCTTGGCTTTATATATCTT GTGGAAAGGACGAAACACCGNNNNNNNNNNNNNNNNNNNGTTTTAGAGCTAGAAATAGC AAGTTAAATAAGGCTAGTCCGTTATCAACTTGAAAAAGTGGCACCGAGTCGGTGCTTTTTT TCTAGACCCAGCTTTCTTGTACAAAGTTGGCATT-3' (Mali et al., 2013); The poly- NNNNNNNNNNNNNNNNNNNNNN represents the 19nt target sequence. The two 19nt target sequences for excision of the shL3 site (Δ 41 deletion) were 5'-*CCTTGTGATCAATGAAACT*-3' (gRNA #1) and 5'-*GTTGTTGCAAGATTGACCC*-3' (gRNA #2). The two target sequences for the Δ 227 deletion of the shR6 site were 5'-*GCACTTGGTATTCTGGGTC*-3' and 5'- *TGTTTGCTCATTTAAACAC*-3'. The two target sequences for Δ 64 deletion of the siL3 site were 5'-*TAAACCGTTTGCTGGGGC*-3' and 5'-*TATCCCAGATCTACTGGG*-3'. Target sequences were identified using the CRISPR gRNA algorithm found at <http://crispr.mit.edu/>; only gRNAs with scores over 50 were used. These 6 gene blocks were sub-cloned into the pSC-B-amp/kan plasmid using the StrataClone Blunt PCR Cloning kit (Agilent Technologies #240207).

The target sites of siL3, shL3, and shR6 were homozygously deleted from target cells by co-transfecting Cas9 plasmid with each corresponding pair of pSC-B-gRNA plasmids. Briefly, 400,000 cells were seeded per well on a 6-well plate the day prior to transfection. Each well was transfected with 940 ng of Cas9-GFP plasmid (pMJ920) (Jinek et al., 2013) and 450 ng of each pSC-B-gRNA plasmid using Lipofectamine 2000. Media was replaced next day. One to two days later, cells were sorted for the top 50% population with the highest green fluorescence. Those cells were cultured for an additional week to let them recover. The cells were then sorted by FACS (BD FACSAria SORP system) directly into 96-well plates containing a 1:1 ratio of fresh media:conditioned media for single cell cloning. Approximately two to three weeks later, single cell clones were expanded and subjected to genotyping. PCR using both a primer pair that flanked the region to be deleted and another pair containing one flanking primer and one internal primer was used to screen clones for homozygous deletion. For detection of the $\Delta 41$ deletion of the shL3 site, the flanking external primers were 5'-TCTGGAATGGGAAGACACCT-3' (Fr primer) and 5'-CCTCCATCATCACCAGATCC-3' (Rev primer), and the internal Rev primer was 5'-ATATACAAAGTACAGCCCAGT-3'. For detection of the $\Delta 227$ deletion of the shR6 site, the flanking external primers were 5'-GGTGTCATGCTGTGACTGTTG-3' (Fr primer) and 5'-TTTAGCTTAAGTGGCCAGCAA-3' (Rev primer), and the internal Rev primer was 5'-AAGTTGGTTTACATCTGCAC-3'. For detection of the $\Delta 64$ deletion of the siL3 site, the flanking external primers were 5'-CTTGAGCAGTCAGCAACAGG-3' (Fr primer) and 5'-CAGAGGTTGGACAGGGAAGA-3' (Rev primer), and the internal Rev primer was 5'-ATATGGGTAATTGAAGGGCTG-3'. After screening the clones, Sanger sequencing was performed to confirm that the proper deletion had occurred. Three clones were pooled for each si/shRNA target site deletion except for HeyA8 Δ shR6 for which only clone #11 showed homozygous deletion of the shR6 site; clones #1 and 2 were not complete shR6 deletion mutants, but frame-shift mutations did occur in each allele (as in clone #11) making them CD95 knockout clones as depicted in **Figure 2 - figure supplement 1A and B**.

Knockdown with pLKO lentiviruses

Cells were infected with the following pLKO.2 MISSION Lentiviral Transduction Particles (Sigma): pLKO.2-puro non-targeting (scramble) shRNA particles (#SHC002V), 8 non-overlapping shRNAs against human CD95L mRNA (accession number #NM_000639), TRCN0000058998 (shL1: GCATCATCTTTGGAGAAGCAA), TRCN0000058999 (shL2:

843 CCCATTAAACAGGCAAGTCCA), TRCN0000059000 (shL3:
844 ACTGGGCTGTACTTTGTATAT), TRCN0000059001 (shL4:
845 GCAGTGTTCATCTTACCAGT), TRCN0000059002 (shL5:
846 CTGTGTCTCCTTGTGATGTTT), TRCN0000372231 (shL6:
847 TGAGCTCTCTCTGGTCAATTT), TRCN0000372232 (shL2': TAGCTCCTCAACTC
848 ACCTAAT), and TRCN0000372175 (shL5': GACTAGAGGCTTGCATAATAA), and 9 non-
849 overlapping shRNAs against human CD95 mRNA (accession number NM_000043),
850 TRCN0000218492 (shR2: CTATCATCCTCAAGGACATTA), TRCN00000 38695 (shR5:
851 GTTGCTAGATTATCGTCCAAA), TRCN0000038696 (shR6: GTGCAGA
852 TGTAACCAAACTT), TRCN0000038697 (shR7: CCTGAAACAGTGGCAATAAAT),
853 TRCN0000038698 (shR8: GCAAAGAGGAAGGATCCAGAT), TRCN0000265627 (shR27':
854 TTTTACTGGGTACATTTTATC), TRCN0000255406 (shR6': CCCTTGTGTTT
855 GGAATTATAA), TRCN0000255407 (shR7': TTAAATTATAATGTTTGACTA), and
856 TRCN0000255408 (shR8': ATATCTTTGAAAGTTTGTATT). Infection was carried out
857 according to the manufacturer's protocol. In brief, 50,000 to 100,000 cells seeded the day before
858 in a 6-well plate were infected with each lentivirus at an M.O.I of 3 in the presence of 8 µg/ml
859 polybrene overnight. Media change was done the next day, followed by selection with 3 µg/ml
860 puromycin 24 hours later. Selection was done for at least 48 hours until puromycin killed the
861 non-infected control cells. For infection of NB7 cells over-expressing pLenti-CD95L cDNAs
862 with pLKO lentiviral particles as in **Figure 1C and D**, cells were seeded at 5,000 per well on a
863 24-well plate and infected with an M.O.I. of 20 to ensure complete infection. For infection of
864 MCF-7 cells over-expressing pLNCX2-CD95 cDNAs with pLKO lentiviruses as in **Figure 1G**,
865 cells were seeded at 7,000 per well on a 24-well plate and infected at an M.O.I. of three. 3 µg/ml
866 puromycin was added 48 hours after infection. For infection of HCT116, Drosha^{-/-}, and Dicer^{-/-}
867 cells in **Figure 3E**, cells were seeded at 100,000 per well in a 24-well plate and infected at an
868 M.O.I of three. 3 µg/ml puromycin was added 48 hours after infection.

869

870 **Knockdown with pTIP-shRNA viruses**

871 Cells were plated at 50,000 to 100,000 cells per well in a 6-well plate. Cells were infected with
872 lentivirus generated in 293T cells from the desired pTIP-shRNA vector in the presence of 8
873 µg/ml Polybrene. Media was replaced 24 hours later. Selection was done 48 hours after infection
874 with 3 µg/ml puromycin. Induction of shRNA expression was achieved by adding 100 ng/ml

Dox to the media. For infection with the LT3REPIR-shRNA viruses cells were plated and infected as described above for pTIP-shRNA viruses. After selection with 3 µg/ml puromycin was complete, they were plated in 96-well plates and the shRNA expression was induced by adding Dox (100 ng/ml) to the media. The cell confluency over time was measured using Incucyte.

Transfection with short oligonucleotides

siRNAs were either purchased from Dharmacon (*Figures 2I and 4D, Figure 1 - figure supplement 1A, Figure 5 - supplement 2*) or synthesized by IDT (*Figure 3A*) as sense and antisense RNA (or DNA for *Figure 3B, Figure 5 - supplement 1B,*) oligos and annealed. The sense RNA oligonucleotides had 3' 2 deoxy-T overhangs. The antisense RNA oligos were phosphorylated at the 5' end and had 3' 2 deoxy-A overhangs. siRNAs targeting CD95L (and controls) were as follows: siRNA (Scr, sense: UGGUUUACAUGUUGUGUGA), siL1 (sense: UACCAGUGCUGAUCAUUUA), siL2 (sense: CAACGUAUCUGAGCUCUCU), siL3 (sense: GCCCUUCAAUUACCCAUAU), siL4 (sense: GGAAAGUGGCCCAUUUAAC), and siL3MUT (sense: GGACUUCAACUAGACAUCU). The siL3 DNA oligos (sense: GCCCTTCAATTACCCATAT) and Scr DNA oligos (sense: TGGTTTACATGTTGTGTGA) were used in *Figure 3B*. Blunt siL3 and siScr RNA oligos without the deoxynucleotide overhangs as well as siL2 and siL3 RNA oligos with Cy5-labelled 5' or 3' ends (IDT) were used in *Figure 3C*. DsiRNA used in *Figure 1 - figure supplement 1* were Dsi13.X (sense RNA oligo: CAGGACUGAG AAGAAGUAAAACCDGdT, antisense RNA oligo: ACGGUUUUACUUCUUCUCAGUCCUGUA), DsiL3 (sense RNA oligo: CAGCCCUUCAAUUACCCAUAUCCdCdC, antisense RNA oligo: GGGGAUAUGGGUAAUUGAAGGGCUGCU), Dsi-13.2 (sense RNA oligo: AUCUU ACCAGUGCUGAUCAUUUAdTdA, antisense RNA oligo: UAUAAAUGAUCAGCACUGGUAAGAUUG), Dsi-13.3 (sense RNA oligo: AAAGUAUACUCCGGGGUCAAUUCdTdT, antisense RNA oligo: AAGAUUGACCCCGGAAGUAUACUUUGG), Dsi-13.9 (sense RNA oligo: CUUCCGGGGUCAAUUCUUGCAACAdAdC, antisense RNA oligo: GUUGUUGC AAGAUUGACCCCGGAAGUA), and a non-targeting DsiRNA control Dsi-NC1 (Sense:5'- CGUUAUUCGCGUAUAAUACGCGUdAdT, antisense:5'- AUACGCGUAUUAUACGCGAUUAACGAC, IDT #51-01-14-03). Predesigned siRNA

SmartPools targeting the 11 downregulated genes were obtained from Dharmacon and used in **Figure 4C** and **Figure 4 - figure supplement 2B and 2C**. Each siRNA SmartPool consisted of 4 siRNAs with On-Target^{plus} modification. The following SmartPools were used: L-014208-02 (NUCKS1); L-012212-00 (CAPZA1); L-018339-00 (CCT3); L-013615-00 (FSTL1); L-011548-00 (FUBP1); L-017242-00 (GNB1); L-014597-01 (NAA50); L-020893-01 (PRELID3B); L-019719-02 (SNRPE); L-003941-00 (TFRC); L-006630-00 (HIST1H1C). On-Target^{plus} non-targeting control pool (D-001810-10) was used as negative control. Transfection efficiency was assessed by transfecting cells with siGLO Red (Dharmacon) followed by FACS analysis.

HeyA8 cells (and modified cells derived from parental HeyA8 cells) were seeded at 750 cells per well on a 96-well plate one day before transfection. Cells were transfected using 0.1 µl of Lipofectamine RNAiMAX reagent per well. HCT116 cells (and modified cells derived from parental HCT116 cells) were seeded at 4000 cells per well on a 96-well plate one day before transfection. 0.2 µl of Lipofectamine RNAiMAX was used for transfection. Media was changed the day after transfection.

Soluble CD95L protein rescue experiments

NB7 cells were seeded at 500 cells per well in a 96-well plate. Next day, cells were infected with the scrambled pLKO lentiviruses or pLKO-shL1 lentiviruses at an M.O.I. of 20 (to achieve 100% transduction efficiency under conditions omitting the puromycin selection step) in the presence of 8 µg/ml polybrene and 100 ng/ml of S2 CD95L or LzCD95L for 16 hrs. Media was replaced the next day with media containing varying concentrations of recombinant CD95L.

Real-time PCR

Total RNA was extracted and purified using QIAzol Lysis reagent (QIAGEN) and the miRNeasy kit (QIAGEN). 200 ng of total RNA was used to generate cDNA using the High-Capacity cDNA reverse Transcription kit (Applied Biosystems #4368814). cDNA was quantified using Taqman Gene expression master mix (ThermoFisher Scientific #4369016) with specific primers from ThermoFisher Scientific for GAPDH (Hs00266705_g1), human CD95 for **Figure 5 -supplement 3** (Hs00163653_m1), human CD95 3'UTR in **Figure 2F** (custom probe, Fr primer: GGCTAACCCCACTCTATGAATCAAT, Rev primer: GGCCTGCCTGTTTCAGTAACT, Probe: CCTTTTGCTGAAATATC), human CD95L (Hs00181226_g1 and Hs00181225_m1), the shL3 target site in CD95L in **Figure 2D** (custom probe, Fr primer: GGTGGCCTTGATCAATGAAA,

Rev primer: *GCAAGATTGACCCCGGAAG TATA*, Probe: *CTGGGCTGTACTTTGTATATT*),
and downstream of the shL3 site in **Figure 2D** (custom probe, Fr primer:
CCCCAGGATCTGGTGATGATG, Rev primer: *ACTGCCCCCAGGTAGCT*, Probe:
CCCACATCTGCCCAGTAGT).

To perform arrayed real-time PCR (**Figure 4 - figure supplement 1**), total RNA was
extracted and used to make cDNA as described for standard real-time PCR. For Taqman Low
Density Array (TLDA) profiling, custom-designed 384-well TLDA cards (Applied Biosystems
#43422489) were used and processed according to the manufacturer's instructions. Briefly, 50 µl
cDNA from each sample (200 ng total input RNA) was combined with 50 µl TaqMan Universal
PCR Master Mix (Applied Biosystems) and hence a total volume of 100 µl of each sample was
loaded into each of the 8 sample loading ports on the TLDA cards that were preloaded with
assays from ThermoFisher Scientific for human GAPDH control (Hs99999905_m1) and for
detection of ATP13A3 (Hs00225950_m1), CAPZA1 (Hs00855355_g1), CCT3
(Hs00195623_m1), FSTL1 (Hs00907496_m1), FUPB1 (Hs00900762_m1), GNB1
(Hs00929799_m1), HISTH1C (Hs00271185_s1), NAA50 (Hs00363889_m1), NUCKS1
(Hs01068059_g1), PRELID3B (Hs00429845_m1), SNRPE (Hs01635040_s1), and TFRC
(Hs00951083_m1) after the cards reached room temperature. The PCR reactions were performed
using Quantstudio 7 (ThermoFisher Scientific). Since each of the port loads each sample in
duplicates on the TLDA card and because two biological replicates of each sample were loaded
onto two separate ports, quadruplicate Ct values were obtained for each sample. Statistical
analysis was performed using Student's t test. Cells were plated at 600,000 per 15 mm dish
(Greiner CELLSTAR, cat#P7237, Sigma) after one day of puromycin selection. Total RNA was
harvested at 50 hours after plating for RNAseq analysis.

Western blot analysis

Protein extracts were collected by lysing cells with RIPA lysis buffer (1% SDS, 1% Triton X-
100, 1% deoxycholic acid). Protein concentration was quantified using the DC Protein Assay kit
(Bio-Rad). 30 µg of protein were resolved on 8-12% SDS-PAGE gels and transferred to
nitrocellulose membranes (Protran, Whatman) overnight at 25 mA. Membranes were incubated
with blocking buffer (5% non-fat milk in 0.1% TBS/Tween-20) for 1 hour at room temperature.
Membranes were then incubated with the primary antibody diluted in blocking buffer over night
at 4°C. Membranes were washed 3 times with 0.1% TBS/Tween-20. Secondary antibodies were

diluted in blocking buffer and applied to membranes for 1 hour at room temperature. After 3 more additional washes, detection was performed using the ECL reagent (Amersham Pharmacia Biotech) and visualized with the chemiluminescence imager G:BOX Chemi XT4 (Synoptics).

CD95 surface staining

Cell pellets of about 300,00 cells were resuspended in about 100 μ l of PBS on ice. After resuspension, 5 μ l of either anti-CD95 primary antibody (BD #556640) conjugated with fluorescein isothiocyanate (FitC), or the matching Isotype control (BD #551954), Mouse IgG1 κ conjugated with FitC, were added. Cells were incubated on ice at 4°C, in the dark, for 25 minutes, washed twice with PBS, and percent green cells were determined by flow cytometry (Becton, Dickinson).

Cell death quantification (DNA fragmentation)

A cell pellet (500,000 cells) was resuspended in 0.1% sodium citrate, pH 7.4, 0.05% Triton X-100, and 50 μ g/ml propidium iodide. After resuspension, cells were incubated 2 to 4 hours in the dark at 4°C. The percent of subG1 nuclei (fragmented DNA) was determined by flow cytometry.

Cell growth and fluorescence over time

After treatment/infection, cells were seeded at 500 to 4,000 per well in a 96-well plate at least in triplicate. Images were captured at indicated time points using the IncuCyte ZOOM live cell imaging system (Essen BioScience) with a 10x objective lens. Percent confluence, red object count, and the green object integrated intensity were calculated using the IncuCyte ZOOM software (version 2015A).

RNA-Seq analysis

The following describes the culture conditions used to produce samples for RNA-Seq in **Figure 4**. HeyA8 Δ shR6 clone #11 cells were infected with pLKO-shScr or pLKO-shR6. A pool of three 293T Δ shL3 clones was infected with either pTIP-shScr or pTIP-shL3. After selection with puromycin for 2 days, the pTIP-infected 293T cells were plated with Dox in duplicate at 500,000 cells per T175 flask. The pLKO-infected HeyA8 cells were plated at 500,000 cells per flask. Total RNA was harvested 50 hours and 100 hours after plating. In addition, 293T cells were infected with either pLKO-shScr or pLKO-shL1 and RNA was isolated (100 hrs after plating) as

described above for the infection with shR6. Finally, HeyA8 cells were transfected with RNAiMAX in 6-wells with siScr (NT2) or siL3 oligonucleotides (Dharmacon) at 25 nM. The transfection mix was removed after 9 hours.

Total RNA was isolated 48 hours after initial transfection using the miRNeasy Mini Kit (Qiagen, Cat.No. 74004) following the manufacturer's instructions. An on-column digestion step using the RNase-free DNase Set (Qiagen, Cat.No.: 79254) was included for all RNA-Seq samples.

RNA libraries were generated and sequenced (Genomics Core facility at the University of Chicago). The quality and quantity of the RNA samples was checked using an Agilent bio-analyzer. Paired end RNA-SEQ libraries were generated using Illumina TruSEQ TotalRNA kits using the Illumina provided protocol (including a RiboZero rRNA removal step). Small RNA-SEQ libraries were generated using Illumina small RNA SEQ kits using the Illumina provided protocol. Two types of small RNA-SEQ sub-libraries were generated: one containing library fragments 140-150 bp in size and one containing library fragments 150-200 bp in size (both including the sequencing adaptor of about 130bp). All three types of libraries (one RNA-SEQ and two small RNA-SEQ) were sequenced on an Illumina HiSEQ4000 using Illumina provided reagents and protocols. The raw counts for RNAs were calculated by HTSeq. The sequenced reads were mapped to hg38 human genome using Tophat and bowtie2. Differential gene expression was analyzed by R Bioconductor DESeq2 package using shrinkage estimation for dispersions and fold changes to improve stability and interpretability of estimates. P values and adjusted P values were calculated using the DESeq2 package. Counts and sequences of small RNAs were extracted from raw fastq file by UNIX shell scripts and then grouped and summarized by SQL language in database tables. To extract small RNAs (shRNA sequences) adaptor sequences were removed using Trim Galore software.

To identify differentially abundant RNAs in cells expressing either shL3 or shR6, using a method unbiased by genome annotation, we also analyzed the raw 100 bp reads for differential abundance. First, the second end in each paired end read was reverse complemented, so that both reads were on the same strand. Reads were then sorted and counted using the core UNIX utilities sort and uniq. Reads with fewer than 128 counts across all 16 samples were discarded. A table with all the remaining reads was then compiled, summing counts from each sequence file corresponding to the same sample. This table contained a little over 100,000 reads. The R package edgeR (<http://bioinformatics.oxfordjournals.org/content/26/1/139>) was used to identify

differentially abundant reads, and then these reads were mapped to the human genome using blat (<http://genome.cshlp.org/content/12/4/656.abstract>) to determine chromosomal location whenever possible. Homer (<http://homer.salk.edu/homer/>) was used to annotate chromosomal locations with overlapping genomic elements (such as genes). Raw read counts in each sequence file were normalized by the total number of unique reads in the file.

To identify the most significant changes in expression of RNAs both methods of RNAs-Seq analyses (alignment and read based) were used to reach high stringency. All samples were prepared in duplicate and for each RNA the average of the two duplicates was used for further analysis. In the alignment-based analysis only RNAs were considered that had a base mean of >2000 reads and were significantly deregulated between the groups (adjusted p-value <0.05). Only RNAs were scored as deregulated when they were more than 1.5 fold changed in the shL3 expressing cells at both time points and in the shR6 expressing cells at either time points (each compared to shScr expressing cells) (*Table S1*). This was done because we found that the pLKO driven expression of shR6 was a lot lower than the pTIP driven expression of shL3 (see the quantification of the two shRNAs in **Figure 5 - figure supplement 1A**) and likely was a result of the cell responses in the shR6 expressing cells were reduced. In the read based analysis, only normalized read numbers of >10 across the samples in each treatment were considered. Only RNA reads were further considered that had a variation between duplicates of less than 2 fold. Only RNAs reads were considered that showed >1.5 change between treatment groups in both cell lines and both time points (*Table S1*). Using the chromosomal localization of each read the gene of origin was determined. Finally, All RNAs were counted that showed deregulation in the same direction with both methods. This resulted in the identification of 11 RNAs that were down and 1 that was upregulated in cells exposed to the shRNAs shL3 and shR6. To determine the number of seed matches in the 3'UTR of downregulated genes, the 3'UTRs of the 11 mRNAs were extracted from the Homo sapiens gene (GRCh38.p7) dataset of the Ensembl 86 database using the Ensembl Biomart data mining tool. For each gene only the longest deposited 3'UTR was considered. Seed matches were counted in all 3'UTRs using in-house Perl scripts.

GSEA used in **Figures 4D** was performed using the GSEA v2.2.4 software from the Broad Institute ([www.http://software.broadinstitute.org/gsea](http://software.broadinstitute.org/gsea)); 1000 permutations were used. The Sabatini gene lists (*Table S2*) were set as custom gene sets to determine enrichment of survival genes versus the nonsurvival control genes in downregulated genes from the RNA seq data; Adjusted p-values below 0.05 were considered significantly enriched. The GO enrichment

analysis shown in **Figure 4F** was performed using all genes that after alignment and normalization were found to be at least 1.5 fold downregulated with an adjusted p values of <0.05, using the software available on www.Metascape.org and default running parameters.

From the RNA-Seq analysis with HeyA8 ΔshR6 infected with pLKO-shR6 and 293T ΔshL3 clones infected pTIP-shL3, we analyzed the mature double-stranded RNAs derived from pLKO-shR6 and pTIP-shL3 and found that the most abundant RNA forms were both shifted by one nucleotide. Based on these most abundant species observed after cellular processing, we converted shL3 and shR6 sequences to siRNAs. The genomic target sequence in shL3 (21nt) is 5'-ACUGGGCUGUACUUUGUAU-3'. For the shL3=>siL3 sense strand, one G was added before the A on the 5' end while the last U on the 3' end was deleted, and second and third to the last ribonucleotides on the 3' end (UA) were replaced with deoxyribonucleotides for stabilization. For shL3=>siL3 antisense strand, the last three nucleotides on the 5' end (AUA) were deleted and one U and two dTs (UdTdT) were added after the last U on the 3' end. The shL3=>siL3 sense strand is 5'-GACUGGGCUGUACUUUGUAdTdA-3' and antisense strand is 5'-/5Phos/UACAAAGUACAGCCCAGUUDtTdT-3'. The shR6=>siRNA was designed in a similar fashion except that two Gs instead of one G were added to the 5' end of the sense strand while UUdTdT instead of UdTdT was added to the 3' end of the antisense strand. The genomic target sequence in shR6 (21nt) is 5'-GUGCAGAUGUAAACCAAACUU-3'. The shR6=>siR6 sense strand is 5'-GGGUGCAGAUGUAAACCAAAdCdT-3' and antisense strand is 5'-/5Phos/UUUGGUUUACAUCUGCACUUDtTdT-3'. Both shL3=>siL3 and ShR6=>siR6 siRNA duplexes were purchased from Dharmacon.

The pTIP-shRNA libraries were constructed by subcloning libraries of 143nt PCR inserts of the form

5'-XXXXXXXXXXXXXXXXXXXXXXXXXXXXXXXXXXXXATAGAGATCGNNNNNNNNNN

possible 21-mer shRNA (i.e. each nearest neighbor shRNA was shifted by 1 nucleotide). These libraries were synthesized together on a chip as 143 bp single-stranded DNA oligos (CustomArray Inc, Custom 12K oligo pool). Each shRNA pool had its own unique 5' end represented by the poly-*X* region. This allowed selective amplification of a particular pool using 1 of 5 unique Fr primers (CD95L ORF: 5'-*TGGCTTTATATATCTCCCTATCAGTG*-3', CD95L 3' UTR: 5'-*GGTCGTCCTATCTATTATTATTCACG*-3', CD95 ORF: 5'-*TCTTGTGTCCAGACCAATTTATTTTCG*-3', CD95 3'UTR: 5'-*CTCATTGACTATCGTTTTAGCTACTG*-3', Venus: 5'-*TATCATCTTTCATGATGACTTTCCGG*-3') and the common reverse primer 5'-*AATCAATGTCAACGCAGCAT*-3'. Phusion High Fidelity Polymerase (NEB #M0530) was used to amplify each library pool; standard PCR conditions were used with an annealing temperature of 61°C and 15 cycles. PCR reactions were purified using PCR Cleanup kit (QIAGEN). The pTIP-shR6 vector and each of the amplified libraries were digested with SphI-HF and BsaBI. Digested PCR products were run on either a 2% Agarose gel or a 20% polyacrylamide (29:1) gel made with 0.5 x TBE buffer. PCR products were extracted using either Gel Extraction kit (QIAGEN) for extraction from Agarose gels or via electro-elution using D-Tube Dialyzer Mini columns (Novagen #71504). Purified PCR inserts were then ligated to the linearized pTIP vector with T4 DNA ligase for 24 hours at 16°C. The ligation mixtures were transformed via electroporation in MegaX DH10B T1 cells (Invitrogen #C6400) and plated on 24 cm ampicillin dishes. At least 10 colonies per pool were picked and sequenced to verify successful library construction. After verification, all colonies per library were pooled together and plasmid DNA extracted using the MaxiPrep kit (QIAGEN). The 5 pTIP-shRNA library DNA preps were used to produce virus in 293T cells.

Lethality screen with pTIP-shRNA libraries

NB7 cells were seeded at 1.5×10^6 per 145 cm² dish. Two dishes were infected with each of the 5 libraries with a transduction efficiency of about 10 to 20%. Media was replaced next day. Infected cells were selected with 1.5 µg/ml puromycin. Cells infected with the Venus, CD95L ORF, and CD95L 3'UTR-targeting libraries were pooled in a 1:1:1 ratio to make the CD95L cell pool. Likewise, cells infected with the Venus, CD95 ORF, and CD95 3'UTR-targeting libraries were pooled to make the CD95 receptor cell pool. The CD95 and the CD95L cell pools were plated separately each in 2 sets of duplicates seeded at 600,000 cells per 145cm² dish. One set received 100 ng/ml Dox, and the other one was left untreated (total of 4 dishes per combined

pool; 2 received no treatment and 2 received Dox). Cells infected with the different libraries were also plated individually in triplicate with or without Dox on a 96-well plate to assess the overall toxicity of each pool. DNA was collected from each 145cm² dish 9 days after Dox addition.

The shRNA barcodes were amplified from the harvested DNA template using NEB Phusion Polymerase with 4 different pairs of primers (referred to as N, N+1, N+2, and N+3) in separate reactions per DNA sample. The N pair consisted of the primers originally used to amplify the CD95L ORF library (Fr: 5'-*TGGCTTTATATATCTCCCTATCAGTG*-3' and Rev: 5'-*AATCAATGTCAACGCAGCAT*-3'). The N+1 primers had a single nucleotide extension at each 5' end of the N primers corresponding to the pTIP vector sequence (Fr: 5'-*TTGGCTTTATATATCTCCCTATCAGTG*-3' and Rev: 5'-*TAATCAATGTCAACGCAGCAT*-3'). The N+2 primers had 2 nucleotide extensions (Fr: 5'-*CTTGGCTTTATATATCTCCCTATCAGTG*-3' and Rev: 5'-*ATAATCAATGTCAACGCAGCAT*-3'), and the N+3 primers had 3 nucleotide extensions (Fr: 5'-*TCTTGGCTTTATATATCTCCCTATCAGTG*-3' and Rev: 5'-*AATAATCAATGTCAACGCAGCAT*-3'). The barcodes from the pTIP-shRNA library plasmid preparations were also amplified using Phusion Polymerase with the N, N+1, N+2, and N+3 primer pairs. The shRNA barcode PCR products were purified from a 2% Agarose gel and submitted for 100 bp paired-end deep sequencing (Genomics Core facility at the University of Chicago). DNA was quantitated using the Qubit. The 4 separate PCR products amplified using N, N+1, N+2, and N+3 were combined in equimolar amounts for each sample. Libraries were generated using the Illumina TruSeq PCR-free kit using the Illumina provided protocol. The libraries were sequenced using the HiSEQ4000 with Illumina provided reagents and protocols. Raw sequence counts for DNAs were calculated by HTSeq. shRNA sequences in the PCR pieces of genomic DNA were identified by searching all reads for the sense sequence of the mature shRNA plus the loop sequence CTCGAG. To avoid a division by zero problem during the subsequent analyses all counts of zero in the raw data were replaced with 1. A few sequences with a total read number <10 across all plasmids reads were not further considered. In the CD95L pool this was only one shRNA (out of 2362 shRNAs) (L792') and in the CD95 20 shRNAs (out of 3004 shRNAs) were not represented (R88, R295, R493, R494, R496, R497, R498, R499, R213', R215', R216', R217', R220', R221', R222', R223', R225', R226', R258', R946', R1197', R423'). While most shRNAs in both pools had a unique sequence two sequences occurred 6 times (L605', L607', L609', L611', L613', L615', and

L604', L606', L608', L610', L612', L614'). In these cases, read counts were divided by 6. Two shRNAs could not be evaluated: 1) shR6 in the CD95 pool. It had a significant background due to the fact that pTIP-shR6 was used as a starting point to clone all other shRNAs. 2) shL3 was found to be a minor but significant contaminant during the infection of some of the samples. For each condition, two technical duplicates and two biological duplicates were available. To normalize reads to determine the change in relative representation of shRNAs between conditions, the counts of each shRNA in a subpool (all replicates and all conditions) was divided by the total number of shRNAs in each subpool (%). First, the mean of the technical replicates (R1 and R2) was taken. To analyze the biological replicates and to determine the changes between conditions, two analyses were performed: 1) The change in shRNA representation between the cloned plasmid library and cells infected with the library and then cultured for 9 days without Dox (infection -Dox). Fold downregulation was calculated for each subpool as $[(\text{plasmid } \%/ -\text{Dox1 } \% + \text{plasmid } \%/ -\text{Dox2 } \%)/2]$. 2) The difference in shRNA composition between the infected cells cultured with (infection +Dox) and without Dox. Fold downregulation was calculated for each subpool as $[(-\text{Dox1 } \%/ + \text{Dox1 } \%) + (-\text{Dox1 } \%/ + \text{Dox2 } \%) + (-\text{Dox2 } \%/ + \text{Dox1 } \%) + (-\text{Dox2 } \%/ + \text{Dox2 } \%)/4]$. Only shRNAs were considered that were at least 5-fold underrepresented in either of the two analyses (data in *Table S3*).

The toxicity index (TI) and GC content analysis

The TI in *Figure 7A* is defined by the sum of the counts of a 6mer or 8mer seed match in the 3'UTRs of critical survival genes divided by the seed match counts in the 3'UTRs of nonsurvival genes. We used the 1882 survival genes recently described in a CRISPR/Cas9 lethality screen by Wang et al. (Wang et al., 2015). The survival genes were defined by having a CRISPR score of <-0.1 and an adjusted p-value of <0.05 . We chose as a control group to these top essential genes the bottom essential genes using inverse criteria (CRISPR score of >0.1 and adjusted p-value of <0.05) and are referring to them as the "nonsurvival genes". Both counts were normalized for the numbers of genes in each gene set. 3'UTRs were retrieved as described above. For the survival genes 1846 and for the nonsurvival genes 416 3'UTRs were found. For each gene, only seed matches in the longest 3'UTR were counted. The TI was calculated for each of the 4096 possible 6mer combinations and each of the 65536 possible 8mer combinations (*Table S4*). These numbers were then assigned to the results of the shRNA screen (*Table S5*). An alternative TI was calculated in *Figure 7 – figure supplement 1B* and is based on the top 850 most highly

expressed survival genes (all expressed >1000 average reads) and 850 expression matched genes not described to be critical for cancer cell survival were selected as controls.

For the analyses in **Figure 7C and D**, the GC content % was calculated for every 6mer in the CD95L ORF shRNA pool. The GC content % was then plotted against the log(Fold down) for each shRNA in the CD95L ORF shRNA after infection (compared to the plasmid composition) in **Figure 7C** and after addition of Dox (compared to cells infected but not treated with Dox) in **Figure 7D**. In **Figure 7E**, the log(TI) and GC content % was extracted for every possible 6mer and plotted. Pearson correlation coefficient and associated p-value were calculated in R3.3.1.

Sylamer analysis

Sylamer is a tool to test for the presence of RNAi-type regulation effects from a list of differentially expressed genes, independently from small RNA measurements (van Dongen et al., 2008) (<http://www.ebi.ac.uk/research/enright/software/sylamer>). For short stretches of RNA (in this case length 6, 7, and 8 in length corresponding to the lengths of the determinants of seed region binding in RNAi-type binding events), Sylamer tests for all possible motifs of this length whether the motif occurrences are shifted in sequences associated with the list under consideration, typically 3'UTRs when analyzing RNAi-type binding events. A shift or enrichment of such a motif towards the down-regulated end of the gene list is consistent with upregulation of a small RNA that has the motif as the seed region. Sylamer tests in small increments along the list of genes, using a hypergeometric test on the counts of a given word, comparing the leading part of the gene list to the universe of all genes in the list. For full details refer to (van Dongen et al., 2008). Enriched motifs stand out from the back-ground of all motifs tested, as visible in the Sylamer plot. The plot consist of many different lines, each line representing the outcomes of a series of tests for a single word, performed along regularly spaced intervals (increments of 200 genes) of the gene list. Each test yields the log-transformed P-value arising from a hypergeometric test as indicated above. If the word is enriched in the leading interval the log-transformed value has its value plotted on the positive y-axis (sign changed), if the word is depleted the log-transformed value is plotted on the negative y-axis. 3' UTRs were used from Ensembl, version 76. As required by Sylamer, they were cleaned of low-complexity sequences and repetitive fragments using respectively Dust (Morgulis, Gertz, Schaffer, & Agarwala, 2006) with default parameters and the RSAT interface (Medina-Rivera et al., 2015) to

the Vmatch program, also run with default parameters. Sylamer (version 12-342) was run with the Markov correction parameter set to 4.

Statistical analyses

Continuous data were summarized as means and standard deviations (except for all IncuCyte experiments where standard errors are shown) and dichotomous data as proportions. Continuous data were compared using t-tests for two independent groups and one-way ANOVA for 3 or more groups. For evaluation of continuous outcomes over time, two-way ANOVA was used with one factor for the treatment conditions of primary interest and a second factor for time treated as a categorical variable to allow for non-linearity. Comparisons of single proportions to hypothesized null values were evaluated using binomial tests. Statistical tests of two independent proportions were used to compare dichotomous observations across groups.

The effects of treatment on wild-type versus either Dicer^{-/-} or Drosha^{-/-} cells were statistically assessed by fitting regression models that included linear and quadratic terms for value over time, main effects for treatment and cell type, and two- and three-way interactions for treatment, cell-type and time. The three-way interaction on the polynomial terms with treatment and cell type was evaluated for statistical significance since this represents the difference in treatment effects over the course of the experiment for the varying cell types.

To test if higher TI is enriched in shRNAs that were highly downregulated, p-values were calculated based on permuted datasets using Mann-Whitney U tests. The ranking of TI was randomly shuffled 10,000 times and the W statistic from our dataset was compared to the distribution of the W statistic of the permuted datasets. Test of enrichment was based on the filtered data of at least 5-fold difference, which we define as a biologically meaningful. Fisher Exact Tests were performed to assess enrichment of downregulated genes (i.e. >1.5 downregulated with adjusted p-value <0.05) amongst genes with at least one si/shRNA seed match. All statistical analyses were conducted in Stata 14 or R 3.3.1.

Data availability

The accession number for the RNA-Seq and expression data reported in this manuscript are GSE87817.

Acknowledgements

We are grateful to Lindsay Stolzenburg and Ann Harris for helping to set up the CRISPR/Cas9 gene editing method and to Matthew Schipma for computational support. We would like to thank the Gene Editing & Screening Core, at Memorial Sloan Kettering in New York City, NY, for RNAi reagents and services. M.H. was supported by the Intramural Research Program of NIAMS. This work was funded by training grants T32CA070085 (to M.P.) and T32CA009560 (to W.P.) R50CA211271 (to J.C.Z.), and R35CA197450 (to M.E.P.).

Author contributions

W.P. planned the study and performed experiments. M.P. established the arrayed qPCR method and performed experiments, Q.Q.G., A.H., A.S., A.H.K., A.A.S, and A.E.M. performed experiments, S.D. performed the SYMALER analysis, E.B. and J.S.Z. provided biocomputational and K.A.K. and D.M.S. biostatistics support, M.H. provided assistance and discussions on the mechanism of RNAi and the RISC, and M.E.P. directed the study and wrote the manuscript.

Competing financial interests

The authors declare no competing financial interests.

Figure legends

Figure 1

Exogenous CD95L or CD95 proteins do not protect cells from toxicity of CD95L/CD95 derived shRNAs.

(A) *Left*: Percent cell confluence over time of NB7 cells after infection with either pLKO-shScr or pLKO-shL1 and concurrent treatment with different concentrations of soluble CD95L protein (S2). Two-way ANOVA was performed for pairwise comparisons of % confluence over time between shScr expressing cells untreated or treated with 100 ng/ml S2. Each data point represents mean \pm SE of three replicates. *Center*: Percent cell confluence over time of NB7 cells after infection with either pLKO-shScr or pLKO-shL1 and concurrent treatment with different concentrations of leucine zipper tagged (Lz)CD95L protein. Two-way ANOVA was performed for pairwise comparisons of % confluence over time between shScr expressing cells untreated or treated with 50 ng/ml LzCD95L. Each data point represents mean \pm SE of three replicates. *Right*: Percent nuclear PI staining of MCF-7 cells 24 hours after adding different amounts of LzCD95L. (B) Schematic of the eight silent mutations introduced to the shL1 and the shL3 target sites of CD95L. (C) Western blot analysis of CD95L and β -actin in NB7 cells over-expressing CD95L-WT, CD95L-L1MUT, or CD95L-L3MUT 3 days after infection with pLKO-shScr, pLKO-shL1, or pLKO-shL3. Shown is one of two repeats of this analysis. (D) Percent nuclear PI staining of NB7 cells expressing empty pLenti vector, CD95L-WT, CD95L-L1MUT, or CD95L-L3MUT 6 days after infection with either pLKO-shScr, pLKO-shL1, or pLKO-shL3. Each bar represents mean \pm SD of three replicates. (E) Schematic of the 8 silent mutations introduced at the shR6 site of CD95. (F) Western blot analysis of CD95 and β -actin in MCF-7 cells over-expressing CD95-WT or CD95-R6MUT. (G) Percent nuclear PI staining of MCF-7 cells expressing empty pLNCX2 vector, CD95-WT, or CD95-R6MUT 6 days after infection with pLKO-shScr, pLKO-shR6, or pLKO-shR7. Each bar represents mean \pm SD of three replicates.

Figure 1 - figure supplement 1.

The majority of siRNAs and shRNAs targeting CD95L or CD95 are toxic.

(A) Location of target sites, growth inhibitory activities and toxicity of all tested siRNAs, DsiRNAs, and pLKO-shRNAs targeting CD95L and CD95. Experiments were performed in HeyA8 cells at an MOI of 3 for pLKO-shRNA infection, transfected with 25 nM of siRNAs, or 5 nM of DsiRNAs. Color code indicates the level of growth reduction caused by each sh/siRNA. sh/siRNAs labeled with an asterisk induced significant cell death as monitored by nuclear PI staining. Both exon/intron structure and protein domains are shown for both CD95L and CD95. EC, extracellular domain; TM, transmembrane domain; IC, intracellular domain. Data on growth reduction of DsiRNAs were performed in triplicates and in two independent experiments. Data on growth reduction of siRNAs were performed in 4 replicates and in two independent experiments. Data on growth reduction of shRNAs were performed in triplicate and in two independent experiments. Data on nuclear fragmentation by siRNAs were performed in triplicate in two independent experiments. Data on nuclear fragmentation by shRNAs were performed in triplicate. (B) PI staining was used to quantify percent subG1 of HeyA8 cells 4 days after transfection with 5 nM of CD95L derived DsiRNAs. Data are representative of three independent experiments. Each bar represents mean \pm SD of four replicates (p-value *** $p < 0.0001$, unpaired t-test). (C) Level of underrepresentation (toxicity) of shRNAs targeting either CD95L (left column) or CD95 (right column) across 216 human cancer cell lines as described in (Cowley et al., 2014). The fraction of cell lines for which an shRNA was found to be toxic is given in percentage For shL5 data on only 197 cell lines were available. This screen

did not include shL3, but another CD95 derived shRNA we did not test (we now call shR3) was found to be toxic to 71.8% of the 216 cell lines.

Figure 1 - figure supplement 2.

Toxicity of si/shRNAs is dose dependent.

(A) Sequences of the 6 toxic TRC shRNAs (pLKO vector) that were converted into miR-30 based shRNAs (Tet inducible LT3REPIR vector). (B) Confluence over time of NB7-Venus-CD95L (left) or NB7-Venus CD95 (right) cells infected with the LT3REPIR vector minus/plus Dox to induce expression of the indicated shRNAs. (C) Total green fluorescence over time of the experiment shown in B. (D) Confluence (top) and total green fluorescence (bottom) over time of NB7-Venus-CD95L (left) or NB7-Venus CD95 (right) cells infected with the pTIP vector minus/plus Dox to induce expression of the indicated shRNAs. (E) Confluence over time of HeyA8 cells transfected with the indicated concentration of either siScr or siL3. Each data point represents mean \pm SE of six replicates. The experiment was repeated three times.

Figure 2.

CD95 and CD95L derived si/shRNAs kill cells in the absence of the targeted sites in CD95 or CD95L.

(A) Schematic of the genomic locations and sequences of the gRNAs used to excise the siL3 (Δ 64bp) and shL3 (Δ 41bp) target sites from CD95L. PAM site is underlined. Green indicates a gRNA targeting the sense strand. Blue indicates a gRNA targeting the antisense strand. (B) Schematic showing the genomic locations and sequences of the gRNAs used to excise the shR6 (Δ 227bp) target site. (C) PCR with flanking (*top panels*) and internal (*bottom panels*) primers used to confirm the Δ 41 deletion in the shL3 site in 293T clones. Cells transfected with Cas9 only (Cas9) are wild-type, clone #3 is heterozygous, and clones #1 and #5 are representative of homozygous deletion clones. (D) Quantitative PCR for endogenous CD95L with a primer downstream of the Δ 41 shL3 deletion and another primer internal to the deleted region. nd, not detectable. Each bar represents mean \pm SD of three replicates. (E) PCR with flanking (*top row*) and internal (*bottom row*) primers used to confirm the presence of the shL3 Δ 41 (*top panel*), siL3 Δ 64 (*middle panel*), and shR6 Δ 227 (*bottom panel*) deletions in HeyA8 clones. Mix, HeyA8 cells after transfection with Cas9 and gRNAs but before single cell cloning. (F) Quantitative PCR for CD95 in HeyA8 cells transfected with Cas9 plasmid (Cas9) alone, or the HeyA8 Δ shR6 clone #11. RNA was extracted 5 days after infection with pLKO-shScr, pLKO-shR6, pLKO-shR2, or pLKO-shR6' (targeting the 3'UTR). Each bar represents mean \pm SD of three replicates. (G) Percent cell confluence over time of 293T cells (*left*) and a pool of three 293T clones with a homozygous deletion of the shL3 target site (*right*) infected with pTIP-shScr or pTIP-shL3 and treatment with or without Dox. Data are representative of two independent experiments. Each data point represents mean \pm SE of six replicates. (H) *Left*: Percent confluence over time of HeyA8 cells infected with pLKO-shScr, pLKO-shR6, or pLKO-shL3. *Center*: Percent confluence over time of a HeyA8 clone with a homozygous deletion of the shR6 target site infected with either pLKO-shScr or pLKO-shR6. *Right*: Percent confluence over time of a pool of three HeyA8 clones with a homozygous deletion of the shL3 site infected with either pLKO-shScr or pLKO-shL3. Data are representative of two independent experiments. Each data point represents mean \pm SE of three replicates. (I) Percent confluence over time of a pool of three HeyA8 clones harboring a homozygous deletion of the siRNA siL3 target site after transfection with different concentrations of siScr or siL3. Data are representative of three independent experiments. Each data point represents mean \pm SE of three replicates.

Figure 2 - figure supplement 1.

Knockout of CD95 in HeyA8 cells.

(A) PCR showing a $\Delta 227$ shR6 deletion and insertions in HeyA8 clones #1 and #2. (B) Schematic of the $\Delta 227$ deletion in allele #1 and partial insertion of a pSC-B plasmid fragment in allele #2 in HeyA8 clone #2 based on Sanger sequencing of isolated bands from PCR shown in A. Note, cl#1 and #2 have the expected $\Delta 227$ shR6 deletion in one allele and an insertion in the other. cl#11 has a homozygous $\Delta 227$ shR6 deletion. The deleted region is shown in green containing the shR6 target site in red. pSC-B vector sequences are shown in blue letters, and the insertion is shown in orange. (C) Western blot for CD95 and β -actin in Cas9-control transfected HeyA8 cells and HeyA8 shR6 k.o. clones #1, #2, and #11. Shown is one of two repeats of this analysis. (D) Surface staining for CD95 in parental HeyA8 cells and HeyA8 shR6 knockout clones #1, #2, and #11. Shown is one of two repeats of this analysis. (E) Images showing apoptosis induction with LzCD95L treatment (4.5 hrs) in parental HeyA8 cells but not in clone #2.

Figure 3.

Toxicity of CD95L derived siRNAs involves canonical RNAi activity.

(A) Percent cell confluence (*left*) and total green object integrated intensity (*right*) over time of a HeyA8 CD95 knockout clone ($\Delta R6$ cl#2) expressing the Venus-CD95L sensor either untreated (Ctr) or after transfection with 25 nM of single-stranded sense, single-stranded antisense, or double-stranded (ds) siScr or siL3 siRNAs. The CD95L sensor is schematically shown and comprises the Venus ORF fused to the CD95L ORF lacking the A of the ATG start codon (X). Data are representative of two independent experiments. Each data point represents mean \pm SE of three replicates. (B) Percent cell confluence (*left*) and total green object integrated intensity (*right*) over time of the HeyA8 CD95L sensor cell used in *Figure 3A* after transfection with 5 nM siScr or siL3 double-stranded RNA (dsRNA) or double-stranded DNA (dsDNA). Data are representative of two independent experiments. Each data point represents mean \pm SE of three replicates. (C) Summary of experiments to test whether siL3 and siL2 siRNAs modified as indicated (*left*) were active (check mark) or not (X) in reducing green fluorescence or cell growth (both $>70\%$ reduction at end point) when transfected at 25 nM (except for blunt end oligonucleotides which were used at 5 nM and compared to 5 nM of siL3) into HeyA8 CD95L sensor cells used in *Figure 3A*. Endpoints were 164 hours for blunt end siRNA transfection, 180 hrs for modified siL3 and 144 hrs for modified siL2 siRNA transfections. Every data row is based on cell growth and green fluorescence quantification data executed as shown in A. Each analysis was done in triplicate and based on two independent repeats. (D) Red object count over time of HeyA8 cells (expressing NucRed) after transfection with different ratios of siL3 and mutant siL3 (siL3MUT). Data are representative of two independent experiments. Each data point represents mean \pm SE of three replicates. (E) Percent cell confluence over time of HCT116 parental (*left*) or Dicer^{-/-} (clone #43, another Dicer^{-/-} clone, #45, gave a similar result, data not shown), or Drosha^{-/-} (*right*) cells after infection with either shScr, shL3 or shR6 pLKO viruses. Inserts show the level of protein expression levels of Drosha/Dicer and AGO2 levels in the tested cells. Data are representative of three independent experiments. Each data point represents mean \pm SE of four replicates. Drosha^{-/-} cells were more sensitive to toxic shRNAs than wt cells ($p < 0.0001$, according to a polynomial fitting model). (F) Western blot analysis of HCT116 wt, Dicer^{-/-} or Drosha^{-/-} cells 4 days after infection with either pLKO-shScr or pLKO-shR6. (G) Percent cell confluence over time of HCT116 wt, Dicer^{-/-} (clone #43) and Drosha^{-/-} cells after transfection with 25 nM siScr or siL3. Data are representative of four independent experiments (Dicer^{-/-} clone #45, gave a similar result, data not shown). Each data point represents the mean \pm

SE of four replicates. Data in insert confirm similar uptake of transfected siRNA (25 nM of siGLO Red) into wild-type, Dicer^{-/-} and Drosha^{-/-} cells. Dicer^{-/-} and Drosha^{-/-} cells were more sensitive to siL3 than wt cells ($p < 0.0001$, according to a polynomial fitting model). **(H)** Percent reduction in Venus expression (green) and in cell number (red object count (red)) over time of HeyA8 cells expressing the Venus-CD95L sensor and red nuclei after transfection with 5 nM of different chimeric siRNAs generated by substituting nucleotides in the toxic siL3 with the scrambled siRNA sequence beginning at either the seed match end (top) or the opposite end (bottom) of siL3 after 188 hours. The schematic in the middle shows the sequence of siL3 and the siScr siRNA (both sense and antisense strands). The 6mer seed sequence region of siL3 (positions 2 to 7) is highlighted in light blue. Nucleotides shared by siScr and siL3 are shown in grey font. Data are representative of two independent experiments. Each data point represents mean of three replicates. In another independent experiment cells were transfected with 25 nM with a very similar result (data not shown).

Figure 4.

Toxic shRNAs derived from CD95 and CD95L cause downregulation of critical survival genes.

(A) Schematic of RNA-Seq work flow for total RNA sample prepared both before (50 hrs) and during (100 hrs) DISE after expressing either shR6 or shL3 from different vector systems (i.e. pLKO-shR6 and pTIP-shL3) in different cells (HeyA8 shR6 Δ 227 cells and 293T shL3 Δ 41 cells). **(B)** One mRNA was up and 11 mRNAs were downregulated in the cells treated with toxic shL3 and shR6 as shown in *Figure 4A*. mRNAs shown in red were found to be essential cancer survival genes in two genome-wide lethality screens. The number of essential genes was enriched from 6.6% of the tested genes (Blomen et al., 2015; Wang et al., 2015) to 54.5% in our study ($p = 3 \times 10^{-6}$ according to binomial distribution). **(C)** The level of growth inhibition observed in HeyA8 cells transfected with siRNA SmartPools (25 nM) individually targeting the listed survival genes. Targeting the seven genes shown significantly reduced cell growth compared to cells transfected with a siScr pool at 140 hrs (samples done in quadruplicate in two independent experiments) with an ANOVA $p < 0.05$. **(D)** Gene set enrichment analysis for a group of 1846 survival genes (*top 4 panels*) and 416 nonsurvival genes (*bottom 4 panels*) identified in a genome-wide CRISPR lethality screen (Wang et al., 2015) after introducing Dox-inducible shL3 in 293T Δ shL3 cells (*left-most panels*), shR6 in HeyA8 Δ shR6 cells (*center-left panels*), shL1 in parental 293T cells (*center-right panels*), and siL3 in HeyA8 cells (*right-most panels*). Scrambled sequences served as controls. p-values indicate the significance of enrichment. **(E)** Schematics showing all RNAs at least 1.5 fold downregulated (adj p-value < 0.05) in cells treated as in *Figure 4A*. Histones that are underlined contain a 3'UTR. **(F)** Metascape analysis of the 4 RNA Seq data sets analyzed. The boxed GO term clusters were highly enriched in all data sets.

Figure 4 - figure supplement 1.

Down-regulation of critical survival genes after treatment with CD95 and CD95L-derived shRNAs and siRNAs.

(A) Arrayed quantitative PCR of genes found to be down-regulated (or upregulated as with ATP13A3) in *Figure 4B* both in 293T Δ shL3-pTIP-shL3 cells 50 hrs post-Dox treatment and HeyA8 Δ shR6-pLKO-shR6 100 hrs post infection and puromycin selection. Data are representative of two independent experiments. Each bar represents mean \pm SD of two biological replicates and two technical replicates (p-value $* < 0.05$, $** < 0.005$, unpaired t-test). **(B)** Venn diagram showing overlap of genes determined to be down-regulated with both read-based and

alignment-based analyses of the RNA-Seq data depicted in *Figure 4A* with the critical survival genes found in the Sabatini and Brummelkamp studies (Blomen et al., 2015; Wang et al., 2015), all listed in **Table S2**. The Venn diagram was generated using <http://bioinformatics.psb.ugent.be/webtools/Venn>. (C) Kinetic quantitative PCR of the down-regulated genes in the 293T Δ shL3 pTIP-shL3 cells. RNA was collected at 14 hrs, 26 hrs, and 50 hrs after treatment with Dox. NS, not significant. Each bar represents mean \pm SD of quadruplicates (p-value $* < 0.05$, $** < 0.005$, unpaired t-test). (D) Table showing which genes were significantly (p < 0.05) down-regulated >1.5 fold (indicated by an "X") in parental HeyA8 cells 80 hrs after transfection with siL3 or 100 hrs after infection and puromycin selection with pLKO-shL1, pLKO-shL3, or pLKO-shR7.

The following describes the 11 genes that were significantly downregulated after introducing the toxic shRNAs shL3 or shR6 into cancer cells (see **Figure 4B**) and some of their cancer relevant activities:

- 1) CAPZA1 (capping actin protein of muscle Z-line alpha subunit 1) is an actin capping protein. CAPZA1 knockdown has been reported to cause disassembly of autophagosomes (Mi et al., 2015). It is overexpressed in malignant melanoma (Sun et al., 2011).
- 2) CCT3 (chaperonin containing TCP1 subunit 3) is part of a chaperone complex that folds various proteins including actin and tubulin. CCT3 is required for proper mitotic progression (Zhang et al., 2016).
- 3) FSTL1 (follistatin-like 1) is a putative activin-binding protein. Knockdown of FSTL1 in lung cancer cells resulted in mitotic arrest followed by apoptosis promoted by the activation of caspase-3 and -9 (Bae et al., 2016). FSTL1 is downregulated during cellular senescence of human mesenchymal stem cells (Yoo, Choi, & Kim, 2013).
- 4) FUBP1 (far upstream element binding protein 1). A lack of FUBP1 causes a cell-autonomous defect in the maintenance of fetal and adult hematopoietic stem cells (HSCs). FUBP1-deficient adult HSCs exhibit significant transcriptional changes, including upregulation of the cell-cycle inhibitor p21 and the pro-apoptotic Noxa molecule, suggesting they undergo apoptosis (Rabenhorst et al., 2015). In addition, FUBP1 binds to an upstream element of the c-myc promoter and regulates c-myc mRNA level, thus regulating proliferation (Jang et al., 2009). Finally, FUBP1 is upregulated in many tumors and acts as an oncoprotein by stimulating proliferation and inhibiting apoptosis (Baumgarten et al., 2014).
- 5) GNB1 (G-protein beta subunit 1) is tumor-promoting in breast cancer. Data suggest that GNB1 plays an important role in the mTOR-related anti-apoptosis pathway (Wazir, Jiang, Sharma, & Mokbel, 2013).
- 6) HIST1H1C. A specific role of this particular histone in cancer cell survival has not yet been described. (Knockdown causes cell cycle arrest in MCF-7 cells; (<http://journals.plos.org/plosgenetics/article?id=10.1371/journal.pgen.1000227>)).
- 7) NAA50 (N(alpha)-acetyltransferase 50, NatE catalytic subunit) is required for sister chromatid separation *in vivo* (Hou, Chu, Kong, Yokomori, & Zou, 2007).
- 8) NUCKS1 (nuclear casein kinase and cyclin dependent kinase substrate 1) is a chromatin-associated protein with a role in the DNA damage response. Knocking down NUCKS1 causes chromosomal breaks (Parplys et al., 2015).
- 9) PRELID3B (PRELI domain containing 3B) is an inner mitochondrial protein. Knocking down PRELID3B decreases cell viability (<http://www.genecards.org/cgi-bin/carddisp.pl?gene=PRELID3B>).
- 10) SNRPE (small nuclear ribonucleoprotein polypeptide E). siRNA-mediated depletion of SNRPE stimulated autophagy and led to a marked reduction of cell viability in breast, lung,

and melanoma cancer cell lines, whereas it had little effect on the survival of the nonmalignant MCF-10A breast epithelial cells (Quidville et al., 2013).
11) TFRC (transferrin receptor). Blocking TFRC function with a neutralizing antibody inhibits cell proliferation and survival (Pham et al., 2014). Suppression of TFRC led to apoptosis of renal cells (Gui et al., 2013) and cell cycle arrest in esophageal squamous cell carcinoma cells (Chan et al., 2014).

Figure 4 - figure supplement 2.

Characterization of the six genes downregulated in shL3 and shR6 treated cells and found to be critical survival genes in lethality screens.

(A) The six downregulated survival genes were queried individually using default settings with all studies selected in the cBioPortal for Cancer Genomics hosted by Memorial Sloan Kettering Cancer Center (<http://www.cbioportal.org/>) (Cerami et al., 2012; Gao et al., 2013). Datasets with alterations in 5 out of the 6 essential genes reporting both copy number alterations and mutational data were included. To avoid reporting duplicate datasets, The Cancer Genome Atlas publications were excluded. After filtering, 33 datasets representing cancers from 23 different sites reported alterations in the downregulated survival genes. (B) Percent confluence over time of HeyA8 cells transfected with increasing concentrations of a pool of siRNAs (28 different siRNAs) targeting 7 different genes: CCT3, TFRC, NAA50, FUBP1, PRELID3B, GNB1 and FSTL1. Each siRNA SmartPool was comprised of 4 individual siRNAs. Data are representative of two independent experiments. Values were calculated from samples done in quadruplicates shown as mean \pm SE. (C) PI staining used to quantify percent subG1 for cells 4 days after transfection with 1 nM and 5 nM of combined siRNA pools targeting the 7 different survival genes as in B. Data are representative of two independent experiments. Values were calculated from samples done in quadruplicates shown as mean \pm SD. *** $p < 0.0001$, unpaired t-test.

Figure 4 - figure supplement 3.

Histones are downregulated in all forms of DISE but are not the most highly expressed genes in cells.

MA plots comparing the expression level (counts per million, CPM) and fold change in the four RNA Seq data sets in this study. Shown are all RNAs that were >1.5 fold deregulated with an adjusted p-value of <0.01 . Significantly downregulated RNAs are shown in green, upregulated RNAs in cyan. All 73 histones are shown as dark blue dots and the 12 histones downregulated in all 4 data sets are shown as red dots.

Figure 5.

DISE inducing si/shRNAs target critical survival genes through RNAi.

(A) Sylamer plots for the list of genes in the shL3 experiment (left) and the shR6 experiment (right) ordered from down-regulated to up-regulated. The most highly enriched sequence is shown which in each case is the 8mer seed match of the introduced shRNA. The red line corresponds to a p-value threshold of 0.05 after Bonferroni correction for the number of words tested (65536). Bonferroni-adjusted p-values are shown. The unadjusted p-values are $1.58E-24$ and $1.35E-26$, respectively. The black line represents the sequences carrying the let-7 8mer seed match. (B) Location of the 6mer seed matches of either shL3 or shR6 in the 3'UTRs of the 11 genes (shown at scale) identified in the RNA-Seq experiment described in *Figure 4A*. Red font indicates a critical survival gene. (C) A series of six 2x2 contingency tables comparing whether or not a critical survival gene is downregulated after treatment with the indicated siRNA or shRNA to whether or not its 3'UTR contains at least 1 seed match for the introduced sh/siRNA.

p-values were calculated using Fisher's Exact Test to determine any significant relationship between gene downregulation and presence of seed matches in 3'UTR.

Figure 5 - figure supplement 1.

Quantification of the mature shRNA forms.

(A) Graphical representation of the percentage of the different Dicer cut sites to produce the mature passenger (top) and guide (bottom) strands of 3 shRNAs expressed from two vectors. All analyses were performed with cells 50 hrs after either Dox addition (in pTIP expressing cells) or infection with the pLKO virus. Letters in green: vector sequences; black: passenger and guide strands of shRNAs; Arrow heads label the most highly cleaved residues; the darker the arrow head the more highly cleaved. Numbers in yellow box represent total number of reads detected for passenger and guide strands. (B) Percent cell confluence in HeyA8 cells after transfection with shL3=>siL3 (shL3 converted to an siRNA) or shR6=>siR6 (shR6 converted to an siRNA). Conversion was based on the most common mature double-stranded RNA form produced as indicated by the results in A. Data are representative of two independent experiments. Each bar represents mean \pm SE of four replicates. Insert: percent DNA fragmentation in the same samples. Data are representative of two independent experiments. Each bar represents mean \pm SD of four replicates, *** p<0.0001, unpaired t-test.

Figure 5 - figure supplement 2.

Identification of seed matches targeted by shL1 and siL3.

Sylamer plots for the list of genes in the shL1 experiment (293T cells 100 hrs after infection with pLKO-shL1) (left) and the siL3 experiment (48 hrs after transfection of HeyA8 cells with siL3) (right) ordered from down-regulated to up-regulated. The most highly enriched sequences are shown which in each case is the 7mer seed match of the introduced shRNA. The red line corresponds to a p-value threshold of 0.05 after Bonferroni correction for the number of words tested. Bonferroni-adjusted p-values are shown.

Figure 5 - figure supplement 3.

Activity to knockdown CD95 does determine shRNA toxicity.

HeyA8 cells infected with the indicated shRNAs in the pLKO vector were analyzed for toxicity (top, % percent reduction at half maximal confluency), CD95 expression by Western blot analysis (center, 2 days after puromycin addition) and qPCR analysis (bottom, 3 days after puromycin addition). Shown data are representative of two independent experiments. +++, >75%; ++, >50%; +, >10%; -, <10% growth reduction.

Figure 6.

Identifying all toxic shRNAs derived from CD95L and CD95.

(A) Schematic showing the cloned shRNAs covering the ORF of Venus and the ORFs and 3'UTRs of CD95L and CD95. The 3'UTR is displayed as a dashed line because it was not included in the full-length Venus-CD95L/CD95 sensors. (B) Work-flow of pTIP-shRNA library synthesis, shRNA screen and data analysis. (C) Ranked fold reduction of shRNAs spanning Venus and CD95L (ORF and 3'UTR) (left 3 panels) and Venus and CD95 (ORF and 3'UTR) (right 3 panels). The ranked lists were separated into the shRNAs derived from Venus (top), the ORFs (center) and the 3'UTRs (bottom). The p-value of enrichment for each ranked set of shRNAs is given. Only the parts of the ranked lists are shown with the downregulated shRNAs. For all 6 panels, the top section of each panel (boxed in blue) contains the data on shRNAs downregulated after infection of cells and cultured for 9 days without Dox when compared to the

composition of the shRNA plasmid library and the bottom half (boxed in orange) contains the data on shRNAs downregulated after culture with Dox for 9 days when compared to the culture without Dox. P-values were calculated using Mann Whitney U tests with a one-sided alternative that the rank was lower. **(D)** The location of all shRNAs significantly downregulated at least 5 fold along the sequences of Venus, CD95L ORF, CD95L 3'UTR (left panel) and Venus, CD95 ORF, and CD95 3'UTR (right panel). The top half of each sub panel (blue ticks) shows the shRNAs downregulated after infection and the bottom half (orange ticks) contains the data on shRNAs downregulated after culture with Dox for 9 days. Significance of enrichment in the different subpanels is shown. p-values were calculated according to statistical tests of two proportions. Each data set was compared to the corresponding Venus distribution. Green line: sequence that corresponds to the intracellular domain of CD95L.

Figure 6 - figure supplement 1.

Toxicity and RNAi of individual shRNA pools.

(A) *Top panels:* Green object intensity over time of NB7 Venus-CD95L sensor cells infected with the pTIP-Venus shRNA pool (*left panel*), pTIP-CD95L ORF shRNA pool (*center panel*), or pTIP-CD95L 3'UTR shRNA pool (*right panel*) with or without Dox treatment. *Bottom panels:* Green object intensity over time of NB7 Venus-CD95 sensor cells infected with the pTIP-Venus shRNA pool (*left panel*), pTIP-CD95 ORF shRNA pool (*center panel*), or pTIP-CD95 3'UTR shRNA pool (*right panel*) with or without Dox treatment. Values were calculated from samples done in quadruplicates shown as mean \pm SE. **(B)** Percent confluence over time of parental NB7 cells infected with the pTIP-Venus shRNA pool (*top left panel*), pTIP-CD95L ORF shRNA pool (*top center panel*), pTIP-CD95L 3'UTR shRNA pool (*top right panel*), pTIP-CD95 ORF-shRNA pool (*bottom center panel*), and pTIP-CD95 3'UTR shRNA pool (*bottom right panel*) with or without Dox treatment. Values were calculated from samples done in triplicate shown as mean \pm SE. P-values were calculated using two-way ANOVA with a factor for Dox treatment and a factor for time. Similar data were obtained when either HCT116 or 293T cells were treated with each of the five shRNA pools (data not shown).

Figure 6 - figure supplement 2.

Fold change in shRNA representation after infection of NB7 cells and after treatment with Dox.

(A) Change in green fluorescence (top panels) and percent cell confluence (bottom panels) over time of NB7 cells expressing either Venus-CD95 (left panels) or Venus-CD95L (right panels). Cells were infected with the Tet-inducible pTIP-shR6 virus, selected for two days with puromycin and then subjected to an analysis in the IncuCyte Zoom. No Dox was added. Two other inducible constructs (pTIP-shL1 and pTIP-shL3) were tested in the same way and no evidence of leakiness was observed (data not shown), supporting the finding in the shRNA screen that certain shRNA constructs display leakiness while others do not. Values were calculated from samples done in triplicate shown as mean \pm SE. **(B)** Scatterplot showing the fold change of shRNAs after infection of cells and culture for 9 days without Dox when compared to the composition of the shRNA plasmid library (X axis) and the fold change of shRNAs after culture with Dox for 9 days when compared to the culture without Dox (Y axis). The red dots are the shRNAs that were significantly downregulated at least 5 fold. The number of shRNAs labeled in red in each quartile is given in blue. Two of the shRNAs tested before are labeled in green.

Figure 7.

In silico prediction of DISE activity tracks with experimental determined toxicity of shRNAs.

(A) *Left*: Schematic showing the preferential targeting of seed matches present in the 3'UTRs (red marks) of survival genes by toxic si/shRNAs. *Right*: The toxicity index (TI) is the normalized ratio of the number of 6mer or 8mer seed matches present in a list of survival genes versus a list of nonsurvival genes. (B) Fold downregulation versus ranked (8mer seed matched based) Toxicity Index for shRNAs of the Venus/CD95L pool (*left three panels*) and the Venus/CD95 pool (*right three panels*). Orange and blue tick marks indicate the same as in *Figure 6D*. To test if higher TI is enriched in shRNAs that were highly downregulated, p-values were calculated based on permuted datasets using Mann-Whitney U tests. The ranking of TI was randomly shuffled 10,000 times and the W statistic from our dataset was compared to the distribution of the W statistic of the permuted datasets. (C, D) Plot of fold downregulation of toxic shRNAs derived from CD95L ORF of the toxicity screens -Dox (left) or +Dox (center) versus GC content the 6mer seed in each shRNA. (E) Plot of the log(TI) of all 4092 possible 6mers versus GC content of the seeds. Pearson correlation coefficient and significance (p values) are given.

Figure 7 - figure supplement 1.

DISE does not just target all highly expressed genes.

(A) Correlation between 850 survival genes (genes identified as critical survival genes in two genome-wide lethality screens (Blomen et al., 2015; Wang et al., 2015) and expressed at least at 100 reads in all of the 16 control RNA Seq samples in this study) and 850 expression matched nonsurvival genes (genes not identified as critical survival genes in two genome-wide lethality screens (Blomen et al., 2015; Wang et al., 2015) and expressed at least at 100 reads in all of the 16 control RNA Seq samples in this study). (B) Reanalysis of the CD95L ORF data in *Figure 7B* using two alternative ways to calculate the toxicity index (TI). *Left*: the analysis shown in *Figure 7B* with the data ranked using the original TI (using all known 3'UTRs for each gene group). *Center*: analysis with the data ranked using the original TI but based on only the longest 3'UTR for each gene. *Right*: analysis with the data ranked using the new TI based on expression matched SGs and nonSGs identified in A and using the longest 3'UTR for each gene. To test if higher TI is enriched in shRNAs that were highly downregulated, p-values were calculated based on permuted datasets using Mann-Whitney U tests.

Supplementary Tables:

Table S1: Results of the RNA-Seq analysis used to generate *Figure 4B*.

Table S2: Gene lists used in this work.

Table S3: shRNA screen data.

Table S4: The 6mer and 8mer toxicity index.

Table S5: Correlation between experimental shRNA toxicity and TI.

References

- Algeciras-Schimmich, A., Pietras, E. M., Barnhart, B. C., Legembre, P., Vijayan, S., Holbeck, S. L., & Peter, M. E. (2003). Two CD95 tumor classes with different sensitivities to antitumor drugs. *Proc Natl Acad Sci U S A*, 100(20), 11445-11450.
- Bae, K., Park, K. E., Han, J., Kim, J., Kim, K., & Yoon, K. A. (2016). Mitotic cell death caused by follistatin-like 1 inhibition is associated with up-regulated Bim by inactivated Erk1/2 in human lung cancer cells. *Oncotarget*, 7(14), 18076-18084. doi: 10.18632/oncotarget.6729
- Barnhart, B. C., Legembre, P., Pietras, E., Bubici, C., Franzoso, G., & Peter, M. E. (2004). CD95 ligand induces motility and invasiveness of apoptosis-resistant tumor cells. *EMBO J*, 23(15), 3175-3185.
- Baumgarten, P., Harter, P. N., Tonjes, M., Capper, D., Blank, A. E., Sahm, F., . . . Mittelbronn, M. (2014). Loss of FUBP1 expression in gliomas predicts FUBP1 mutation and is associated with oligodendroglial differentiation, IDH1 mutation and 1p/19q loss of heterozygosity. *Neuropathol Appl Neurobiol*, 40(2), 205-216. doi: 10.1111/nan.12088
- Bernstein, E., Caudy, A. A., Hammond, S. M., & Hannon, G. J. (2001). Role for a bidentate ribonuclease in the initiation step of RNA interference. *Nature*, 409(6818), 363-366. doi: 10.1038/35053110
- Birmingham, A., Anderson, E. M., Reynolds, A., Ilsley-Tyree, D., Leake, D., Fedorov, Y., . . . Khvorova, A. (2006). 3' UTR seed matches, but not overall identity, are associated with RNAi off-targets. *Nat Methods*, 3(3), 199-204. doi: 10.1038/nmeth854
- Blomen, V. A., Majek, P., Jae, L. T., Bigenzahn, J. W., Nieuwenhuis, J., Staring, J., . . . Brummelkamp, T. R. (2015). Gene essentiality and synthetic lethality in haploid human cells. *Science*, 350(6264), 1092-1096. doi: 10.1126/science.aac7557
- Bramsen, J. B., Laursen, M. B., Nielsen, A. F., Hansen, T. B., Bus, C., Langkjaer, N., . . . Kjems, J. (2009). A large-scale chemical modification screen identifies design rules to generate siRNAs with high activity, high stability and low toxicity. *Nucleic Acids Res*, 37(9), 2867-2881. doi: 10.1093/nar/gkp106
- Ceppi, P., Hadji, A., Kohlhapp, FJ., Pattanayak, A., Hau, A., Xia, L., . . . Peter, M. E. (2014). CD95 and CD95L promote and protect cancer stem cells. *Nature Commun*, 5, 5238.
- Cerami, E., Gao, J., Dogrusoz, U., Gross, B. E., Sumer, S. O., Aksoy, B. A., . . . Schultz, N. (2012). The cBio cancer genomics portal: an open platform for exploring multidimensional cancer genomics data. *Cancer Discov*, 2(5), 401-404. doi: 10.1158/2159-8290.CD-12-0095
- Chan, K. T., Choi, M. Y., Lai, K. K., Tan, W., Tung, L. N., Lam, H. Y., . . . Law, S. (2014). Overexpression of transferrin receptor CD71 and its tumorigenic properties in esophageal squamous cell carcinoma. *Oncol Rep*, 31(3), 1296-1304. doi: 10.3892/or.2014.2981
- Chen, L., Park, S. M., Tumanov, A. V., Hau, A., Sawada, K., Feig, C., . . . Peter, M. E. (2010). CD95 promotes tumour growth. *Nature*, 465(7297), 492-496.
- Chiu, Y. L., & Rana, T. M. (2003). siRNA function in RNAi: a chemical modification analysis. *RNA*, 9(9), 1034-1048.
- Cowley, G. S., Weir, B. A., Vazquez, F., Tamayo, P., Scott, J. A., Rusin, S., . . . Hahn, W. C. (2014). Parallel genome-scale loss of function screens in 216 cancer cell lines for the identification of context-specific genetic dependencies. *Sci Data*, 1, 140035. doi: 10.1038/sdata.2014.35

- 1753 Dow, L. E., Premisrur, P. K., Zuber, J., Fellmann, C., McJunkin, K., Miething, C., . . . Lowe,
1754 S. W. (2012). A pipeline for the generation of shRNA transgenic mice. *Nat Protoc*, 7(2),
1755 374-393. doi: 10.1038/nprot.2011.446
- 1756 Drachsler, M., Kleber, S., Mateos, A., Volk, K., Mohr, N., Chen, S., . . . Martin-Villalba, A.
1757 (2016). CD95 maintains stem cell-like and non-classical EMT programs in primary
1758 human glioblastoma cells. *Cell death & disease*, 7, e2209. doi: 10.1038/cddis.2016.102
- 1759 Fedorov, Y., Anderson, E. M., Birmingham, A., Reynolds, A., Karpilow, J., Robinson, K., . . .
1760 Khvorova, A. (2006). Off-target effects by siRNA can induce toxic phenotype. *RNA*,
1761 12(7), 1188-1196. doi: 10.1261/rna.28106
- 1762 Friesen, C., Fulda, S., & Debatin, K. M. (1999). Cytotoxic drugs and the CD95 pathway.
1763 *Leukemia*, 13(11), 1854-1858.
- 1764 Gao, J., Aksoy, B. A., Dogrusoz, U., Dresdner, G., Gross, B., Sumer, S. O., . . . Schultz, N.
1765 (2013). Integrative analysis of complex cancer genomics and clinical profiles using the
1766 cBioPortal. *Science signaling*, 6(269), pl1. doi: 10.1126/scisignal.2004088
- 1767 Grimm, D., Streetz, K. L., Jopling, C. L., Storm, T. A., Pandey, K., Davis, C. R., . . . Kay, M. A.
1768 (2006). Fatality in mice due to oversaturation of cellular microRNA/short hairpin RNA
1769 pathways. *Nature*, 441(7092), 537-541. doi: 10.1038/nature04791
- 1770 Gu, S., Jin, L., Zhang, Y., Huang, Y., Zhang, F., Valdmann, P. N., & Kay, M. A. (2012). The
1771 loop position of shRNAs and pre-miRNAs is critical for the accuracy of dicer processing
1772 in vivo. *Cell*, 151(4), 900-911. doi: 10.1016/j.cell.2012.09.042
- 1773 Gu, S., Zhang, Y., Jin, L., Huang, Y., Zhang, F., Bassik, M. C., . . . Kay, M. A. (2014). Weak
1774 base pairing in both seed and 3' regions reduces RNAi off-targets and enhances si/shRNA
1775 designs. *Nucleic Acids Res*, 42(19), 12169-12176. doi: 10.1093/nar/gku854
- 1776 Gui, S., Sang, X., Zheng, L., Ze, Y., Zhao, X., Sheng, L., . . . Tang, M. (2013). Intragastric
1777 exposure to titanium dioxide nanoparticles induced nephrotoxicity in mice, assessed by
1778 physiological and gene expression modifications. *Part Fibre Toxicol*, 10, 4. doi:
1779 10.1186/1743-8977-10-4
- 1780 Guo, H., Ingolia, N. T., Weissman, J. S., & Bartel, D. P. (2010). Mammalian microRNAs
1781 predominantly act to decrease target mRNA levels. *Nature*, 466(7308), 835-840.
- 1782 Ha, M., & Kim, V. N. (2014). Regulation of microRNA biogenesis. *Nat Rev Mol Cell Biol*,
1783 15(8), 509-524. doi: 10.1038/nrm3838
- 1784 Hadji, A., Ceppi, P., Murmann, A. E., Brockway, S., Pattanayak, A., Bhinder, B., . . . Peter, M.E.
1785 (2014). Death induced by CD95 or CD95 ligand elimination. *Cell Reports*, 10, 208-222.
- 1786 Hart, T., Brown, K. R., Sircoulomb, F., Rottapel, R., & Moffat, J. (2014). Measuring error rates
1787 in genomic perturbation screens: gold standards for human functional genomics. *Mol Syst*
1788 *Biol*, 10, 733. doi: 10.15252/msb.20145216
- 1789 Hart, T., Chandrashekar, M., Aregger, M., Steinhart, Z., Brown, K. R., MacLeod, G., . . .
1790 Moffat, J. (2015). High-Resolution CRISPR Screens Reveal Fitness Genes and
1791 Genotype-Specific Cancer Liabilities. *Cell*, 163(6), 1515-1526. doi:
1792 10.1016/j.cell.2015.11.015
- 1793 Hou, F., Chu, C. W., Kong, X., Yokomori, K., & Zou, H. (2007). The acetyltransferase activity
1794 of San stabilizes the mitotic cohesin at the centromeres in a shugoshin-independent
1795 manner. *J Cell Biol*, 177(4), 587-597. doi: 10.1083/jcb.200701043
- 1796 Jackson, A. L., Burchard, J., Schelter, J., Chau, B. N., Cleary, M., Lim, L., & Linsley, P. S.
1797 (2006). Widespread siRNA "off-target" transcript silencing mediated by seed region
1798 sequence complementarity. *RNA*, 12(7), 1179-1187. doi: 10.1261/rna.25706
- 1799 Jang, M., Park, B. C., Kang, S., Chi, S. W., Cho, S., Chung, S. J., . . . Park, S. G. (2009). Far
1800 upstream element-binding protein-1, a novel caspase substrate, acts as a cross-talker

1801 between apoptosis and the c-myc oncogene. *Oncogene*, 28(12), 1529-1536. doi:
1802 10.1038/onc.2009.11

1803 Jinek, M., East, A., Cheng, A., Lin, S., Ma, E., & Doudna, J. (2013). RNA-programmed genome
1804 editing in human cells. *Elife*, 2, e00471. doi: 10.7554/eLife.00471

1805 Khan, A. A., Betel, D., Miller, M. L., Sander, C., Leslie, C. S., & Marks, D. S. (2009).
1806 Transfection of small RNAs globally perturbs gene regulation by endogenous
1807 microRNAs. *Nat Biotechnol*, 27(6), 549-555.

1808 Kim, D. H., Behlke, M. A., Rose, S. D., Chang, M. S., Choi, S., & Rossi, J. J. (2005). Synthetic
1809 dsRNA Dicer substrates enhance RNAi potency and efficacy. *Nat Biotechnol*, 23(2), 222-
1810 226. doi: 10.1038/nbt1051

1811 Kim, Y. K., Kim, B., & Kim, V. N. (2016). Re-evaluation of the roles of DROSHA, Exportin 5,
1812 and DICER in microRNA biogenesis. *Proc Natl Acad Sci U S A*, 113(13), E1881-1889.
1813 doi: 10.1073/pnas.1602532113

1814 Kleber, S., Sancho-Martinez, I., Wiestler, B., Beisel, A., Gieffers, C., Hill, O., . . . Martin-
1815 Villalba, A. (2008). Yes and PI3K Bind CD95 to Signal Invasion of Glioblastoma.
1816 *Cancer Cell*, 13(3), 235-248.

1817 Krammer, P. H. (2000). CD95's deadly mission in the immune system. *Nature*, 407(6805), 789-
1818 795.

1819 Krol, J., Loedige, I., & Filipowicz, W. (2010). The widespread regulation of microRNA
1820 biogenesis, function and decay. *Nat Rev Genet*, 11(9), 597-610.

1821 Lin, X., Ruan, X., Anderson, M. G., McDowell, J. A., Kroeger, P. E., Fesik, S. W., & Shen, Y.
1822 (2005). siRNA-mediated off-target gene silencing triggered by a 7 nt complementation.
1823 *Nucleic Acids Res*, 33(14), 4527-4535. doi: 10.1093/nar/gki762

1824 Lu, J., Getz, G., Miska, E.A., varez-Saavedra, E., Lamb, J., Peck, D., . . . Golub, T.R. (2005).
1825 MicroRNA expression profiles classify human cancers. *Nature*, 435(7043), 834-838.

1826 Mali, P., Yang, L., Esvelt, K. M., Aach, J., Guell, M., DiCarlo, J. E., . . . Church, G. M. (2013).
1827 RNA-guided human genome engineering via Cas9. *Science*, 339(6121), 823-826. doi:
1828 10.1126/science.1232033

1829 Marques, J. T., & Williams, B. R. (2005). Activation of the mammalian immune system by
1830 siRNAs. *Nat Biotechnol*, 23(11), 1399-1405. doi: 10.1038/nbt1161

1831 Medina-Rivera, A., Defrance, M., Sand, O., Herrmann, C., Castro-Mondragon, J. A., Delerce, J.,
1832 . . . van Helden, J. (2015). RSAT 2015: Regulatory Sequence Analysis Tools. *Nucleic*
1833 *Acids Res*, 43(W1), W50-56. doi: 10.1093/nar/gkv362

1834 Mi, N., Chen, Y., Wang, S., Chen, M., Zhao, M., Yang, G., . . . Yu, L. (2015). CapZ regulates
1835 autophagosomal membrane shaping by promoting actin assembly inside the isolation
1836 membrane. *Nat Cell Biol*, 17(9), 1112-1123. doi: 10.1038/ncb3215

1837 Morgens, D. W., Deans, R. M., Li, A., & Bassik, M. C. (2016). Systematic comparison of
1838 CRISPR/Cas9 and RNAi screens for essential genes. *Nat Biotechnol*, 34(6), 634-636. doi:
1839 10.1038/nbt.3567

1840 Morgulis, A., Gertz, E. M., Schaffer, A. A., & Agarwala, R. (2006). A fast and symmetric DUST
1841 implementation to mask low-complexity DNA sequences. *J Comput Biol*, 13(5), 1028-
1842 1040. doi: 10.1089/cmb.2006.13.1028

1843 Murmann, A. E., McMahon, K. M., Halluck-Kangas, A., Ravindran, N., Patel, M., Law, C., . . .
1844 Peter, M. E. (2017). Induction of DISE in ovarian cancer cells in vivo. *BioRxive*.

1845 Parpys, A. C., Zhao, W., Sharma, N., Groesser, T., Liang, F., Maranon, D. G., . . . Wiese, C.
1846 (2015). NUCKS1 is a novel RAD51AP1 paralog important for homologous
1847 recombination and genome stability. *Nucleic Acids Res*, 43(20), 9817-9834. doi:
1848 10.1093/nar/gkv859

- Patel, M., & Peter, M.E. (2017). Identification of DISE-inducing shRNAs by monitoring cellular responses. *BioRxive*.
- Peter, M. E., Budd, R. C., Desbarats, J., Hedrick, S. M., Hueber, A. O., Newell, M. K., . . . Lynch, D. H. (2007). The CD95 receptor: apoptosis revisited. *Cell*, 129(3), 447-450.
- Petri, S., & Meister, G. (2013). siRNA design principles and off-target effects. *Methods Mol Biol*, 986, 59-71. doi: 10.1007/978-1-62703-311-4_4
- Pham, D. H., Moretti, P. A., Goodall, G. J., & Pitson, S. M. (2008). Attenuation of leakiness in doxycycline-inducible expression via incorporation of 3' AU-rich mRNA destabilizing elements. *Biotechniques*, 45(2), 155-156. doi: 10.2144/000112896
- Pham, D. H., Powell, J. A., Gliddon, B. L., Moretti, P. A., Tsykin, A., Van der Hoek, M., . . . Pitson, S. M. (2014). Enhanced expression of transferrin receptor 1 contributes to oncogenic signalling by sphingosine kinase 1. *Oncogene*, 33(48), 5559-5568. doi: 10.1038/onc.2013.502
- Pratt, A. J., & MacRae, I. J. (2009). The RNA-induced silencing complex: a versatile gene-silencing machine. *J Biol Chem*, 284(27), 17897-17901. doi: 10.1074/jbc.R900012200
- Qadir, A. S., Ceppi, P., Brockway, S., Law, C., Mu, L., Khodarev, N. N., . . . Peter, M. E. (2017). CD95/Fas Increases Stemness in Cancer Cells by Inducing a STAT1-Dependent Type I Interferon Response. *Cell Rep*, 18(10), 2373-2386. doi: 10.1016/j.celrep.2017.02.037
- Quidville, V., Alsafadi, S., Goubar, A., Commo, F., Scott, V., Pioche-Durieu, C., . . . Andre, F. (2013). Targeting the deregulated spliceosome core machinery in cancer cells triggers mTOR blockade and autophagy. *Cancer Res*, 73(7), 2247-2258. doi: 10.1158/0008-5472.CAN-12-2501
- Rabenhorst, U., Thalheimer, F. B., Gerlach, K., Kijonka, M., Bohm, S., Krause, D. S., . . . Zornig, M. (2015). Single-Stranded DNA-Binding Transcriptional Regulator FUBP1 Is Essential for Fetal and Adult Hematopoietic Stem Cell Self-Renewal. *Cell Rep*, 11(12), 1847-1855. doi: 10.1016/j.celrep.2015.05.038
- Robbins, M. A., Li, M., Leung, I., Li, H., Boyer, D. V., Song, Y., . . . Rossi, J. J. (2006). Stable expression of shRNAs in human CD34+ progenitor cells can avoid induction of interferon responses to siRNAs in vitro. *Nat Biotechnol*, 24(5), 566-571. doi: 10.1038/nbt1206
- Schoggins, J. W., Wilson, S. J., Panis, M., Murphy, M. Y., Jones, C. T., Bieniasz, P., & Rice, C. M. (2011). A diverse range of gene products are effectors of the type I interferon antiviral response. *Nature*, 472(7344), 481-485. doi: 10.1038/nature09907
- Shao, D. D., Tsherniak, A., Gopal, S., Weir, B. A., Tamayo, P., Stransky, N., . . . Mesirov, J. P. (2013). ATARIS: computational quantification of gene suppression phenotypes from multisample RNAi screens. *Genome Res*, 23(4), 665-678. doi: 10.1101/gr.143586.112
- Siomi, H., & Siomi, M. C. (2009). On the road to reading the RNA-interference code. *Nature*, 457(7228), 396-404. doi: 10.1038/nature07754
- Stark, A., Brennecke, J., Bushati, N., Russell, R. B., & Cohen, S. M. (2005). Animal MicroRNAs confer robustness to gene expression and have a significant impact on 3'UTR evolution. *Cell*, 123(6), 1133-1146. doi: 10.1016/j.cell.2005.11.023
- Sun, D., Zhou, M., Kowolik, C. M., Trisal, V., Huang, Q., Kernstine, K. H., . . . Shen, B. (2011). Differential expression patterns of capping protein, protein phosphatase 1, and casein kinase 1 may serve as diagnostic markers for malignant melanoma. *Melanoma Res*, 21(4), 335-343. doi: 10.1097/CMR.0b013e328346b715
- Teitz, T., Wei, T., Valentine, M. B., Vanin, E. F., Grenet, J., Valentine, V. A., . . . Kidd, V. J. (2000). Caspase 8 is deleted or silenced preferentially in childhood neuroblastomas with amplification of MYCN. *Nat Med*, 6(5), 529-535.

- 1897 Ting, A. H., Suzuki, H., Cope, L., Schuebel, K. E., Lee, B. H., Toyota, M., . . . Baylin, S. B.
- 1898 (2008). A requirement for DICER to maintain full promoter CpG island
- 1899 hypermethylation in human cancer cells. *Cancer Res*, 68(8), 2570-2575. doi:
- 1900 10.1158/0008-5472.CAN-07-6405
- 1901 Ui-Tei, K., Naito, Y., Takahashi, F., Haraguchi, T., Ohki-Hamazaki, H., Juni, A., . . . Saigo, K.
- 1902 (2004). Guidelines for the selection of highly effective siRNA sequences for mammalian
- 1903 and chick RNA interference. *Nucleic Acids Res*, 32(3), 936-948. doi: 10.1093/nar/gkh247
- 1904 van Dongen, S., Abreu-Goodger, C., & Enright, A. J. (2008). Detecting microRNA binding and
- 1905 siRNA off-target effects from expression data. *Nat Methods*, 5(12), 1023-1025. doi:
- 1906 10.1038/nmeth.1267
- 1907 Wang, T., Birsoy, K., Hughes, N. W., Krupczak, K. M., Post, Y., Wei, J. J., . . . Sabatini, D. M.
- 1908 (2015). Identification and characterization of essential genes in the human genome.
- 1909 *Science*, 350(6264), 1096-1101. doi: 10.1126/science.aac7041
- 1910 Watanabe, C., Cuellar, T. L., & Haley, B. (2016). Quantitative evaluation of first, second, and
- 1911 third generation hairpin systems reveals the limit of mammalian vector-based RNAi. *RNA*
- 1912 *Biol*, 13(1), 25-33. doi: 10.1080/15476286.2015.1128062
- 1913 Wazir, U., Jiang, W. G., Sharma, A. K., & Mokbel, K. (2013). Guanine nucleotide binding
- 1914 protein beta 1: a novel transduction protein with a possible role in human breast cancer.
- 1915 *Cancer Genomics Proteomics*, 10(2), 69-73.
- 1916 Yoo, J. K., Choi, S. J., & Kim, J. K. (2013). Expression profiles of subtracted mRNAs during
- 1917 cellular senescence in human mesenchymal stem cells derived from bone marrow. *Exp*
- 1918 *Gerontol*, 48(5), 464-471. doi: 10.1016/j.exger.2013.02.022
- 1919 Zamore, P. D., Tuschl, T., Sharp, P. A., & Bartel, D. P. (2000). RNAi: double-stranded RNA
- 1920 directs the ATP-dependent cleavage of mRNA at 21 to 23 nucleotide intervals. *Cell*,
- 1921 101(1), 25-33. doi: 10.1016/S0092-8674(00)80620-0
- 1922 Zare, H., Khodursky, A., & Sartorelli, V. (2014). An evolutionarily biased distribution of
- 1923 miRNA sites toward regulatory genes with high promoter-driven intrinsic transcriptional
- 1924 noise. *BMC Evol Biol*, 14, 74. doi: 10.1186/1471-2148-14-74
- 1925 Zhang, Y., Wang, Y., Wei, Y., Wu, J., Zhang, P., Shen, S., . . . Yu, L. (2016). Molecular
- 1926 chaperone CCT3 supports proper mitotic progression and cell proliferation in
- 1927 hepatocellular carcinoma cells. *Cancer Lett*, 372(1), 101-109. doi:
- 1928 10.1016/j.canlet.2015.12.029
- 1929
- 1930

Figure 1

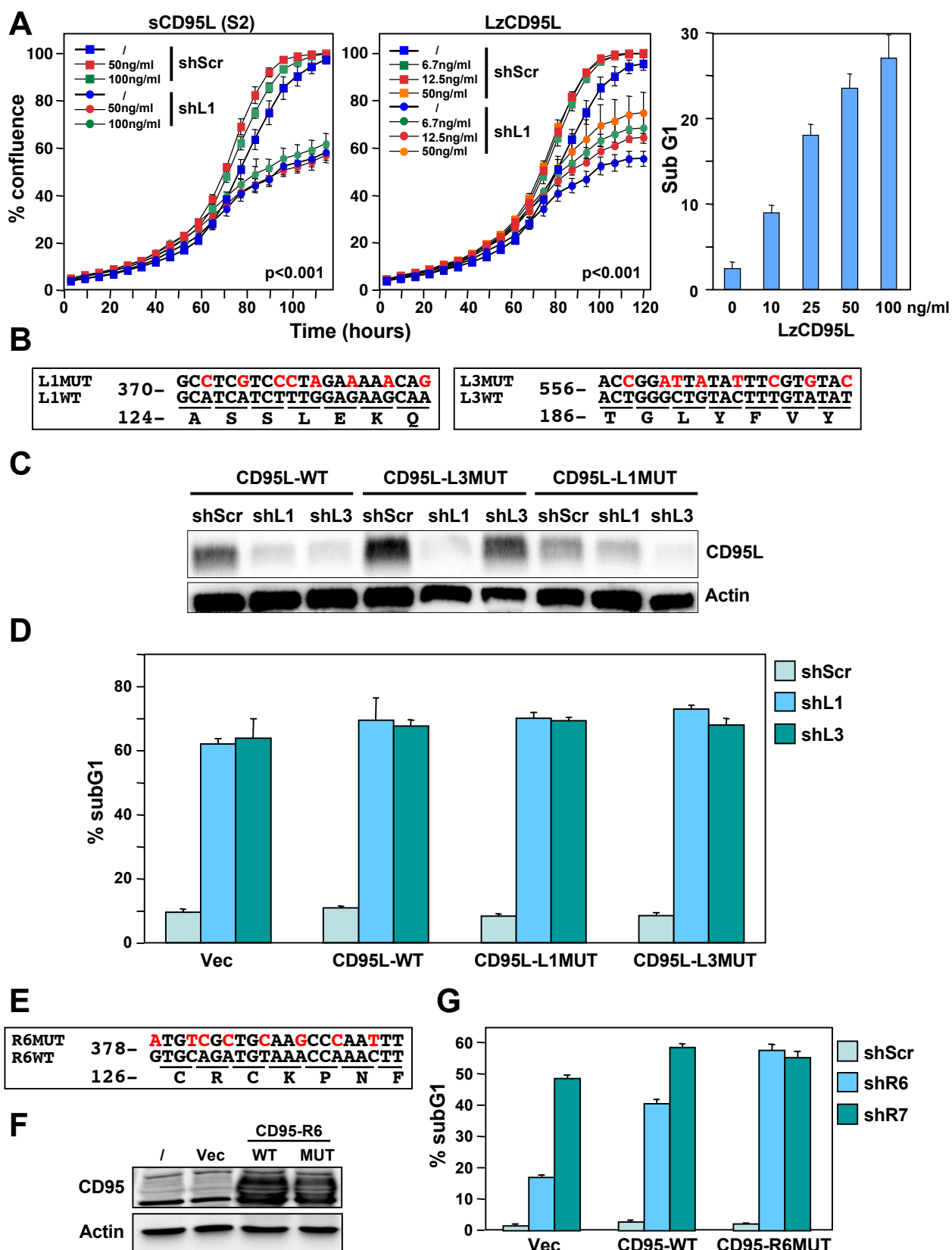


Figure 1 - figure supplement 1

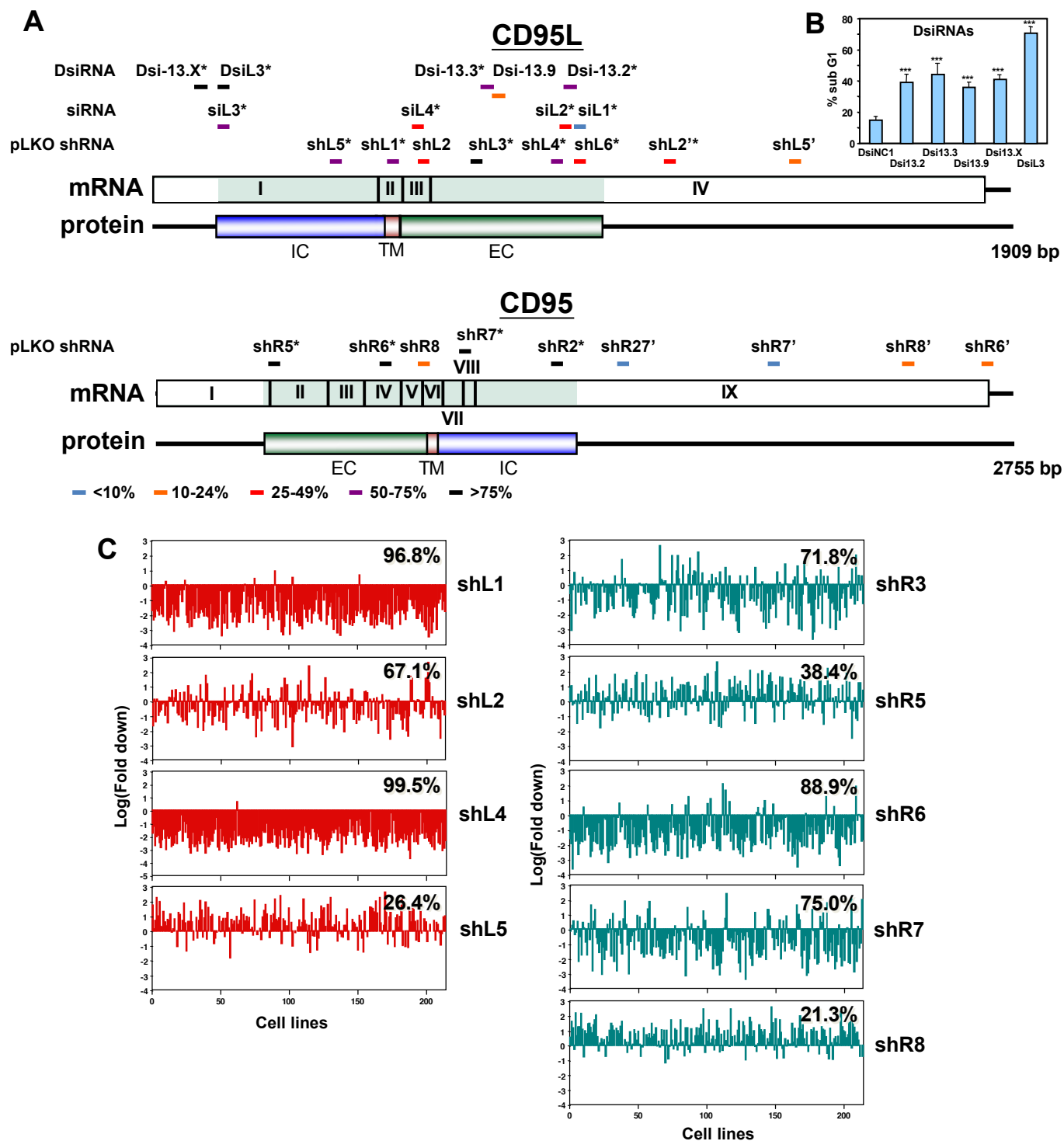


Figure 1 - figure supplement 2

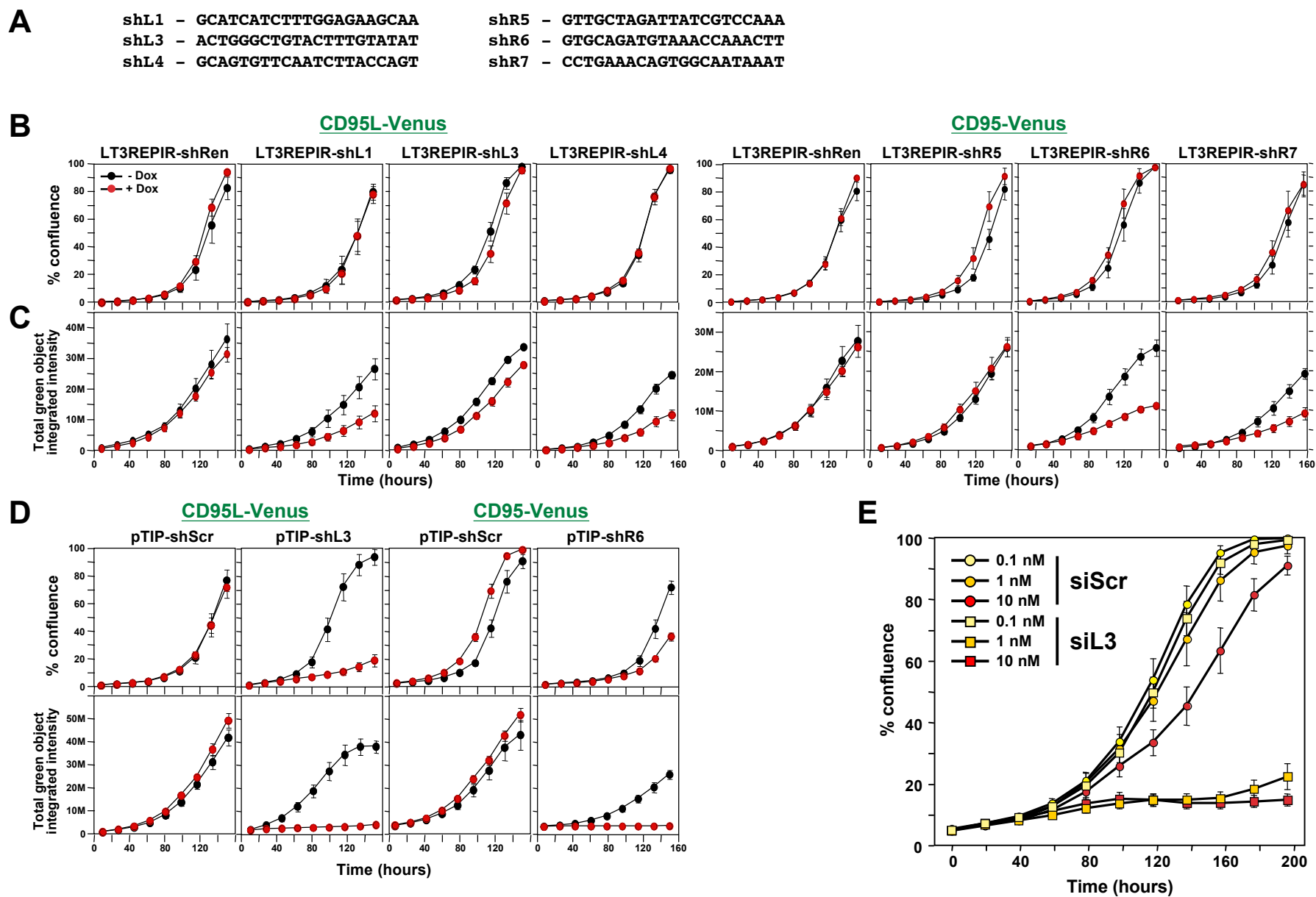


Figure 2

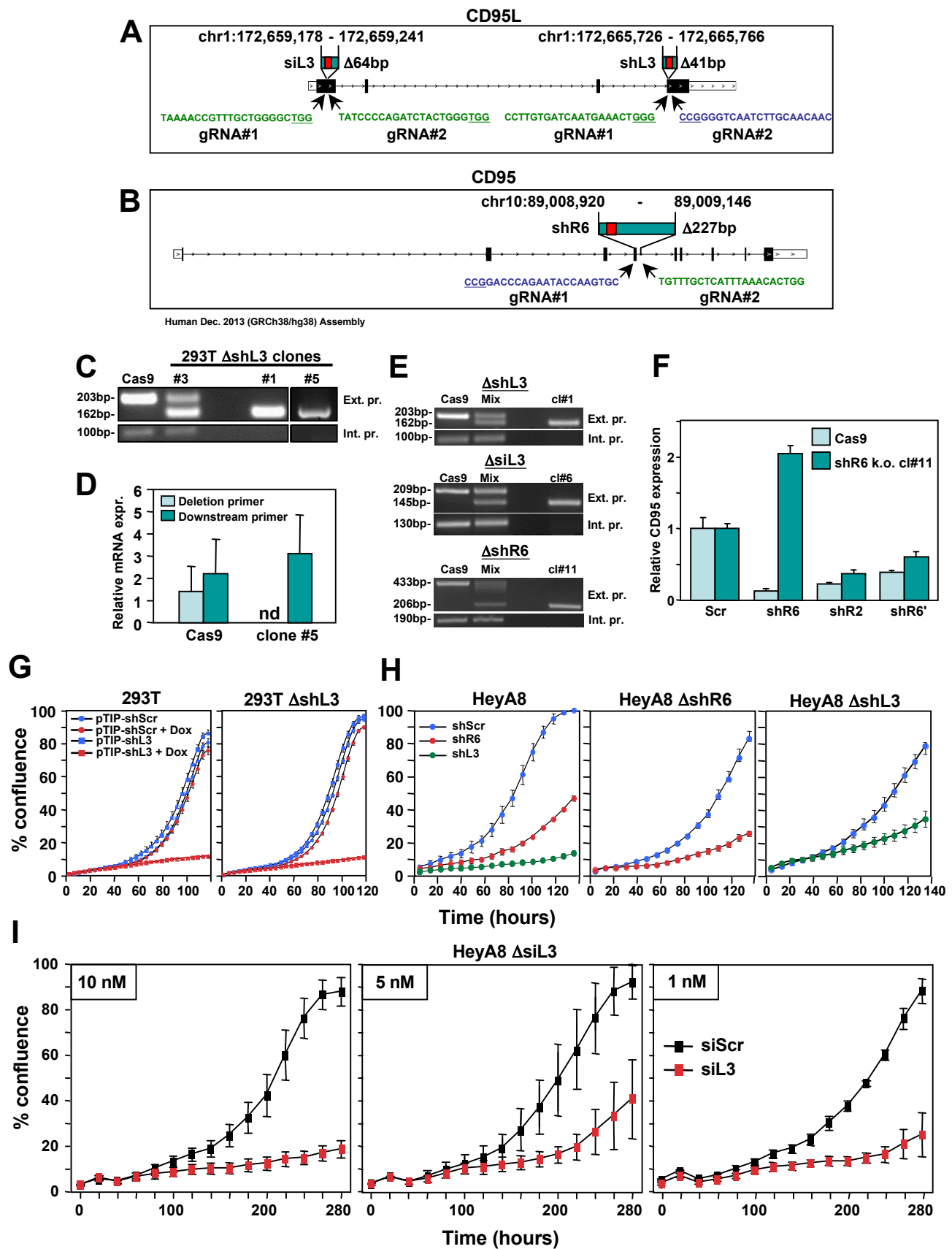


Figure 2 - figure supplement 1

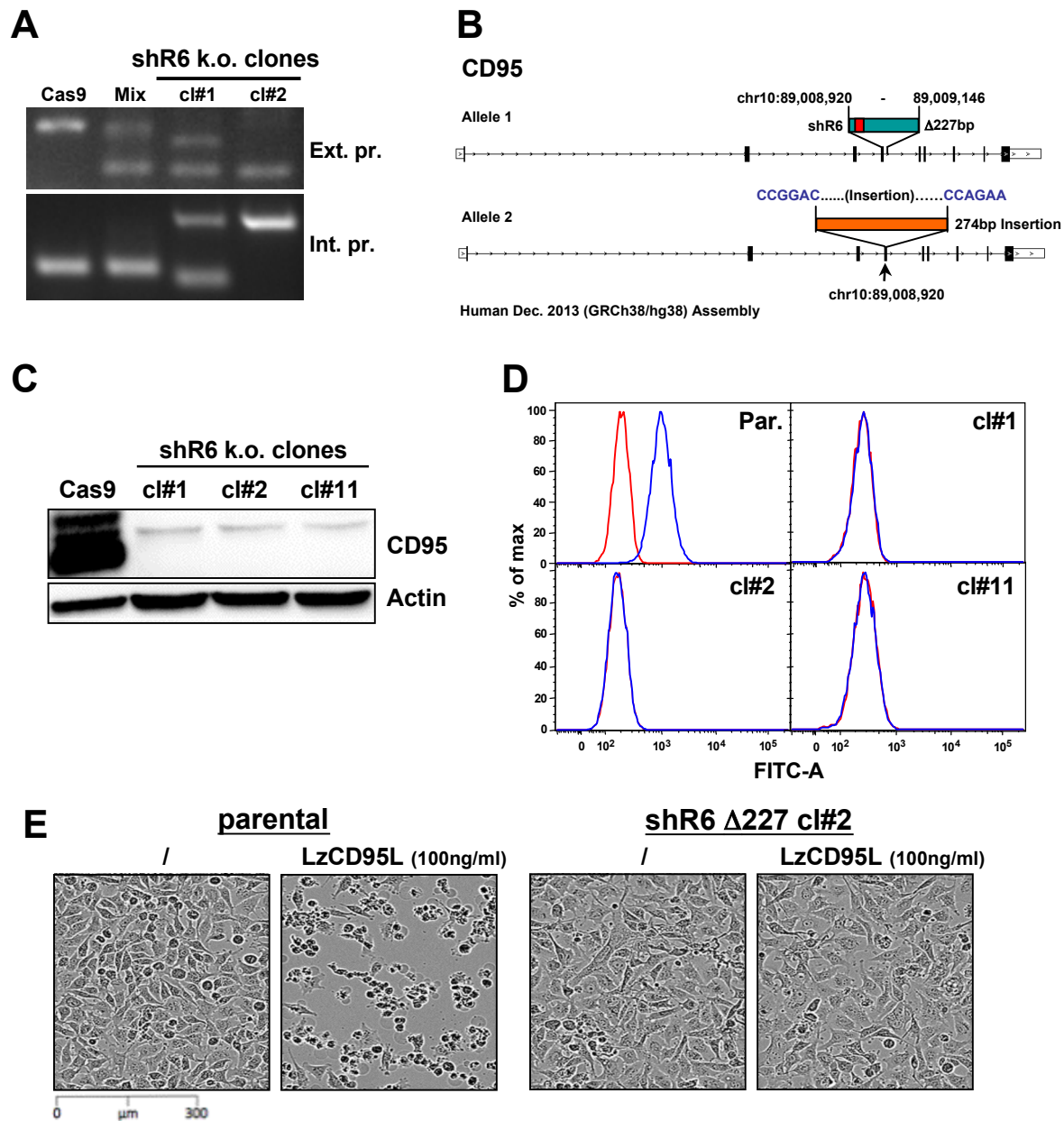


Figure 3

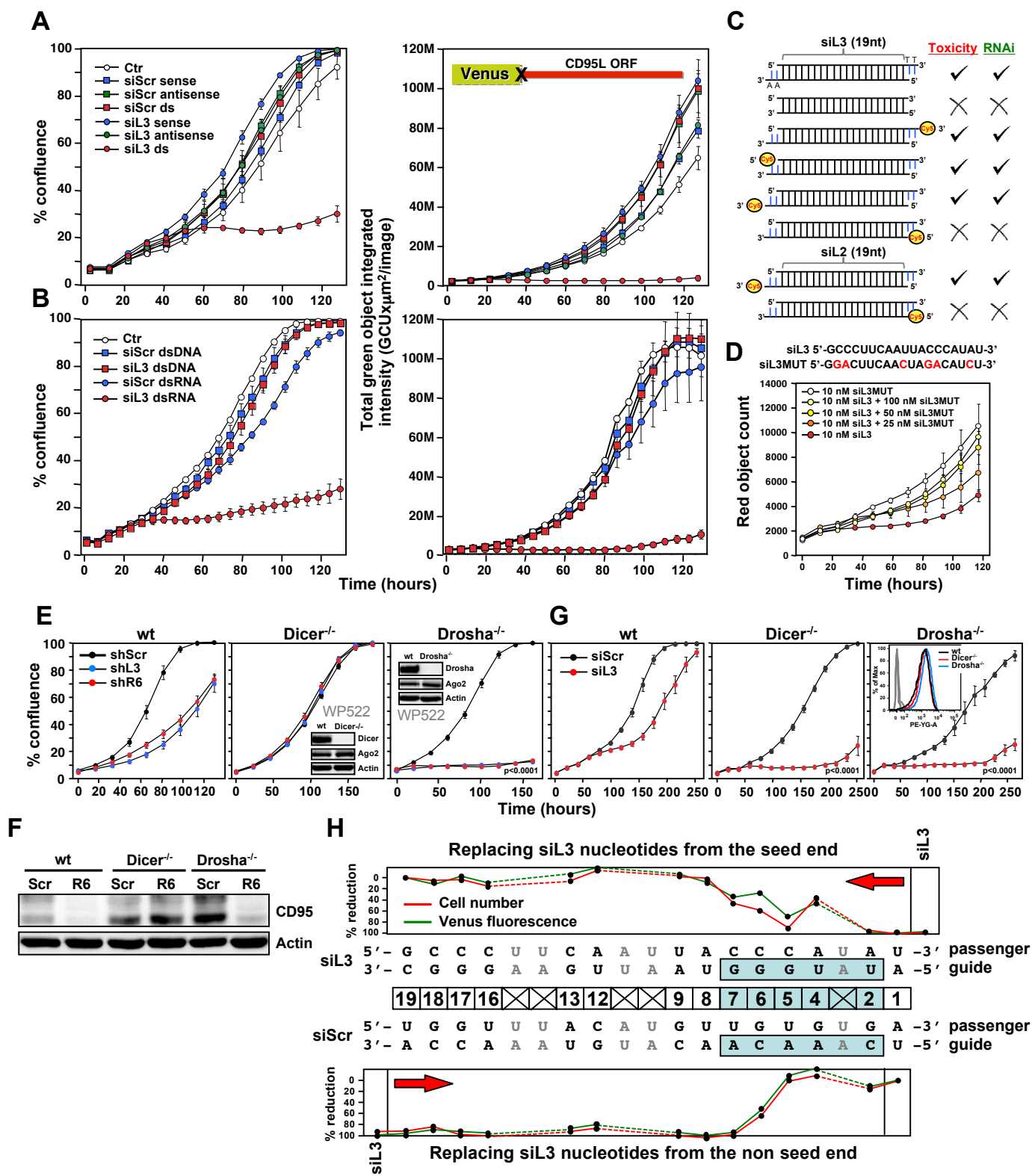
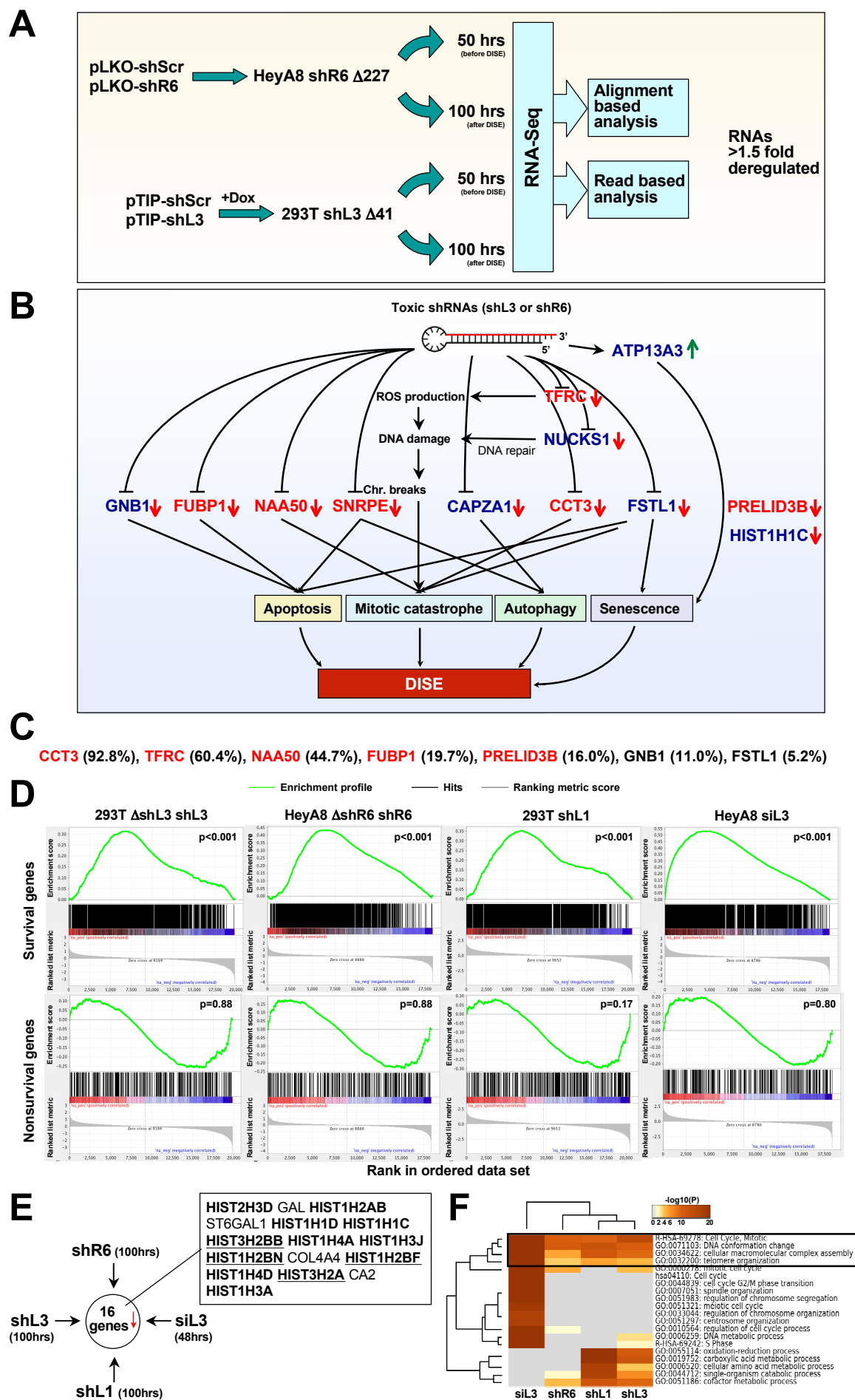
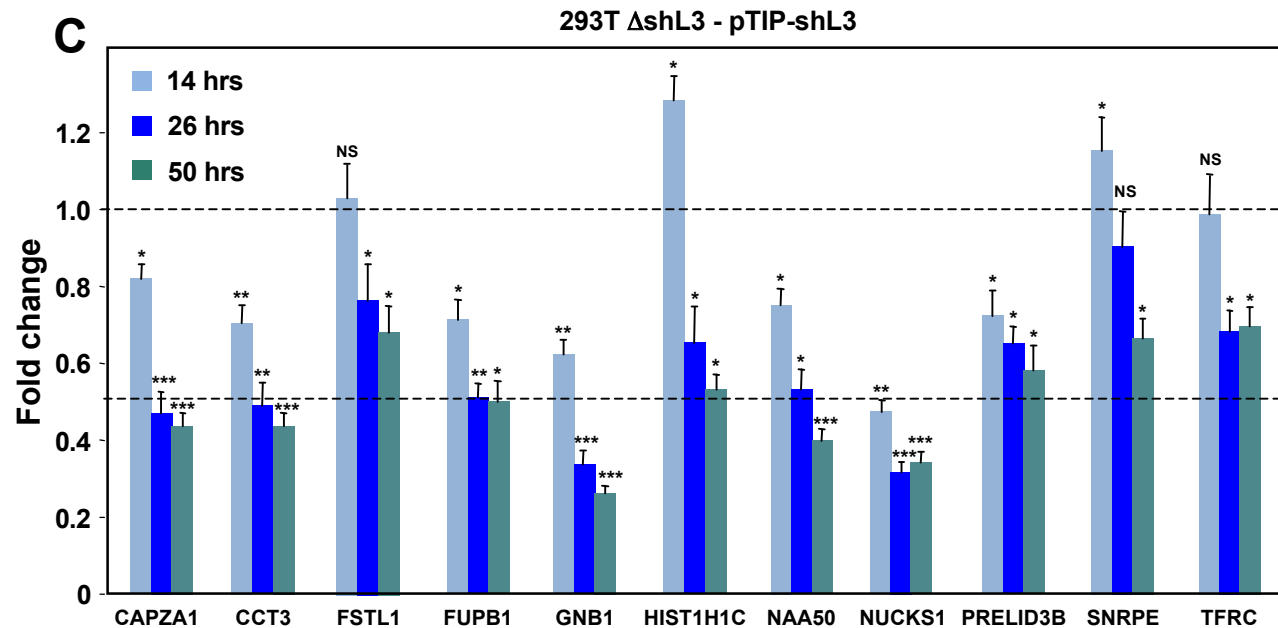
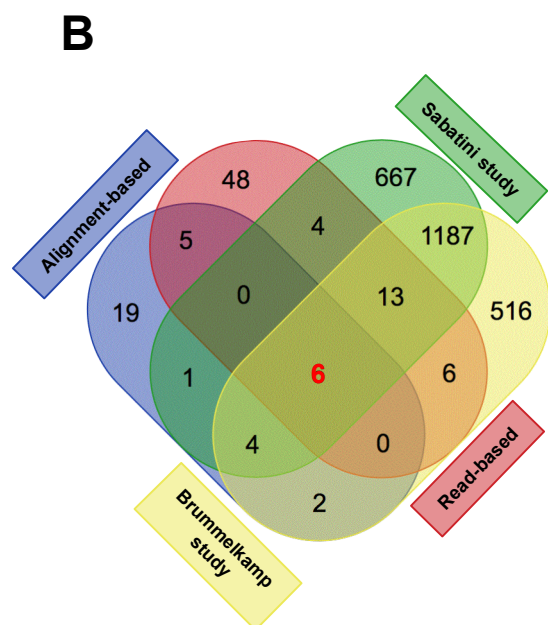
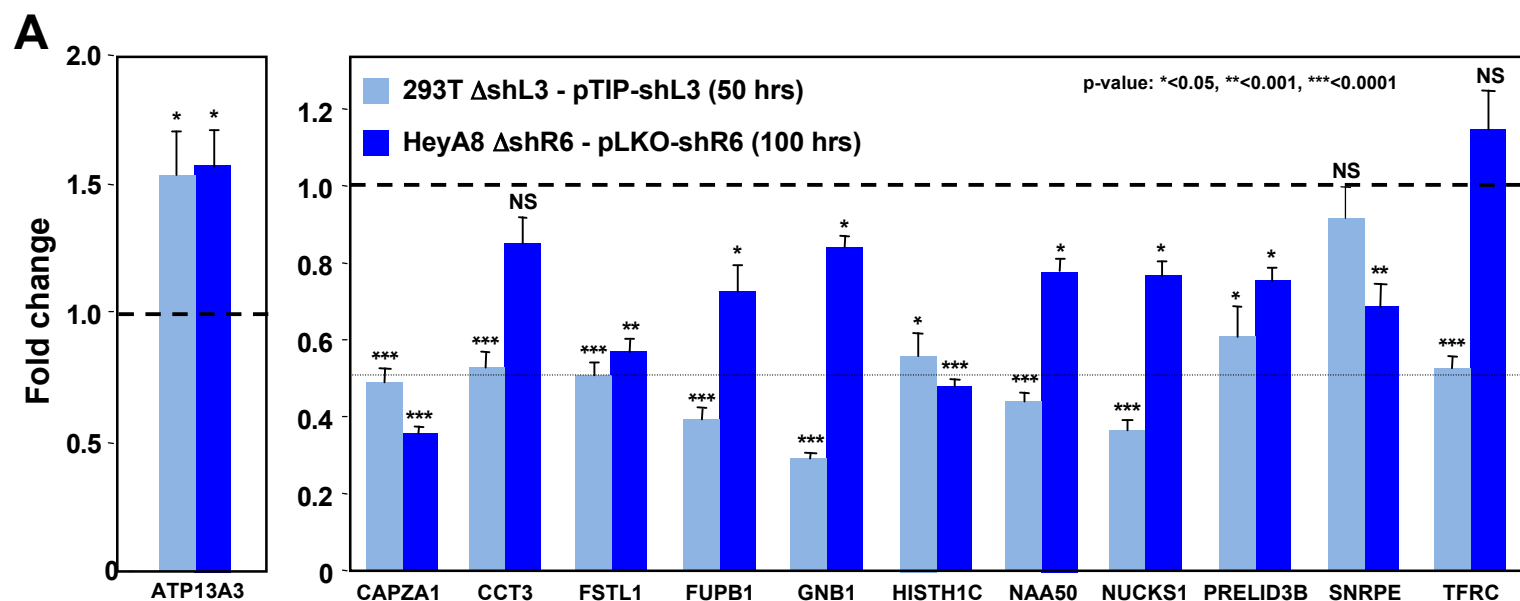


Figure 4





D

siL3			X	X		X					X
shL1						X					
shL3		X		X		X	X	X	X	X	X
shR7	X	X		X		X	X	X	X	X	

Figure 4 - figure supplement 2

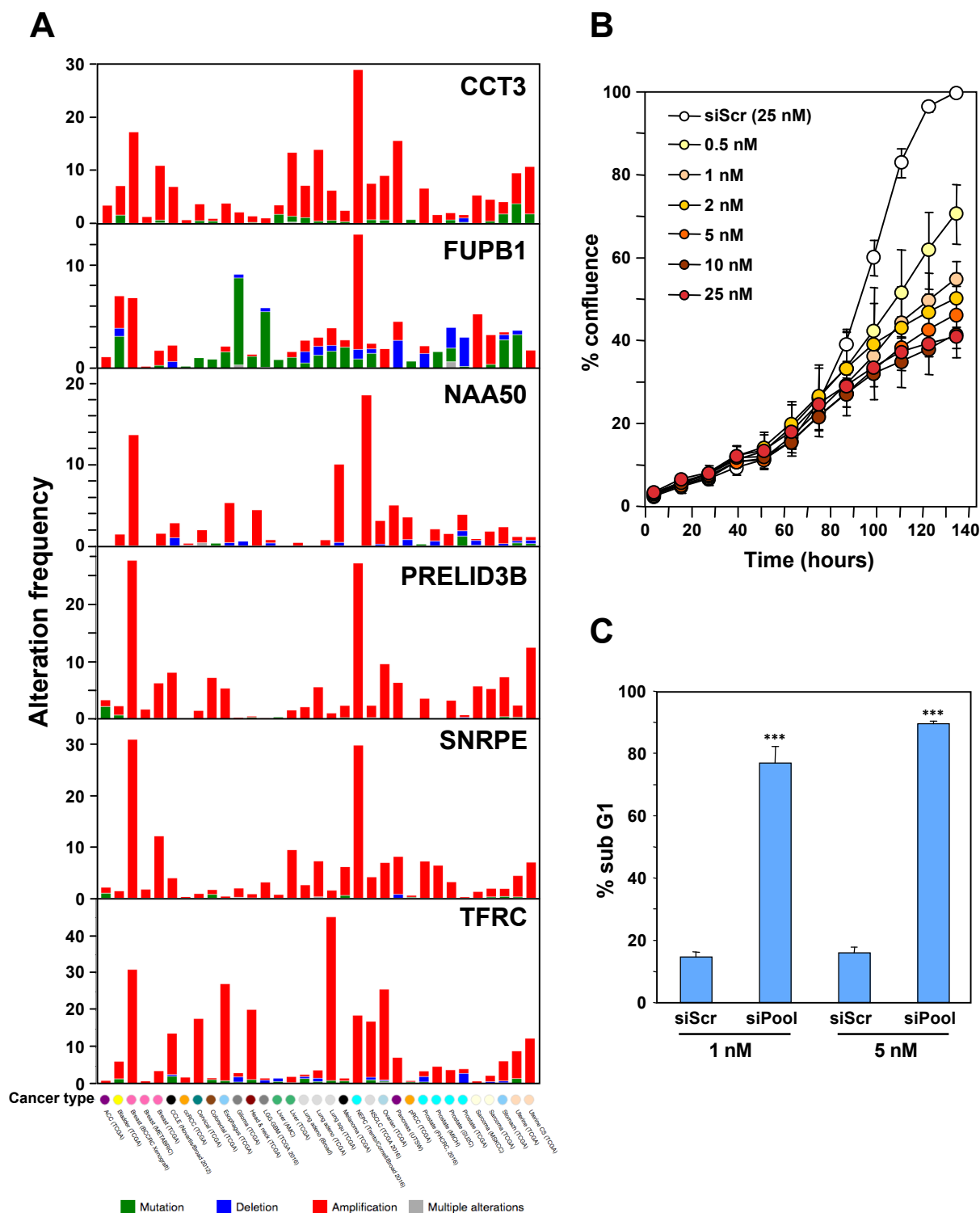


Figure 4 - figure supplement 3

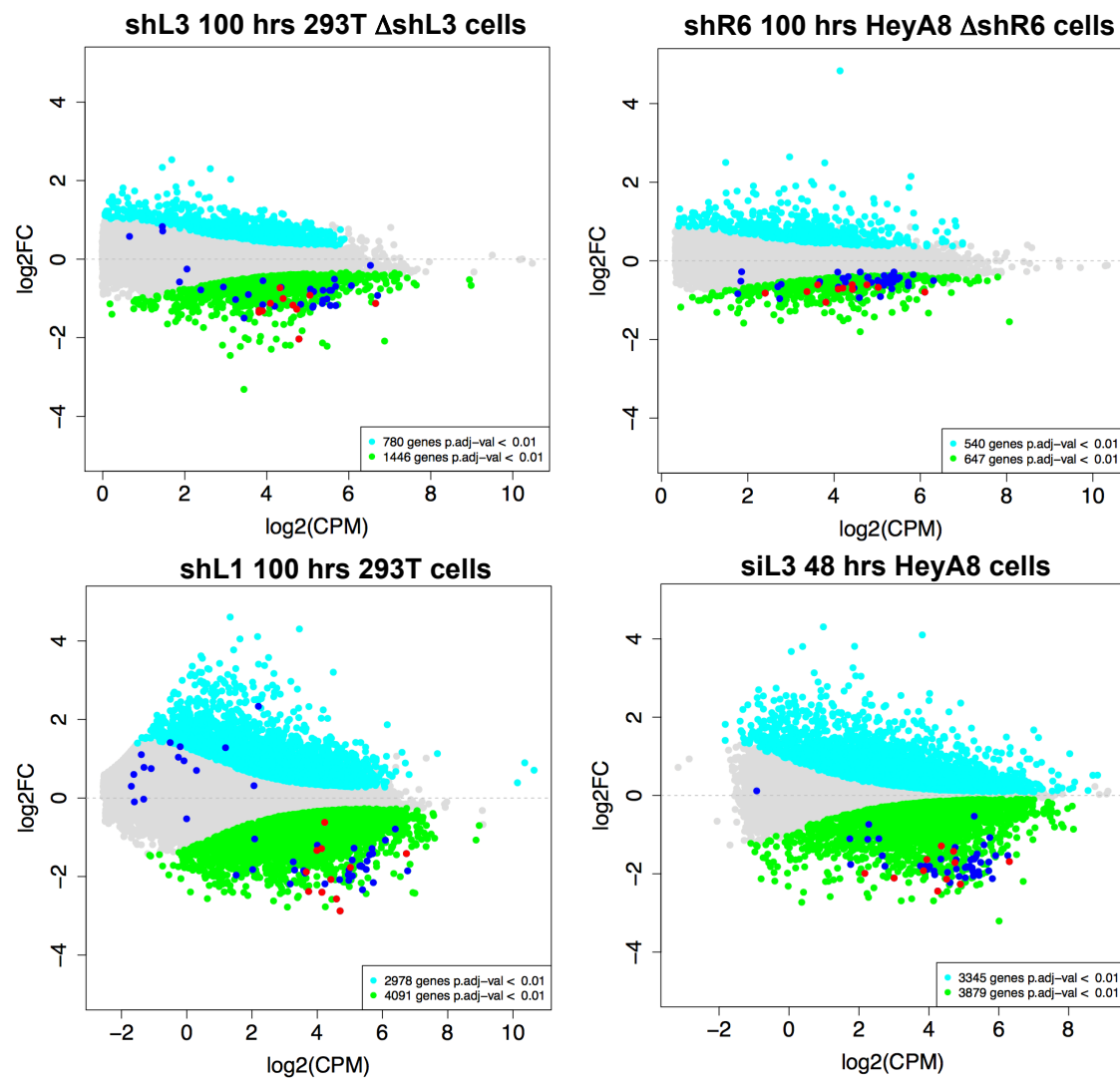
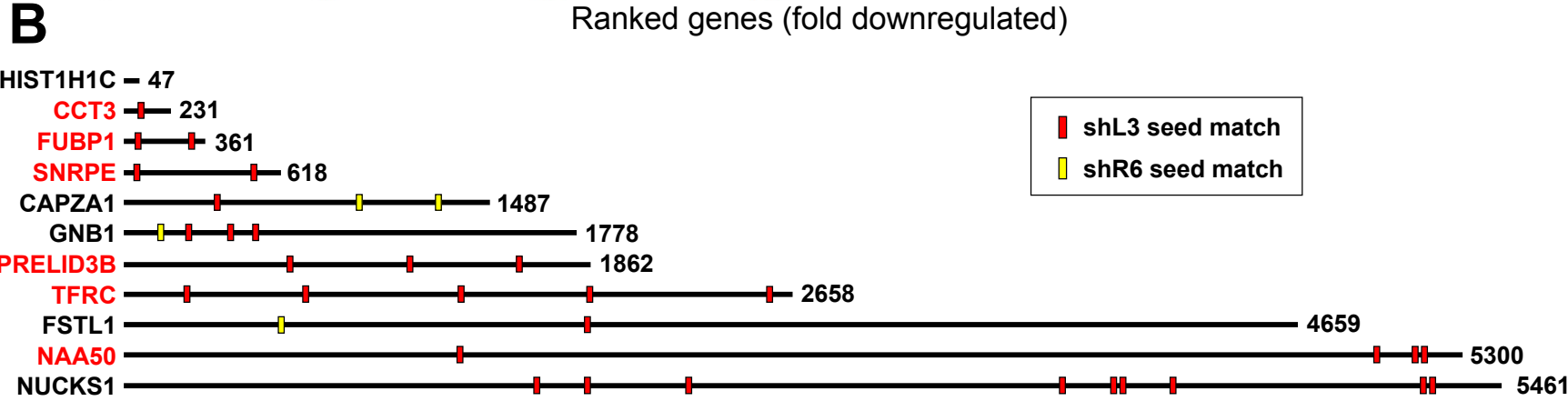
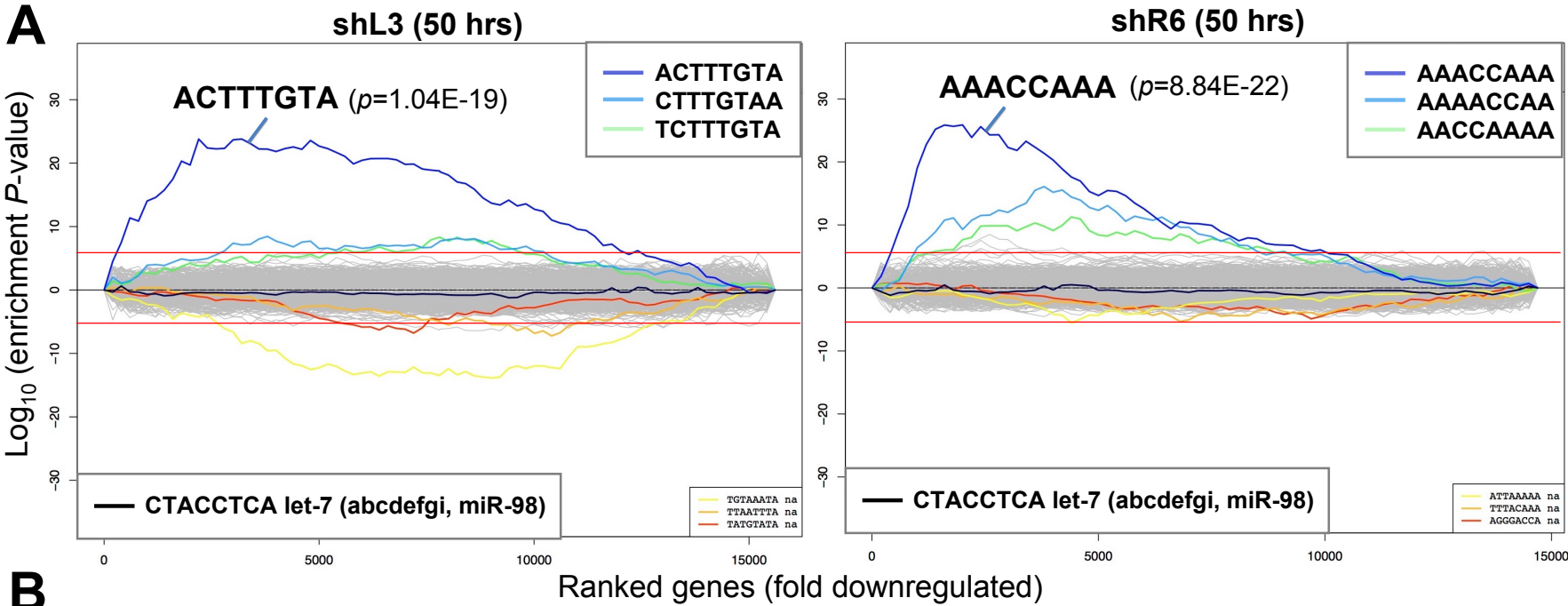


Figure 5



C

Downregulated

Seed match present		shL3 (50hrs)		shL3 (100hrs)		shR6 (50hrs)		shR6 (100hrs)		shL1 (100hrs)		siL3 (48hrs)	
		No	Yes	No	Yes	No	Yes	No	Yes	No	Yes	No	Yes
	No	825	2	783	48	1113	13	1108	16	600	189	1205	238
	Yes	904	55	850	109	612	40	619	31	746	259	244	93
P-value		2.83E-13		2.58E-05		6.65E-09		4.31E-05		0.38		5.74E-06	

Figure 5 - figure supplement 1

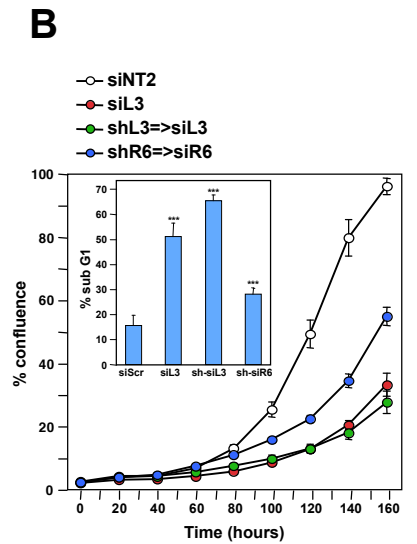
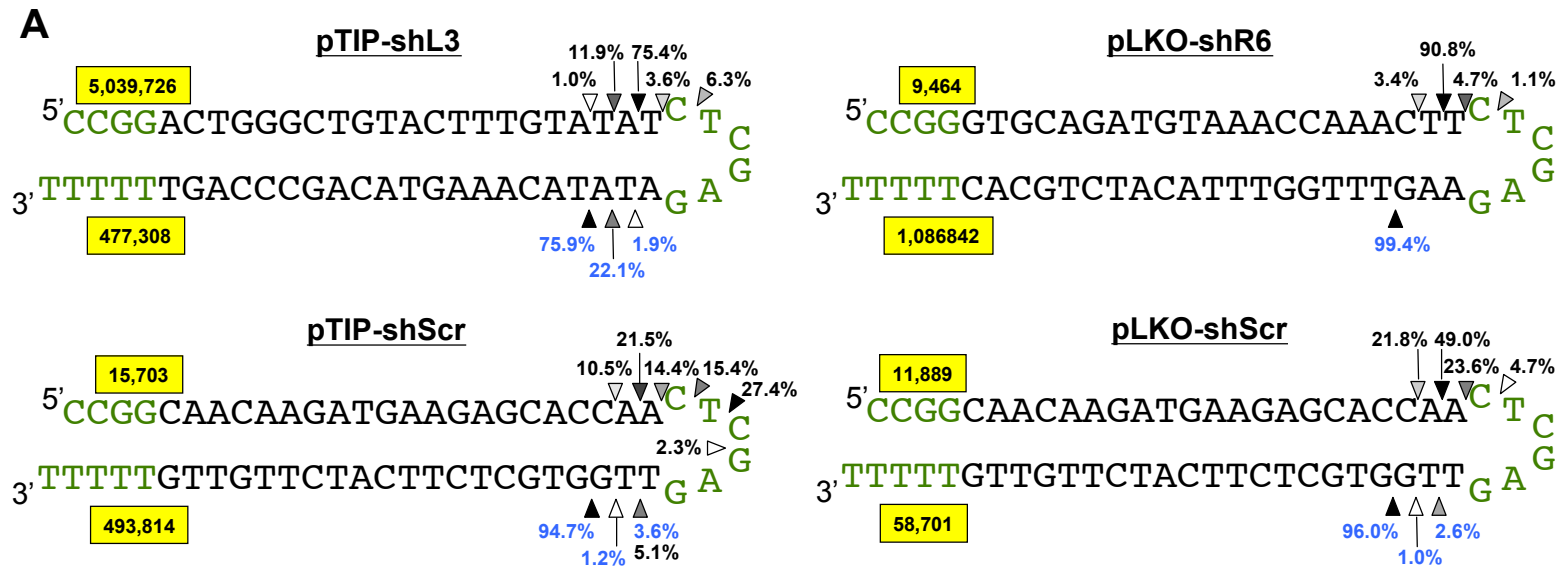


Figure 5 - figure supplement 2

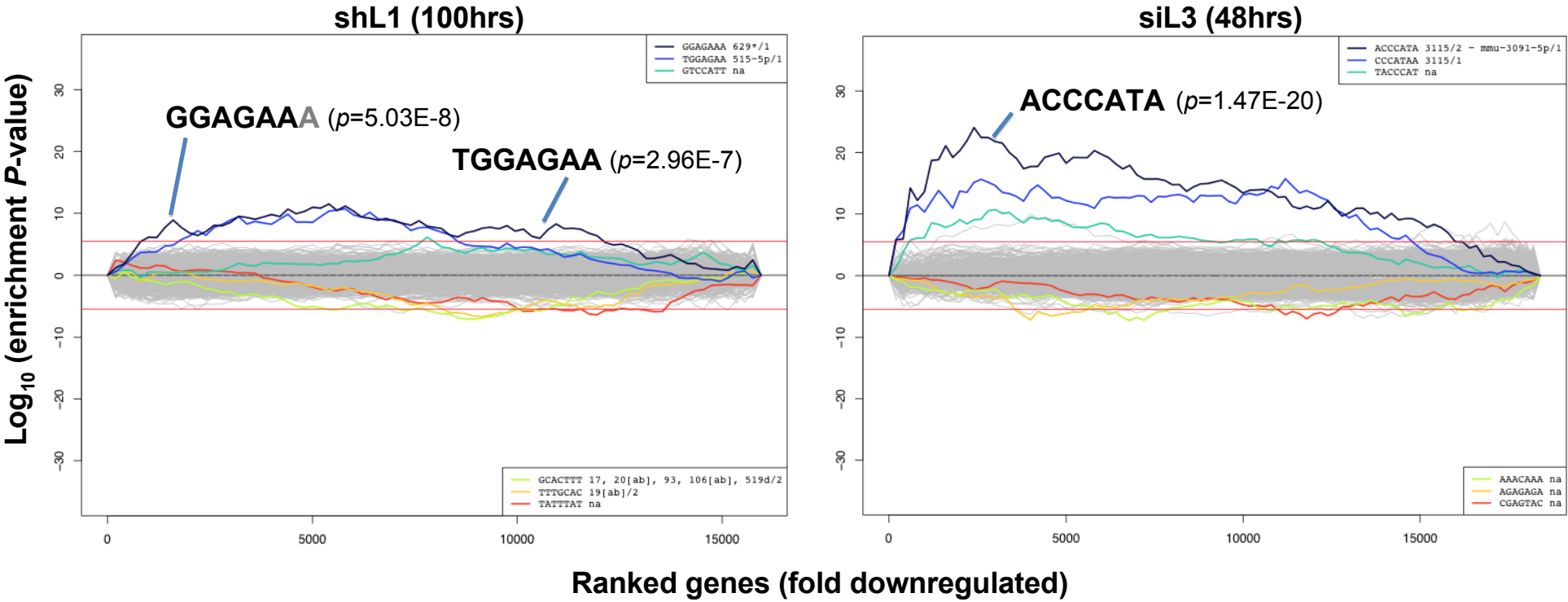


Figure 5 - figure supplement 3

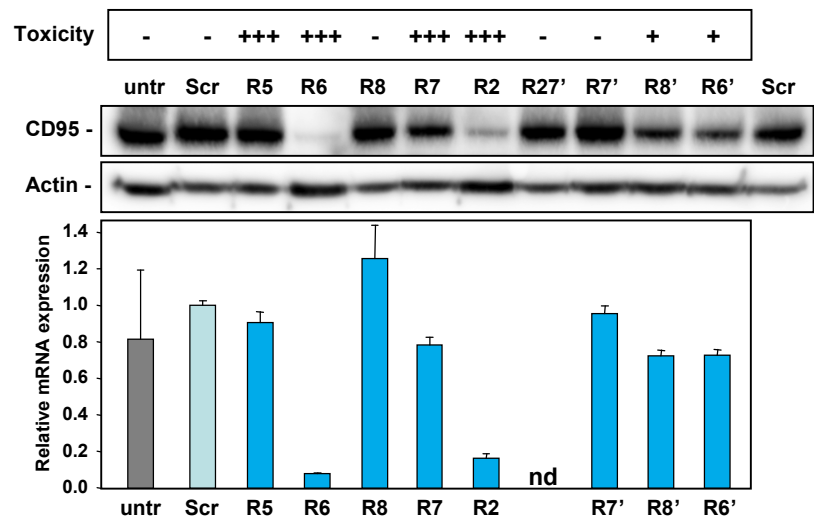


Figure 6

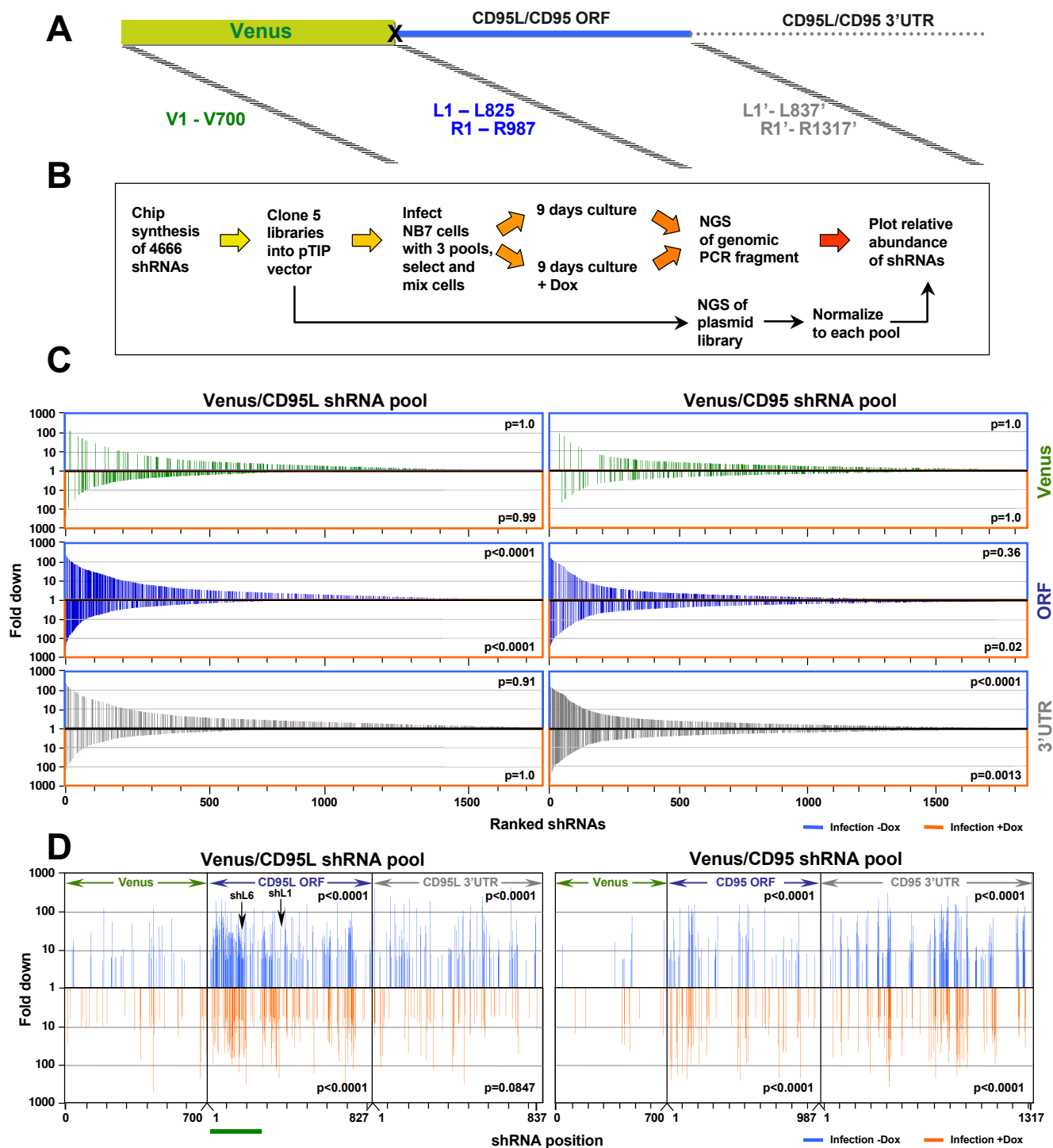


Figure 6 - figure supplement 1

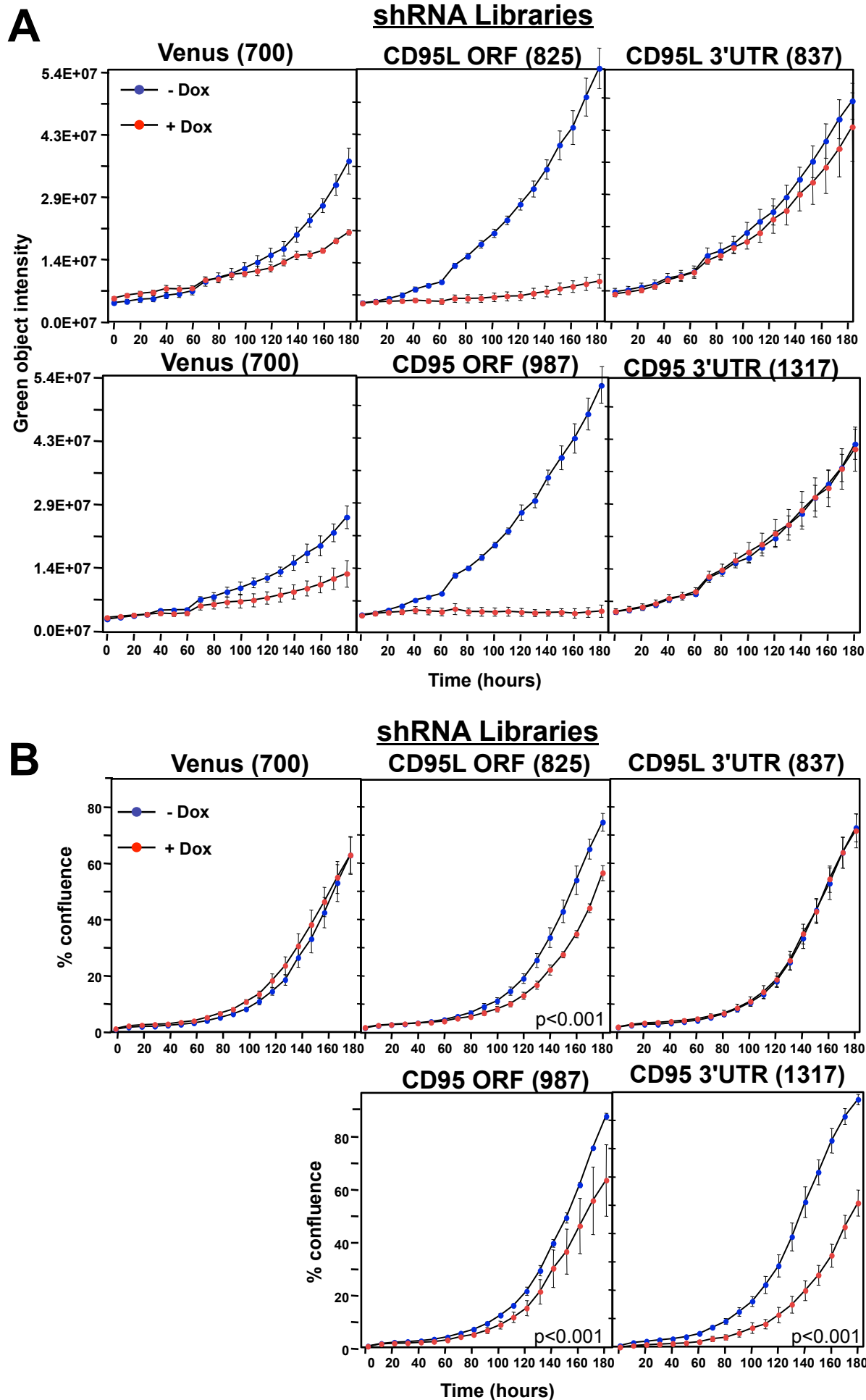


Figure 6 - figure supplement 2

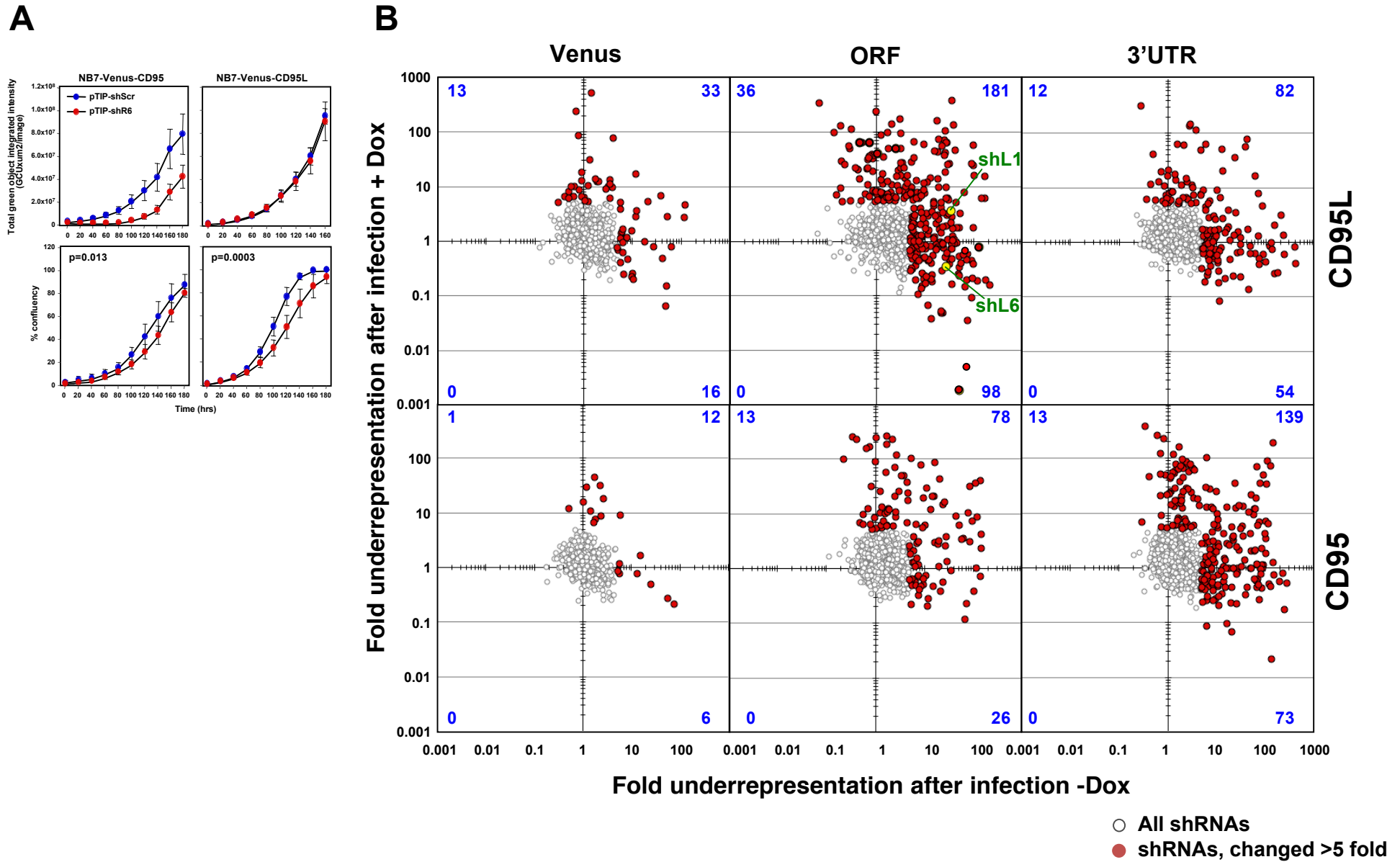


Figure 7

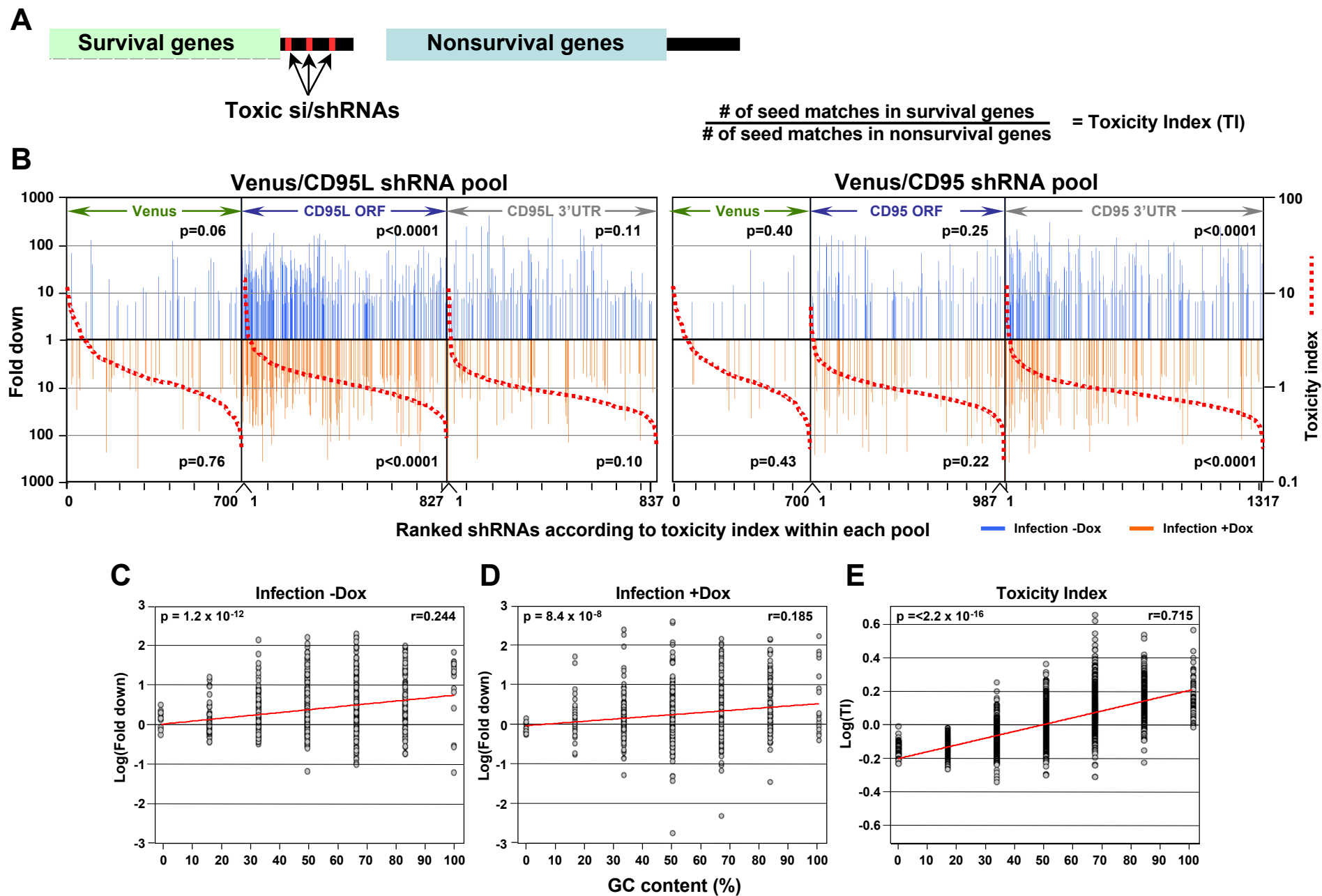


Figure 7 - figure supplement 1

